Control of Nano-Structure of Thin Film by Spray Layer-by-Layer Method and the Optical Applications

March 2011

A thesis submitted in partial fulfilment of the requirements for the degree of Doctor of Philosophy in Engineering

Keio University

Graduate School of Science and Technology
School of Integrated Design Engineering

Kyung, KyuHong

Table of contents

Chapter 5 Control of structure and film thickness using spray layer-by-layer method for application to double-layer anti-reflection film

Control of Nano-Structure of Thin film
by Spray Layer-by-Layer Method and the Optical Applications

Chapter 1

Various techniques for fabrication of thin film
and layer-by-layer self assembly method

Chapter 2

Establishment of   condition
and application to Anti- reflection film
(Investigation of TiO_2 Thin Film Growth by LBL-SA method)

Chapter 3

Spray layer-by-layer method
(principle and optimization)

Chapter 4

Control of nano-structure and
film thickness
using spray-layer-by-layer method

Chapter 5

Application to double-layer
anti-reflection thin films
using spray-layer-by-layer method

Chapter 6

Summary

CHAPTER 1

General introduction

1. 1 Background

Several techniques besides vapor deposition [1-2] and drop-casting [3] have intensively been developed over the years to fabricate the nano-structured thin film by controlling molecule. Among them in the early 1970s, Kuhn fabricated the nano-scale multicomposites consisted of organic molecules by langmuir-blodgett (LB) technique [4-5]. In addition, Sagiv and co-works also introduced the self-assembly of organic molecules which have specific functional groups [6-10]. However, this mono or multilayers thin film assembled by the LB technique has many applications [11], researchers have difficulty in fabrication thick and stable films. The LB technique has several disadvantages. Only amphiphilic materials can be used to construct LB films, which limit the choice of material incorporated in the film. The constructionof the monolayer requires very clean conditions, and it would be hard to mass-produce devices using LB methods. On the other hand, Decher and co-workers introduced the layer-by-layer (LBL) self-assembly method which fabricates the multilayers thin film by the electrostatic force of oppositely charged materials in aqueous solution [12-19]. The principle of LBL self-assembly method using colloidal particles was first described by Iler in 1966 [20]. The schematic process of film deposition via LBL self-assembly method was shown in Fig. 1 [21]. Therefore the LBL method can be applied to the wide variety of starting materials such as small organic molecules or inorganic compounds

[22-33], macromolecules [34-45], biomacromolecules [46-60], and colloids such as metallic or oxidic colloids as well as latex particles [61-89].

These multilayers thin films fabricated the LBL self-assembly method have been applied for the coating films with surface interactions such as corrosion protection [90], anti-reflective coatings [91], surface induced nucleation [92-93], antifouling [94-95], hydorphilicity or hydrophobicity [96-97], antibacterial properties, chemical or biosensing [98-106]. In addition, by controlling and designing the multilayer architecture of nanocomposites, this technique has been a promising method to manufacture several devices such as membrane reactors [107-108], light emitting diodes [109-119], and separation membranes [120-124].

Especially, the LBL self-assembly method has been paid much attention to the manufacture of multilayers thin films because the LBL deposition is very simple, environmentally friendly, and low-cost technique and does not need a vacuum system as well as other complicated apparatus. Moreover the prepared multilayers thin film can be successfully assembled with the controlling of morphology and thickness with nanoscale range by monitoring the in-situ deposition phenomenon of polyelectrolytes or nanoparticles assembled on the electrode of quartz crystal microbalance (QCM) [125].

Though LBL method has many advantages, it requires long fabrication time. Because the process is driven in part by diffusion, LBL cycles usually take on the order of several minutes to complete. This presents unacceptable demerits if this technology is to evolve into industrial applications.

Several LBL modifications have been proposed recently, including spray-LBL [126-134], spin-assisted LBL [135-139], or dewetting-LBL (d-LBL) [140]. These new methods have primarily focused on decreasing the cycle time required by LBL, and

have achieved reductions from cycle times of about 20 min to 60–80 s. And they succeeded in shorting the deposition time at least one order down to 6 s for a polymer/polymer film [127]. They also have provided some abilities to build LBL films on unique substrates, such as fiber substrates [128] or to control the in-plane nanostructure of nano-particles or polymers [129].

1. 2 Various techniques for fabrication of thin film

Techniques for fabrication of thin film can be largely categorized as dry process and wet process. Table simply shows the characterization of fabricated thin film by dry and wet process.

Table 1 Characterization of fabricated thin film by dry and wet process.

	Dry process **(Sputtering, Vacuum evaporation)**	**Wet process** **(spray, gravure coating)**
Film performance	High	Low
Cost	High	Low
Materials	Low	High
Line speed	Low	High

1. 2. 1 Dry process

(1) Vacuum deposition

Vacuum deposition is a family of processes used to deposit layers atom-by-atom or molecule-by-molecule at sub-atmospheric pressure (vacuum) on a solid surface. The layers may be as thin as one atom to millimeters thick (freestanding structures). There may be multiple layers of different materials (e.g. optical coatings). A thickness of less

than one micrometer is generally called a thin film while a thickness greater than one micrometer is called a coating. The vacuum environment may serve one or more purposes including: [141-143]

- reducing the particle density so that the mean free path for collision is long

- reducing the particle density of undesirable atoms and molecules (contaminants)

- providing a low pressure plasma environment

- providing a means for controlling gas and vapor composition

- providing a means for mass flow control into the processing chamber.

Applications:

- Electrical conduction: metallic films, transparent conductive oxides (TCO), superconducting films & coatings

- Semiconductor devices: semiconductor films, electrically insulating films

- Solar cells.

- Optical films: antireflective coatings, optical filters

- Reflective coatings: mirrors, heat mirrors

- Tribological coating: hard coatings, erosion resistant coatings, solid film lubricants

- Energy conservation & generation: low-E glass coatings, solar absorbing coatings, mirrors, solar thin film photovoltaic cells, smart films

- Magnetic films: magnetic recording

- Diffusion barrier: gas permeation barriers, vapor permeation barriers, solid state diffusion barriers

- Corrosion protection:

- Automotive applications: lamp reflectors and trim applications

(2) Sputter deposition

Sputter deposition is a physical vapor deposition (PVD) method of depositing thin films by sputtering, that is ejecting, material from a "target," that is source, which then deposits onto a "substrate," such as a silicon wafer. Resputtering is re-emission of the deposited material during the deposition process by ion or atom bombardment. Sputtered atoms ejected from the target have a wide energy distribution, typically up to tens of eV (100000 K). The sputtered ions (typically only a small fraction — order 1% — of the ejected particles are ionized) can ballistically fly from the target in straight lines and impact energetically on the substrates or vacuum chamber (causing resputtering). Alternatively, at higher gas pressures, the ions collide with the gas atoms that act as a moderator and move diffusively, reaching the substrates or vacuum chamber wall and condensing after undergoing a random walk. The entire range from high-energy ballistic impact to low-energy thermalized motion is accessible by changing the background gas pressure. The sputtering gas is often an inert gas such as argon. For efficient momentum transfer, the atomic weight of the sputtering gas should be close to the atomic weight of the target, so for sputtering light elements neon is preferable, while for heavy elements krypton or xenon are used. Reactive gases can also be used to sputter compounds. The compound can be formed on the target surface, in-flight or on the substrate depending on the process parameters. The availability of many parameters that control sputter deposition make it a complex process, but also allow experts a large degree of control over the growth and microstructure of the film.

Sputtering is used extensively in the semiconductor industry to deposit thin films of

various materials in integrated circuit processing. Thin antireflection coatings on glass for optical applications are also deposited by sputtering. Because of the low substrate temperatures used, sputtering is an ideal method to deposit contact metals for thin-film transistors. Perhaps the most familiar products of sputtering are low-emissivity coatings on glass, used in double-pane window assemblies. The coating is a multilayer containing silver and metal oxides such as zinc oxide, tin oxide, or titanium dioxide. Sputtering is also used to metalize plastics such as potato chip bags. A large industry has developed around tool bit coating using sputtered nitrides, such as titanium nitride, creating the familiar gold colored hard coat. Sputtering is also used as the process to deposit the metal (e.g. aluminum) layer during the fabrication of CD and DVD discs.

Hard disk surfaces use sputtered CrO_x and other sputtered materials. Sputtering is one of the main processes of manufacturing optical waveguides and is another way for making efficient photovoltaic solar cells. [141-143]

(3) Chemical vapor deposition

Chemical vapor deposition (CVD) is a chemical process that uses a chamber of reactive gas to synthesize high-purity, high-performance solid materials, such as electronics components. Certain components of integrated circuits require electronics made from the materials polysilicon, silicon dioxide, and silicon nitride. An example of a chemical vapor deposition process is the synthesis of polycrystalline silicon from silane (SiH_4), using this reaction: [141-143]

$$SiH_4 \rightarrow Si + 2H_2$$

6

In the silane reaction, the medium would either be pure silane gas, or silane with 70-80 % nitrogen. Using a temperature between 600 and 650 ℃ (1100 - 1200 ℉), and pressure between 25 and 150 Pa - less than a thousandth of an atmosphere - pure silicon can be deposited at a rate of between 10 and 20 nm per minute, perfect for many circuit board components, whose thickness is measured in microns. In general, temperatures inside a chemical vapor temperature deposition machine are high, while pressures are very low. The lowest pressures, under 10^{-6} Pa, are called ultrahigh vacuum. This is different than the use of the term "ultrahigh vacuum" in other fields, where it usually refers to a pressure below 10^{-7} Pa instead.

Some products of chemical vapor deposition include silicon, carbon fiber, carbon nano-fibers, filaments, carbon nano-tubes, silicon dioxide, silicon-germanium, tungsten, silicon carbide, silicon nitride, silicon oxynitride, titanium nitride, and diamond. Mass-producing materials using chemical vapor deposition can get very expensive due to the power requirements of the process, which partially accounts for the extremely high cost (hundreds of millions of dollars) of semiconductor factories. Chemical vapor deposition reactions often leave byproducts, which must be removed by a continuous gas flow.

There are several main classification schemes for chemical vapor deposition processes. These include classification by the pressure (atmospheric, low-pressure, or ultrahigh high vacuum), characteristics of the vapor (aerosol or direct liquid injection), or plasma processing type (microwave plasma-assisted deposition, plasma-enhanced deposition, remote plasma-enhanced deposition).

(4) Laser ablation

Laser ablation is the process of removing material from a solid (or occasionally liquid) surface by irradiating it with a laser beam. At low laser flux, the material is heated by the absorbed laser energy and evaporates or sublimates. At high laser flux, the material is typically converted to plasma. Usually, laser ablation refers to removing material with a pulsed laser, but it is possible to ablate material with a continuous wave laser beam if the laser intensity is high enough.

The depth over which the laser energy is absorbed, and thus the amount of material removed by a single laser pulse, depends on the optical properties of the materials and the laser wavelength. Laser pulses can vary over a very wide range of duration (milliseconds to femto seconds) and fluxes, and can be precisely controlled. This makes laser ablation very valuable for both research and industrial applications.

(5) Ion plating

Ion plating is a physical vapor deposition (PVD) process that is sometimes called ion assisted deposition (IAD) or ion vapor deposition (IVD) and is a version of vacuum deposition. Ion plating utilizes concurrent or periodic bombardment of the substrate and depositing film by atomic-sized energetic particles. Bombardment prior to deposition is used to sputter clean the substrate surface. During deposition the bombardment is used to modify and control the properties of the depositing film. It is important that the bombardment be continuous between the cleaning and the deposition portions of the process to maintain an atomically clean interface.

1. 2. 2 Wet process

(1) Dip-coating

Dip coating is a popular way of creating thin films for research purposes. Uniform films can be applied onto flat or cylindrical substrates. The dip coating process can be separated into five stages: [141-144]

- Immersion: The substrate is immersed in the solution of the coating material at a constant speed (preferably judder free).

- Start-up: The substrate has remained inside the solution for a while and is started to been pulled up.

- Deposition: The thin layer deposits itself on the substrate while it is pulled up. The withdrawing is carried out at a constant speed to avoid any judders. The speed determines the thickness of the coating (faster withdrawal gives thicker coating material).

- Drainage: Excess liquid will drain from the surface.

- Evaporation: The solvent evaporates from the liquid, forming the thin layer. For volatile solvents, such as alcohols, evaporation starts already during the deposition and drainage steps.

In the continuous process, the steps are carried out directly after each other.

(2) Sol-gel method

The sol-gel process, also known as chemical solution deposition, is a wet-chemical

technique widely used in the fields of materials science and ceramic engineering. Such methods are used primarily for the fabrication of materials (typically a metal oxide) starting from a chemical solution (or sol) that acts as the precursor for an integrated network (or gel) of either discrete particles or network polymers. Typical precursors are metal alkoxides and metal chlorides, which undergo various forms of hydrolysis and polycondensation reactions. [141-143, 145]

In this chemical procedure, the sol gradually evolves towards the formation of a gel-like diphasic system containing both a liquid phase and solid phase whose morphologies range from discrete particles to continuous polymer networks. In the case of the colloid, the volume fraction of particles (or particle density) may be so low that a significant amount of fluid may need to be removed initially for the gel-like properties to be recognized. This can be accomplished in any number of ways. The simplest method is to allow time for sedimentation to occur, and then pour off the remaining liquid. Centrifugation can also be used to accelerate the process of phase separation.

Removal of the remaining liquid (solvent) phase requires a drying process, which is typically accompanied by a significant amount of shrinkage and densification. The rate at which the solvent can be removed is ultimately determined by the distribution of porosity in the gel. The ultimate microstructure of the final component will clearly be strongly influenced by changes imposed upon the structural template during this phase of processing.

Afterwards, a thermal treatment, or sintering process, is often necessary in order to favor further polycondensation and enhance mechanical properties and structural stability via final sintering, densification and grain growth. One of the distinct advantages of using this methodology as opposed to the more traditional processing

techniques is that densification is often achieved at a much lower temperature.

The precursor sol can be either deposited on a substrate to form a film (e.g., by dip coating or spin coating), cast into a suitable container with the desired shape (e.g., to obtain monolithic ceramics, glasses, fibers, membranes, aerogels), or used to synthesize powders (e.g., microspheres, nanospheres). The sol-gel approach is a low cost and low-temperature technique that allows for the fine control of the product's chemical composition. Even small quantities of dopants, such as organic dyes and rare earth elements, can be introduced in the sol and end up uniformly dispersed in the final product. It can be used in ceramics processing and manufacturing as an investment casting material, or as a means of producing very thin films of metal oxides for various purposes. Sol-gel derived materials have diverse applications in optics, electronics, energy, space, bio-sensors, medicine (e.g., controlled drug release), reactive material and separation (e.g., chromatography) technology.

(3) Spin coating

Spin coating is a procedure used to apply uniform thin films to flat substrates. In short, an excess amount of a solution is placed on the substrate, which is then rotated at high speed in order to spread the fluid by centrifugal force. A machine used for spin coating is called a spin coater, or simply spinner. [141-143]

Rotation is continued while the fluid spins off the edges of the substrate, until the desired thickness of the film is achieved. The applied solvent is usually volatile, and simultaneously evaporates. So, the higher the angular speed of spinning, the thinner the film. The thickness of the film also depends on the concentration of the solution and the

solvent. [146]

Spin coating is widely used in micro-fabrication, where it can be used to create thin films with thicknesses below 10 nm. It is used intensively in photolithography, to deposit layers of photoresist about 1 μm thickness. Photoresist is typically spun at 20 to 80 revolutions per second for 30 to 60 s.

1. 3 Assembly of thin films by dipping (layer-by-layer self assembly method)

Fabrication of functional thin films can be achieved via several deposition techniques including physical or chemical vapor deposition, electroplating, spin assisted or spray coating, layer-by-layer (LBL) deposition, and several other techniques. Among all the techniques mentioned above, LBL has several significant advantages that make this technique very useful for fabrication of functional thin films. One key feature of the LBL technique is that any species with multiple ionic charges can be used as one of the components of the LBL assembled thin films. This phenomenon, along with the fact that charged species can be deposited from aqueous solutions, make a wide range of materials available to be used with this technique such as ionic polymers [147-149], nano-particles [150-152], dendrimers [153-155], quantum dots [156-158], proteins [159, 160], and DNA [161, 162]. The LBL assembly technique was first developed and introduced in 1966 by Iler [163] at Dupont. The technique did not receive much credit nor attention from the scientific community until it was reintroduced in 1991 by Decher et al [164] as a solution for deposition of charged polymers. Since its redevelopment in 1991, the LBL assembly technique has become one of the most preferred techniques for fabrication of thin films and has been practiced by numerous research groups

12

worldwide.

The LBL assembly technique is based on sequential deposition of oppositely charged species on a charged substrate [163, 165-167]. Although different types of chemical bonds may be involved in formation of the multilayer thin films [168, 169], the most common form of LBL deposition is based on ionic bonds between ionic species [167, 170]. Figure 2 shows a schematic of formation of two bilayer via ionic attraction between two ionic polymers.

Exposure of the charged substrate to a dilute aqueous ionic solution of opposite charge forms an ultra thin layer of the charged molecules on the surface of the substrate. The substrate is then rinsed with deionized (DI) water to wash the loosely bound molecules and immersed in the other dilute aqueous ionic solution with a charge opposite to the charge of the first ionic solution to form another ultra thin film on the top of the existing, first, ultrathin film. This step is also followed by rinsing with DI water. The two-layer system forms one bilayer. Repetition of these steps results in formation of thin films consisting of several bilayers.

1. 3. 1 Controlled Assembly

Control over the thickness and morphology of each bilayer, and the thin film as a whole, is significantly important in characterization and performance of the functional thin films. The LBL assembly technique can be adopted to fabricate thin films of a variety of properties. The morphology and properties of the bilayers can be determined by conditions of the deposition process and characteristics of the ionic species. Deposition conditions such as dipping duration and number of bilayers, along with

solution characteristics such as pH, [171,172] ion concentration, [173] ion type [174], ion strength, [175] and molecular weight [174] can influence the composition of the thin films.

Adjusting and optimizing these factors can manipulate the thin films to have desired properties. The dipping duration can vary from 1 to approximately 30 minutes. After a certain amount of time, depending on the conditions and materials, the deposition rate approaches zero due to charge balance between the existing and depositing layers and repulsion of the outer layer towards the polymers in solution. The charge strength of the materials also affects the deposition quality significantly [176-178].

In the case of ionic polymers, varying the charge density of the polymer backbone chains also influence the morphology and the thickness of the thin films. Normally, the polymer molecules are in the form of long chains and the ionic charge is homogeneously distributed along them. Addition of counter ions, usually through addition of salt, neutralizes some fraction of the charges and reduces the repulsion force along the polymer chain; following the lack of enough repulsion force, the polymer chains curl and form cluster conformations [179-181]. As shown in Figure 3, layers deposited from such solutions are generally thicker due to globular arrangement of the polymer molecules.

Another way to manipulate the charge on the polymer backbone is to adjust the pH of the solution [173, 182-185]. This method is especially useful for cases in which the electrolyte is weak, which means that it can be neutralized near neutral pH. Increasing or decreasing the pH increases the charge of carboxyl or amine groups respectively [186-188]. Polyanions are fully charged at high pH and polycations are fully charged at low pH.

1. 3. 2 Influence of pH dependence

Shiratori et al. introduced the pH dependent thickness behavior of multilayers thin film consisted of weak polyelectrolytes poly (acrylic acid, PAA) and poly (allylamine hydrochloride, PAH) as shown in Fig. 4 [189]. The thickness of thin film was outstandingly influenced by the charge density of PAH and PAA which are adjusted to various pH range. In case of PAH, as the pH value is increased, the thickness of PAH adsorption was increased. On the other hand, as the pH value in increased, the thickness of PAA adsorption was decreased because the segments of PAH which is almost fully ionized in low pH region form a tail structure with small thickness and the segment of PAA which is seldom ionized in low pH region form a loop structure with large thickness. The dissociation ratio of PAH and PAA as a function of pH value of solution was shown in Fig. 5 [190].

Therefore the final thickness of multilayers thin film is directly changed by the segments structure of PAH and PAA that is ionized or not in the various pH ranges and it was confined that the thickness of multilayers thin film assembled by LBL self-assembly method is readily controlled with nano-scale order.

1. 3. 3 Influence of salt concentration in polyelectrolyte solution

Several literatures have introduced the role of salt concentration in the assemble phenomenon of polyelectrolytes [191-197]. Fig. 6 shows the schematic diagram of multilayers formation of polyelectrolytes with NaCl [191]. In step a, the negatively or positively charged polyelectrolytes are compensated by counter-ions and the polyelectrolyte charges are compensated by the other charges of polyelectrolytes during

multilayers deposition in step b (intrinsic compensation). In step c, the adding of NaCl result in the swelling of polyelectrolytes pair (extrinsic compensation) and the multilayers may be decomposed or weakly associated by the sufficient swelling. If additional negative or positive polyelectrolyte (negative one in Figure) is present, overcompensation occurs near the surface in step d, which makes the segment structure of polyelectrolyte loopy. Multilayers thin films are assembled by the cycle of steps from b to d simultaneously.

In the presence of salt, the binding sites between positively and negatively charged polyelectrolyte are decreased, which more polyelectrolytes can be absorbed on the surface and the segments of polyelectrolyte become a loopy structure because of charge screening at high ionic strength. Therefore the thickness as well as absorbance of multilayers thin film is gradually increased according to the concentration of NaCl and the surface roughness is also increased [198].

1. 3. 4 pH-induced phase separation of weak polyelectrolyte

Mendelsohn and co-worker introduced the simple way to fabricate the high surface area as well as uniform microporous thin films [199]. The multilayers thin film consisted of weak polyelectrolyte, PAH adjusted to pH 7.5 and PAA adjusted to pH 3.5, is irreversibly transformed in acidic solution (pH 2.5) with 60 s immersion. During this procedure, the thickness of film is increased with 2 ~ 3 times compared with that of original film and the relative density is correspondingly decreased with 1/2 ~ 1/3 because of the ionic bond breakages of oppositely charged weak polyelectrolytes in low pH solution. In addition this microporous multilayers thin film is reorganized in neutral

water for 15 s. The refractive index of multilayers thin film is also changed from 1.54 to 1.18. Therefore microporous multilayers thin films obtained by the deposition of polyelectrolytes adjusted to a unique pH value and immersion in acidic water for short time exhibits the high possibility for microelectronic and biomaterial applications. Fig. 9 shows the surface of PAH 7.5/PAA 3.5 thin film with 21 bilayers before and after immersion into acidic water (pH 2.5) [199]. Fig. 10 presents the surface morphology of microporous thin film immersed into acidic water and then immersed into neutral water for 10 h [199].

1. 3. 5 Applications of LBL assembled films

Versatility of LBL self-assembly, a surface functionalization by combining any substance on any substrates regardless what their form and size offers the accessibility of this technique to real commercial applications. Derived from original "Bola" molecules [13, 14] the LBL self-assembly technique has been used in many different fields. For example, catalytic membranes can be prepared by using LBL adsorption of polyelectrolyte/metal nano-particle in porous supports [200]. LBL assembled polyelectrolyte multilayer with embedded liposomes can be used as immobilized submicronic reactors for mineralization [201]. Besides traditional planar substrate, polyelectrolyte multilayer can be assembled on spherical substrate by using nano-particle template, which makes the fabrication of hollow capsule possible. This hollow capsule fabrication has already been reported by several groups [202, 203]. These well defined hollow polymeric capsules have direct applications in drug delivery, catalysis, and dye dispersion industries.

Shimomura et al. reported the fabrication of uniform, conformal multi stack nanoparticle thin films for optical applications with precise thickness control over each stack using the electrostatic layer-by-layer assembly method. [204]

Optical reflection is a fundamental phenomenon occurring when light propagates across a boundary between two media, which have di!erent refractive indices. There are two approaches to achieve low reflection: [205, 206]

(1) inhomogeneous layer (or called graded index layer)

Inhomogeneous layers have long been used for optical coatings. They differ from normal homogeneous layers only in the smooth variation of their optical constants throughout their thickness. The reduction of reflection occurs when the difference in the refractive index between the two media is reduced using an inhomogeneous surface layer. Fig. 11 illustrates normal incident light reflected at a surface coated with a graded index layer. The reflectance of a non-absorbing inhomogeneous thin film can be expressed as [207]

$$RP* = \frac{(n_1 n_3 P + n_2 n_2' Q)^2 + (n_1 n_2' T + n_2 n_3 S)^2}{(n_1 n_3 P - n_2 n_2' Q)^2 - (n_1 n_2' T - n_2 n_3 S)^2}$$

(1)

where J, Y are Bessel functions, and

$$P = Y_0(\propto)J_0(\beta) - J_0(\propto)J_0(\beta),$$

$$Q = J_1(\propto)Y_1(\beta) - Y_1(\propto)J_1(\beta),$$

$$S = Y_1(\propto)J_0(\beta) - J_1(\propto)Y_0(\beta),$$

$$T = Y_0(\propto)J_1(\beta) - J_0(\propto)Y_1(\beta),$$

$$\propto = \frac{2\pi n_2}{\ln(\frac{n_2'}{n_2})}\frac{d}{\lambda}, \quad \beta = \frac{2\pi n_2'}{\ln(\frac{n_2'}{n_2})}\frac{d}{\lambda}$$

(2)

The characteristic of this type of AR coating is optical neutrality. It was found that

different index profiles, such as simple linear, exponential and quadratic on a halfwave thick inhomogeneous layer did not affect the residual reflectance of the coating dramatically. The calculation was done by modeling the inhomogeneous layer as a multilayer system composed of many thin homogeneous layers that have index values matching different idealistic profiles, as mentioned above. If the layer is thicker than a halfwave then the reflectance is simply that associated with the outermost index.

(2) interference-type multiple layer stack.

This type of AR structure utilizes of the light-matter interaction principles of thin film optics to produce destructive interference of the light reflected at the upper and the lower interfaces of the thin film/substrate system. The principle of this type of AR coating may be illustrated by using vector methods [206]. The basic assumptions of this method are

• No (or negligible) absorption in the layers.

• Only consider one reflection from each interface.

The amplitude of reflected light from the interface *mn*, between medium *m* and the subsequent medium *n*, may be represented by the amplitude reflection coefficient, R_{mn}, expressed as follows:

$$R_{mn} = (n_m - n_n)/(n_m + n_n) \tag{3}$$

where nm and n_n are the refractive index of medium m and n respectively.

The phase thickness of each layer is

$$\delta_n = \frac{2\pi n_n \cos\theta_n d_n}{\lambda}, \tag{4}$$

where Θ_n is the angle of refraction in each layer, d_n is the physical thickness of the layer and is λ the wavelength of light. This represents the phase change of the reflected light

19

after travel across layer n. The reflection of the light from interface mn may be expressed as vector

$$R_{mn} = R_{mn}exp^{-2(\delta_m+\delta_n)} \tag{5}$$

In polar coordinates, we may express the reflected light from an interface as a vector. The length of the vector is the reflection amplitude R_{mn}, while the angle of the vector is indicated as $2\delta n$, due to the light wave passing across the layer twice, i.e. in and out each layer. The resultant reflection from a coating stack may be represented by the vector sum of reflection from each interface.

For a four-layer AR stack, as shown in Fig. 12, the reflection of light will occur at each interface of the coating system. Each reflection has specific amplitude and phase characteristics, as described in Eq. (5). In the case of a four-layer coating stack, the resultant reflection from all interfaces in the system may be expressed as the vector sum as follows

$$R_{sum} = R_{01} + R_{12} + R_{23} + R_{34} + R_{4s} \tag{6}$$

where

$$R_{01} = R_{01} = (n_0 - n_1)/(n_0 + n_1) \ ,$$

$$R_{12} = R_{12}exp^{-2(\delta_1)} = (n_1 - n_2)/(n_1 + n_2)exp^{-2(\delta_1)} \ ,$$

$$R_{23} = R_{23}exp^{-2(\delta_1+\delta_2)} = (n_2 - n_3)/(n_2 + n_3)exp^{-2(\delta_1+\delta_2)},$$

$$R_{34} = R_{34}exp^{-2(\delta_1+\delta_2+\delta_3)} = (n_3 - n_4)/(n_3 + n_4)exp^{-2(\delta_1+\delta_2+\delta_3)},$$

$$R_{4s} = R_{4s}exp^{-2(\delta_1+\delta_2+\delta_3+\delta_4)} = (n_4 - n_s)/(n_4 + n_s)exp^{-2(\delta_1+\delta_2+\delta_3+\delta_4)} \tag{7}$$

and the phase angle of each reflection is given in the following

$$\delta_1 = 2\pi n_1 cos\theta_1 d_1/\lambda$$

$$\delta_2 = 2\pi n_2 cos\theta_2 d_2/\lambda,$$

$$\delta_3 = 2\pi n_3 cos\theta_3 d_3/\lambda,$$

$$\delta_4 = 2\pi n_4 \cos\theta_4 d_4/\lambda, \tag{8}$$

To achieve anti-reflection effect for the multi-layer coating system, the R_{sum} should be minimized by adjusting the refractive index and film thickness of each layer. This interference-type AR coating stack may contain single layer or multiple layers, depending on the need of the optical performance. A single layer normally can only cover a very narrow bandwidth. Therefore, a V-shape reflection performance curve is the characteristic of the coating. In order to achieve broadband optical performance, a multi-layer stack is necessary. In this type of AR coating, the optical property is very sensitive to the optical constants and the coating thickness.

The angle-dependent reflectance performance of an interference-type AR coating is more pronounced than the inhomogeneous type AR. The shift of the reflectance band toward short wavelengths will cause a change in residual color to the observer. Therefore, a multi-layer AR stack is optimized to a specific viewing angle pertinent to the application.

1. 4 Purpose of the present study

In this study, the multilayers thin films consisted of inorganic nanoparticles and polyelectrolytes have been fabricated and the properties of prepared thin films were investigated. In addition by controlling the coating sequence, morphology, thickness, the applications for optical was researched.

Negatively charged titanium (IV) bis (ammonium lactato) dihydroxide (TALH) has been used to fabricate the TiO_2 thin films with positively charged polyelectrolytes because TALH is promising precursor of TiO_2 with anatase crystalline and high

21

refractive index in low temperature deposition. In Chapter 2, the effects of the pH and concentration of a solution, immersion time, number of rinsing times, and the addition of NaCl on the film thickness, morphology, surface roughness, and transmittance of fabricated thin films in order to increase film fabrication speed. In this chapter also present high-quality films with high-speed deposition that maintains the optical flatness of the TiO_2 thin film surface.

Introduction and principle of spray-LBL method was researched in Chapter 3.

Chapter 4 reports the important factor to control the surface morphology of polyelectrolyte multilayer thin film by spray-LBL method. Polyelectrolyte multilayer thin films by LBL have strongly been paid attention to the various applications. LBL technique is based on the alternate adsorption of oppositely charged materials in aqueous solutions via electrostatic attraction. However, it requires long fabrication time. And, this technique is also wasteful, limiting its practicality in manufacturing. Because the process is driven in part by diffusion, LBL cycles usually take on the order of several minutes to complete. This presents unacceptable demerits if this technology is to evolve into industrial applications. In this study, poly (allylamine hydrochloride) (PAH) and poly (acrylic acid) (PAA) for weak polyelectrolyte multilayer thin films by sequential spraying was employed. Using spray-LBL method, the nanoscale texture structure was fabricated by changing the condition such as concentration of spray solution, spray quantity, and flow rate of spray solution. It was found that the formation of nanoscale texture structure was dependent on all the three factors. It was clearly demonstrated that we can control nanoscale texture structure and thickness of (PAH/PAA) thin film by spray-LBL.

Chapter 5, Fabrication of thin film by conventional LBL method requires long

fabrication time. Because the process is driven in part by diffusion, LBL cycles usually take on the order of several minutes to complete. The recently developed practice of spraying solutions onto a substrate in order to fabricate thin film via LBL method has been further investigated and extended.

Double-layer anti-reflectance film consisted of low refractive index layer and high refractive index layer have been researched to increase the efficiency of AR range than the single block anti-reflectance film. In particular, for AR films, the uniformity of the film and the precise control of film thickness and refractive index are essential. The AR film by depositing a low refractive index layer consisting of $(PAH/PAA)_7$ and a high refractive index layer composed of $(PDDA/TALH)_{10}$ by spray-LBL method while controlling the thickness and roughness of the thin film. This AR thin film showed the maximum transmittance (94.5 %) and the minimum reflection (0.5 %) around 550 nm in wavelength. Moreover, deposition speed was able to be increase more than 10 times compare with conventional LBL method, with keeping the optical characteristics of the films.
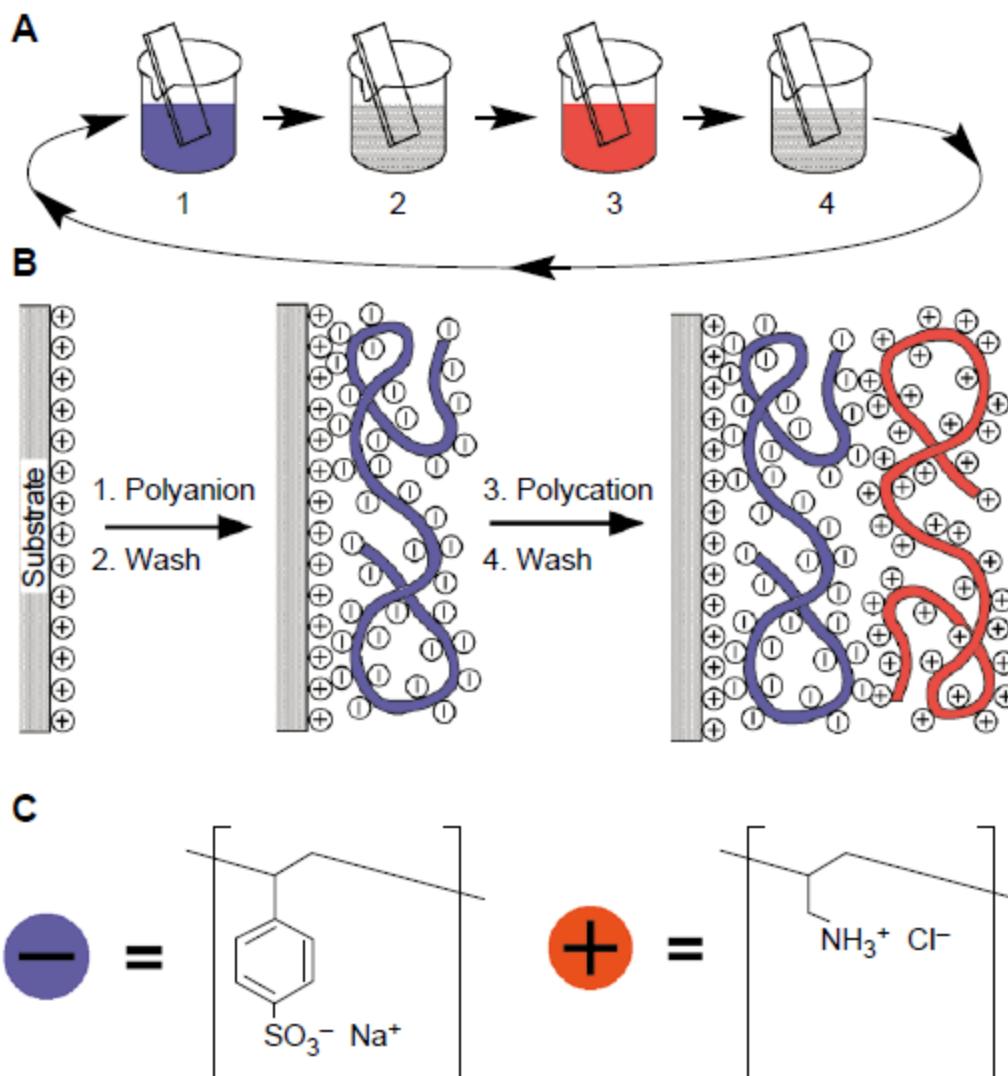
Fig. 1. (A) Schematic of the film deposition process using slides and beakers. Steps 1 and 3 represent the adsorption of a polyanion and polycation, respectively, and steps 2 and 4 are washing steps. (B) Simplified molecular picture of the first two adsorption steps, depicting film deposition starting with a positively charged substrate. (C) Chemical structures of two typical polyions, the sodium salt of poly(styrene sulfonate, PSS) and poly(allylamine hydrochloride, PAH). This Figure is adapted from [21].

Table 1 Characterization of fabricated thin film by dry and wet process.

	Dry process (Sputtering, Vacuum evaporation)	Wet process (spray, gravure coating)
Film performance	High	Low
Cost	High	Low
Materials	Low	High
Line speed	Low	High

Fig. 2. Formation of two bilayers of ionic polymers via LBL assembly technique
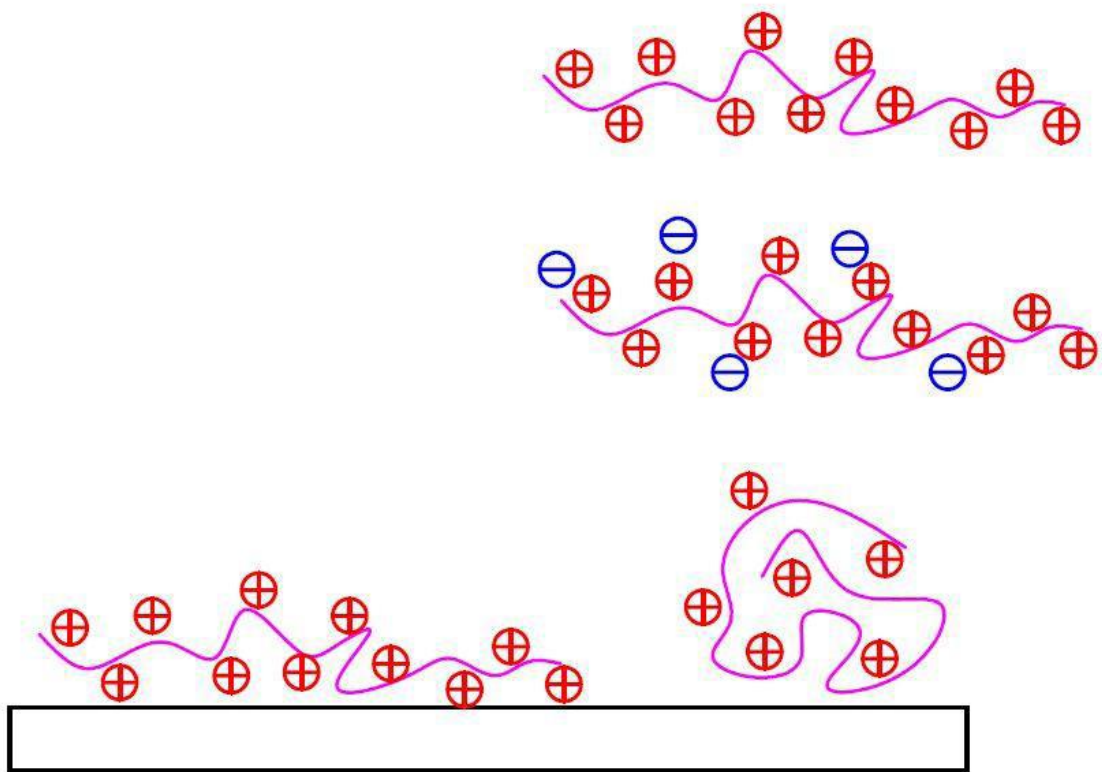
Fig. 3. Schematic of globular conformation of a polymer chain with low charge density (right) is shown in comparison with a polymer chain with high charge density (left). Polymer chains with lower charge density form globular conformations and so thicker layers.
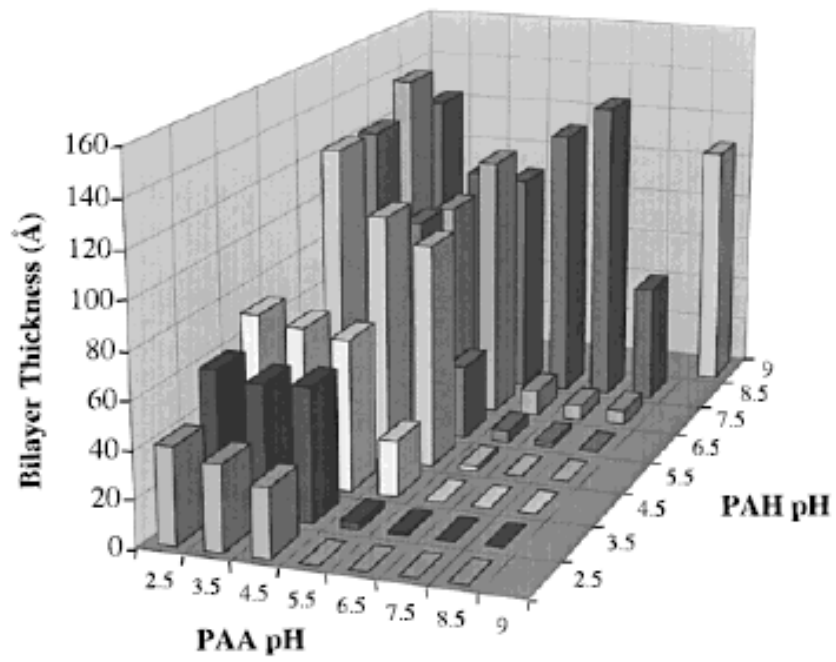
Fig. 4. Complete pH matrix showing the average incremental thickness contributed by a

PAH/PAA bilayer as a function of dipping solution pH. Figure is adapted from [189].
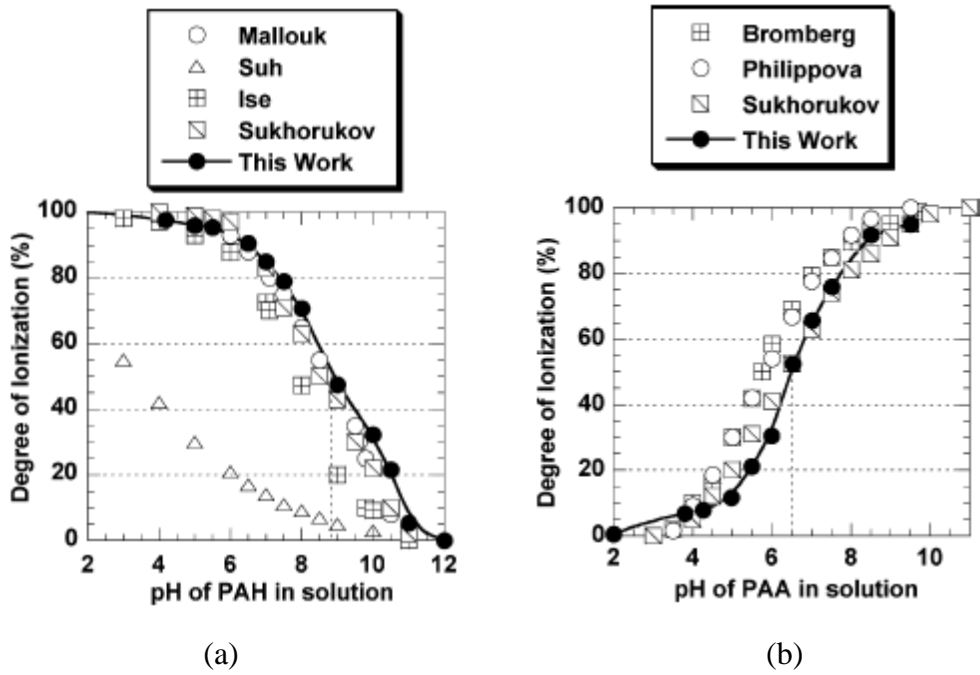
Fig. 5. Estimated degree of ionization of (a) PAH and (b) PAA in solution s a function of pH. Figure is adapted from [190].
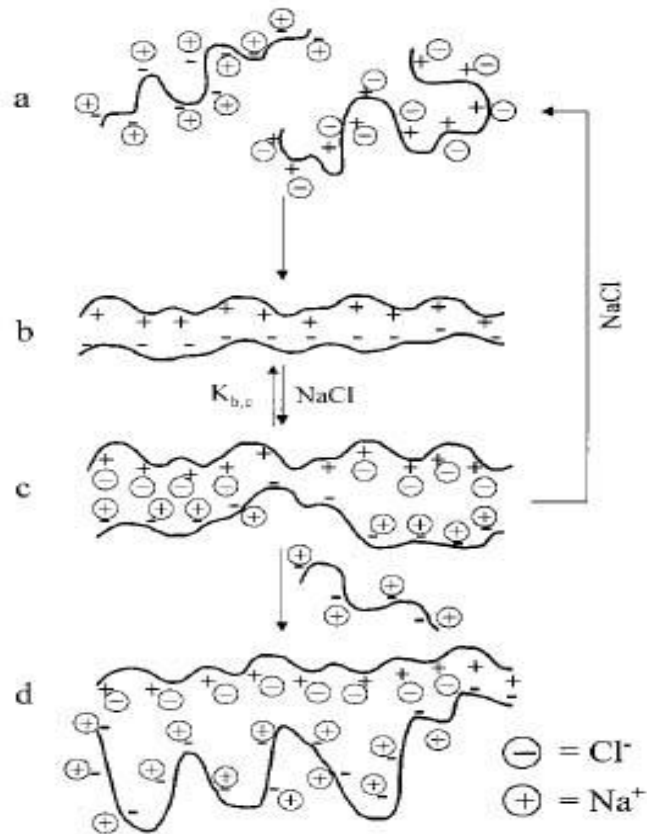
Fig. 6. Various stages during the formation, swelling, and decomposition of polyelectrolyte multilayer. Figure is adapted from [191].
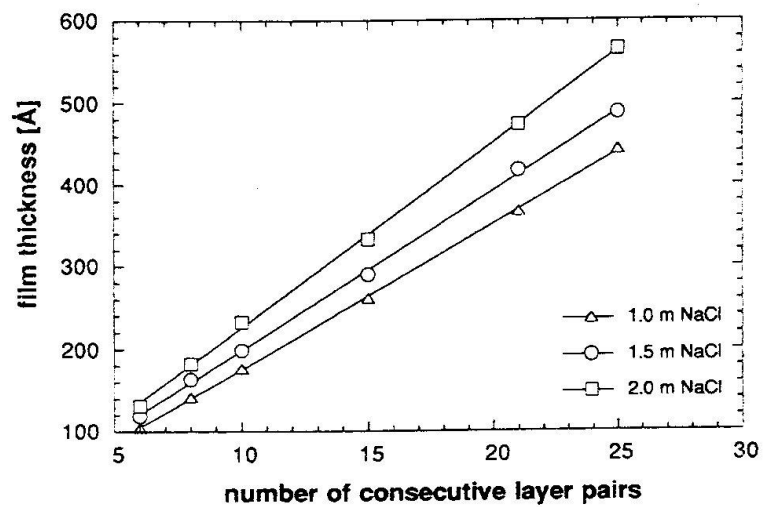
Fig. 7. Dependence of the film thickness on the number of layers for different concentration of NaCl in poly (styrenesulfonate sodium salt, PSS) solution. Figure is adapted from [192].
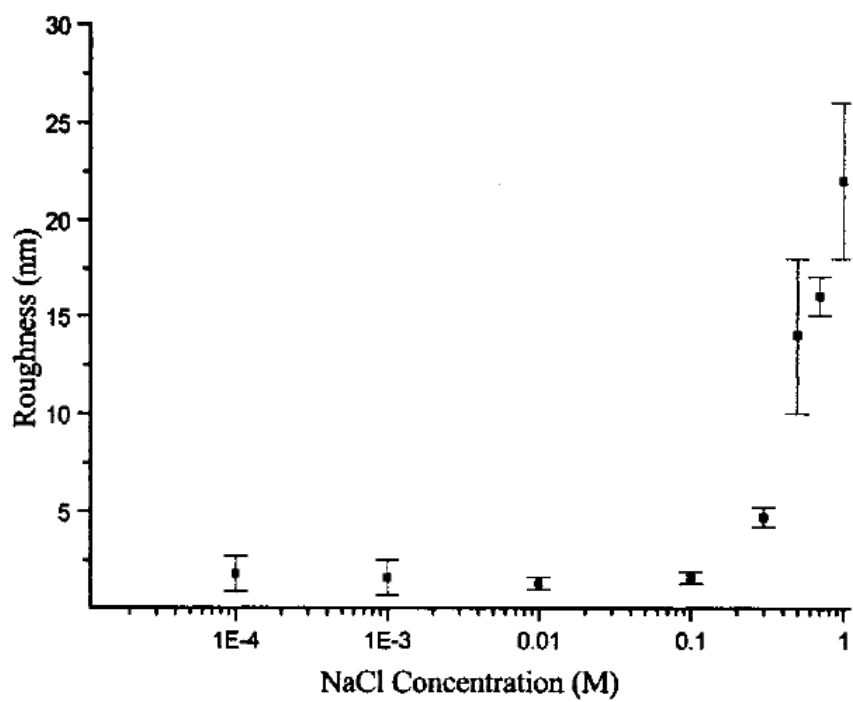
Fig. 8. The surface roughness of 10 bilayers thin film of PDDA/PSS as a function of the concentration of NaCl. Figure is adapted from [198].

<center>(a)</center>

<center>(b)</center>
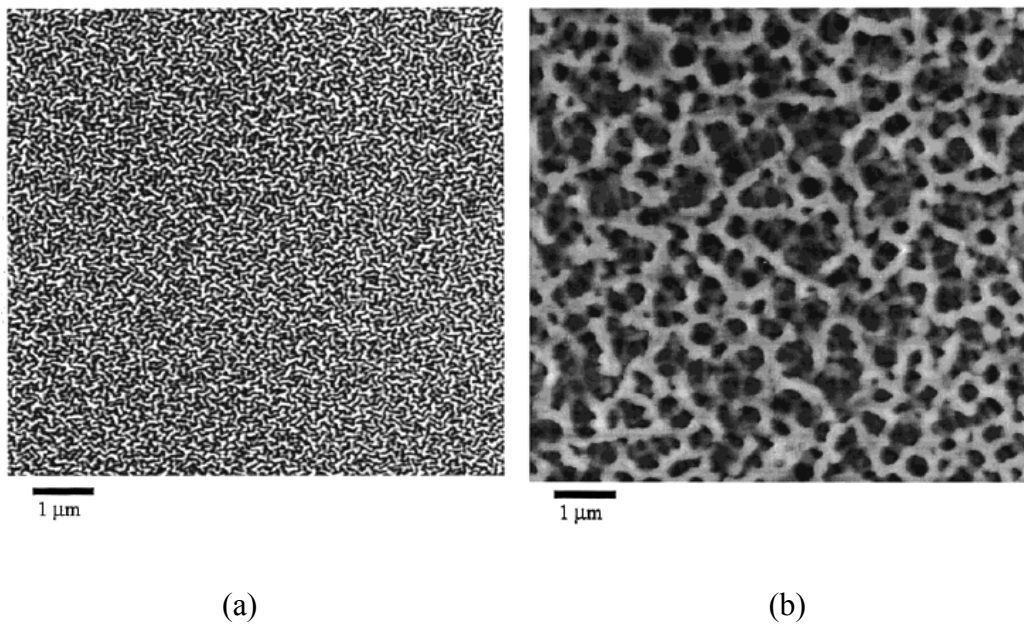
Fig. 9. AFM images of PAH 7.5/PAA3.5 multilayers thin film before (a) and after (b) immersion in acidic water (pH 2.5). Figure is adapted from [199].

100 nm
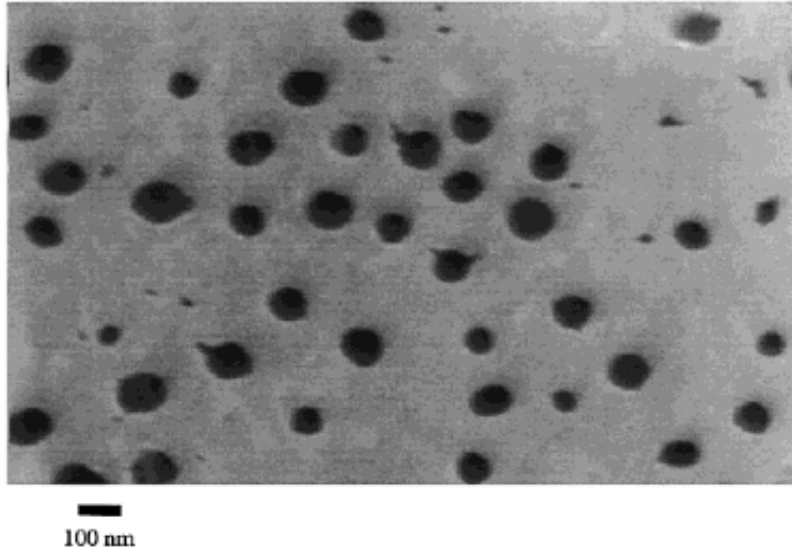
Fig. 10. SEM image of microporous PAH7.5/PAA3.5 multilayers thin film immersed

into acidic water and neutral water for 10 h. Figure is adapted from [199].
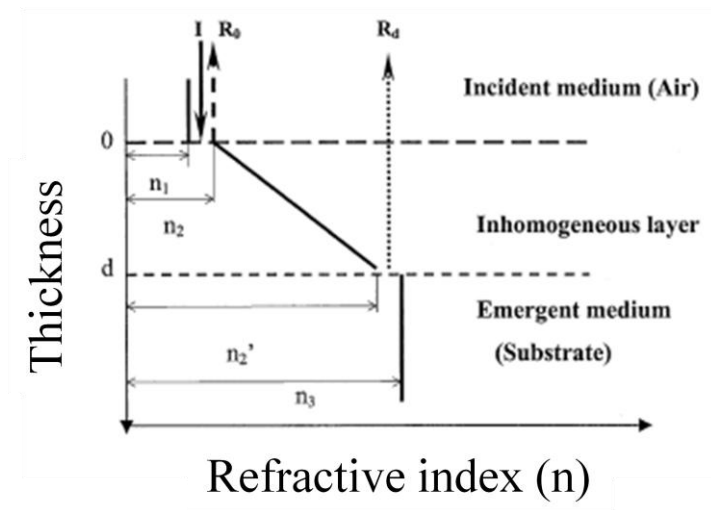
Fig. 11. The representation of a layer exhibiting linear inhomogeneity and small refractive index steps at layer boundaries. Figure is adapted from [207].

$R_{01} = R_{01}$

$R_{12} = R_{12} \exp^{-2(\delta 1)}$

$R_{23} = R_{23} \exp^{-2(\delta 1 + \delta 2)}$

$R_{34} = R_{34} \exp^{-2(\delta 1 + \delta 2 + \delta 3)}$

$R_{4s} = R_{4s} \exp^{-2(\delta 1 + \delta 2 + \delta 3 + \delta 4)}$

Incident medium

n_1 d_1

n_2 d_2 Thin film

n_3 d_3

n_4 d_4

n_s Transmission

Substrate
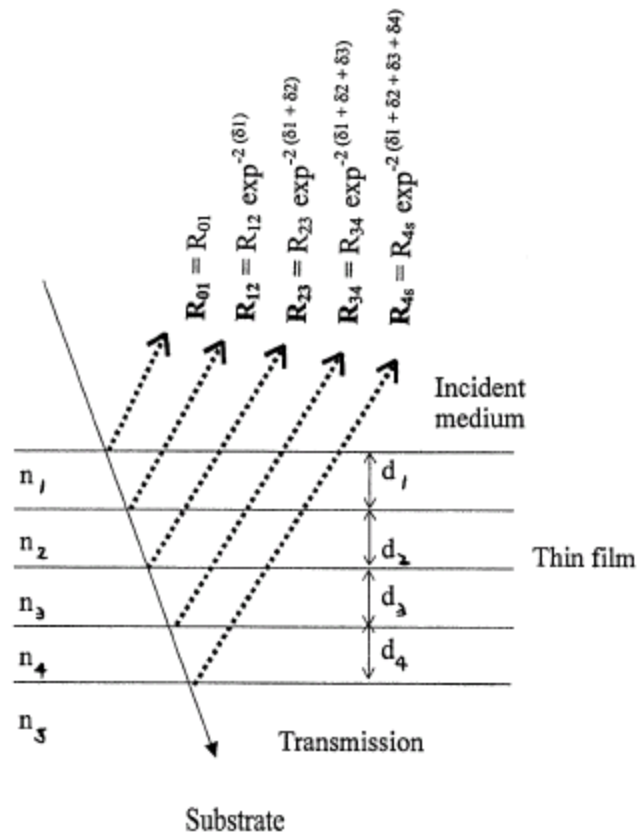
Fig. 11. The reflection from a coating stack is the resultant vector summation of the reflection from each interface in the system. This is an example of a four-layer coating stack. Figure is adapted from [207].

References

[1-1] H. Usui, Thin Solid Films, 365 (2000) 22.

[1-2] M. Tamada, H. Koshikawa, T. Suwa, T. Yoshioka, H. Sui, H. Sato, Polymer 41 (2000) 5661.

[1-3] M. S. Johal, Y. W. Cao, X. D. Chai, L. B. Smilowitz, J. M. Robinson, T. J. Li, D. McBranch, D. Q. Li, Chem. Mater. 11 (1999) 1962.

[1-4] H. Kuhn, D. Möbius, Angew. Chem. 83 (1971) 672.

[1-5] O. Inacker, H. Kuhn, D. Möbius, Chem, Neue Folge 101 (1976) 337.

[1-6] L. Netzer, J. Sagiv, J. Am. Chem. Soc. 105 (1983) 674.

[1-7] A. Ulman, Academic Press, New York, 1991.

[1-8] N. Tillman, A. Ulman, T. L. Penner, Langmuir 5 (1989) 101.

[1-9] R. Maoz, J. Sagiv, Langmuir 3, (1987) 1045.

[1-10] S. D. Evans, E. Urankar, A. Ulman, N. Ferris, J. Am. Chem. Soc. 113 (1991) 4121.

[1-11] Y. Xia, J. A. Rogers, K. E. Paul, G. M. Whitesides, Chem. Rev. 99 (1999) 1823.

[1-12] G. Decher, J. D. Hong, Germ. Pat. DE 402 (1990) 6978.

[1-13] G. Decher, J. D. Hong, Macromol. Chem., Macro. Symp. 46 (1991) 321.

[1-14] G. Decher, J. D. Hong, J. Schmitt, Thin Solid Films, 210-211 (1992) 831.

[1-15] G. Decher, J. Schmitt, Progr. Collid Polym. Sci. 89 (1992) 160.

[1-16] G. Decher, J. D. Hong, US Pat. US 520 (1993) 8111.

[1-17] G. Decher, J. Schmitt, H. U. Siegmund, L. Heiliger, Cerm. Pat. DE 433 (1993) 3107.

[1-18] J. Schmitt, T. Grünewakd, G. Decher, P. Pershan, K. Kjaer, M. Lösche,

Macromolecules 26 (1993) 7058.

[1-19] G. Decher, J. D. Hong, Eur. Pat. EP 472 990 B1, 1995.

[1-20] R. K. Iler, J. Colloid Interface. Sci. 21 (1966) 569.

[1-21] G. Decher, Science 277 (1997) 1233.

[1-22] G. Decher, J. D. Hong, Ber. Bunsen-Ges. Phys. Chem. 95 (1991) 1430.

[1-23] G. Mao, Y. Tsao, M. Tirrell, H. T. Davis, V. Hessel, H. Ringsdorf, Langmuir 9 (1993) 3461.

[1-24] T. M. Cooper, A. L. Campbell, R. L. Crane, Langmuir 11 (1995) 2713.

[1-25] F. Saremi, B. Tieke, Adv. Mater. 7 (1995) 378.

[1-26] K. Aremi, M. J. Wagner, M. S. Wrighton, Langmuir 12 (1996) 5393.

[1-27] B. Sellergren, A. Swietlow, T. Arnebrandt, K. Unger, Anal. Chem. 68 (1996) 402.

[1-28] K. Ariga, Y. Lvov, T. Kunitake, J. Am. Chem. Soc. 119 (1997) 2224.

[1-29] F. Auer, D. W. Schubert, M. Stamm, T. Arnebrandt, A. Swietlow, M. Zizlsperger, B. Sellergren, Chem. Eur. J. 5 (1999) 1150.

[1-30] L. Cheng, L. Niu, J. Gong, S. J. Dong, Chem. Mater. 11 (1999) 1465.

[1-31] L. Cheng. S. J. Dong, Electrochem. Soc. 147 (2000) 606.

[1-32] H. Jiang, W. Su, J. Hazel, J. T. Grant, V. V. Tsukruk, T. M. Cooper, Thin Solid Films 372 (2000) 85.

[1-33] B. Zou, L. Y. Wang, T. Wu, X. Y. Zhao, L. X. Wu, X. Zhang, S. Gao, M. Gleiche, L. F. Chi, H. Fuchs, Langmuir 17 (2001) 3682.

[1-34] Y. Lvov, G. Decher, H. Höhwald, Langmuir 9 (1993) 481.

[1-35] Y. Lvov, H. Haas, G. Decher, H. Höhwald, A. Kalachev, J. Phys. Chem. 97 (1993) 12835.

[1-36] M. Ferreira, J. H. Cheung, M. F. Rubner, Thin Solid Films 244 (1994) 806.

[1-37] R. Pommersheim, J. Schrenzenmeir, W. Vogt, Macromol. Chem. Phys. 195 (1994) 1557.

[1-38] S. Watanabe, S. L. Regen, J. Am. Chem. Soc. 116 (1994) 8855.

[1-39] M. Ferreira, M. F. Rubner, Macromolecules 28 (1995) 7107.

[1-40] A. C. Fou, M. F. Rubner, Macromolecules 28 (1995) 7115.

[1-41] G. J. Kellog, A. M. Mayes, W. B. Stockton, M. Ferreira, M. F. Rubner, Langmuir 12 (1996) 5109.

[1-42] A. Laschewsky, B. Mayer, E. Wischerhoff, X. Arys, P. Bertrand, A. Delcorte, A. Jonas, Thin Solid Films 284/285 (1996) 334.

[1-43] R. Advincula, E. Aust, W. Meyer, W. Knoll, Langmuir 12 (1996) 3536.

[1-44] B. Lehr, M. Seufert, G. Wenz, G. Decher, Supramol. Sci. 2 (1996) 199.

[1-45] J. B. Schlenoff, M. Li, Ber. Bunsen-Ges. Phys. Chem. 100 (1996) 943.

[1-46] R. Kayushina, Y. Lvov, N. Stepina, V. Belyaev, Y. Khurgin, Thin Solid Films 284/285 (1996) 246.

[1-47] C. Sun, X. Zhang, C. Sun, B. Shen, Macromol. Chem. Phys. 197 (1996) 147.

[1-48] T. Cassier, K. Lowack, G. Decher, Supramol. Sci. 5 (1998) 309.

[1-49] J. Lang, M. H. Lin, J. Phys. Chem. B 103 (1999) 11393.

[1-50] S. A. Sukhishvili, S. Granick, J. Chem. Phys. 110 (1999) 10153.

[1-51] E. J. Calvo, F. Battagjini, C. Danilowicz, A. Wolosiuk, M. Otero, Faraday Discuss. 116 (2000) 47.

[1-52] E. S. Forzani, V. M. Solis, E. J. Calvo, Anal. Chem. 72 (2000) 5300.

[1-53] Z. Q. Lu, Y. Lvov, I. Jansson, J. B. Schenkman, J. F. Rusling, J. Colloid Interface Sci. 224 (2000) 162.

[1-54] Y. Lvov, B. Munge, O. Giraldo, I. Ichinose, S. L. Suib, J. F. Rusling, Langmuir

16 (2000) 8850.

[1-55] M. K. Ram, M. Adami, S. Paddeu, C. Nicolini, Nanotechnology 11 (2000) 112.

[1-56] W. Tachaboonyakiat, T. Serizawa, T. Endo, M. Akashi, Polym. J. 32 (2000) 481.

[1-57] G. Ladam, P. Schaaf, F. J. G. Cuisinier, G. Decher, J. C. Voegel, Langmuir 17 (2001) 878.

[1-58] M. Muller, T. Rieser, P. L. Dubin, K. Lunkwitz, Macromol. Rapid Commun. 22 (2001) 390.

[1-59] C. Picart, P. Lavalle, P. Hubert, F. J. G. Cuisinier, G. Decher, P. Schaaf, J. C. Voegel, Langmuir 17 (2001) 7414.

[1-60] L. W. Wang, N. F. Hu, Bioelectrochemistry 53 (2001) 205.

[1-61] S. W. Keller H. N. Kim, T. E. Mallouk, J. Am. Chem. Soc. 116 (1994) 8817.

[1-62] E. R. Kleinfeld, G. S. Ferguson, Science 265 (1994) 370.

[1-63] M. Gao, X. Zhang, Y. Yang, B. Yand, J. Shen, J. Chem. Soc. Chem. Commun. (1994) 2777.

[1-64] G. S. Ferguson, E. R. Kleinfeld, Adv. Mater. 7 (1995) 414.

[1-65] E. R. Kleinfeld, G. S. Ferfuson, Chem. Mater. 7 (1995) 2327.

[1-66] D. L. Feldheim, K. C. Grabar, M. J. Natan, T. E. Mallouk, J. Am. Chem. Soc. 118 (1996) 7640.

[1-67] D. M. Kaschak, T. E. Mallouk, J. Am. Chem. Soc. 118 (1996) 4222.

[1-68] Y. Lvov, K. Ariga, I. Ichinose, T. kunitake, Langmuir 12 (1996) 3038.

[1-69] M. Gao, B. Richter, S. Kirstein, Adv. Mater. 9 (1997) 802.

[1-70] V. N. Bliznyuk, A. Campbeli, V. V. Tsukruk, ACS Symp. Ser. 695 (1998) 220.

[1-71] N. A. Kotov, T. Haraszti, L. Turi, G. Zavala, R. E. Geer, I. Dékány, J. H. Fendler, J. Am. Chem. Soc. 119 (1998) 6821.

[1-72] Y. M. Lvov, J. F. Rusling, D. L. Thomsen, F. Papadimitrakopoulos, T. Kawakami, T. Kunitake, Chem. Commun. (1998) 1229.

[1-73] L. C. Boudreau, J. A. Kuck, M. Tsapatsis, J. Membr. Sci. 152 (1999) 41.

[1-74] J. A. He, K. Yang, J. Kumar, S. K. Tripathy, L. A. Samuelson, T. Oshikiri, H. Katagi, H. Kasai, S. Okada, H. Oikawa, J. Phys. Chem. B 103 (1999) 11050.

[1-75] A. Gole, S. R. Sainkar, M. Sastry, Chem. Mater. 12 (2000) 1234.

[1-76] E. C. Hao, T. Q. Lian, Chem. Mater. 12 (2000) 3392.

[1-77] D. W. Kim, A. Blumstein, J. Kumar, S. K. Tripathy, Chem. Mater. 13 (2001) 243.

[1-78] N. I. Kovtyukhova, E. V. Buzaneva, C. C. Waraksa, T. E. Mallouk, Mater. Sci. Eng. B 69 (2000) 411.

[1-79] A. Kumar, A. B. Mandale, M. Sastry, Langmuir 16 (2000) 6921.

[1-80] Y. Lvov, R. R. Price, J. V. Selinger, A. Singh, M. S. Spector, J. M. Schnur, Langmuir 16 (2000) 5932.

[1-81] A. Mamedov. J. Ostrander, F. Aliev, N. A. Kotov, Langmuir 16 (2000) 3941.

[1-82] M. D. Musick, C. D. Keating, L. A. Lyon, S. L. Botsko, D. J. Pena, W. D. Holliway, T. M. Mcevoy, J. N. Richardson, M. J. Natan, Chem. Mater. 12 (2000) 2869.

[1-83] T. Sasaki, Y. Ebina, M. Watanabe, G. Decher, Chem. Commun. (2000) 2163.

[1-84] R. A. Caruso, A. Susha, F. Crauso, Chem. Mater. 13 (2001) 400.

[1-85] H. Hattori, Thin Solid Films 385 (2001) 302.

[1-86] J. W. Ostrander, A. A. Mamedov, N. A. Kotov, J. Am. Chem. Soc. 123 (2001) 1101.

[1-87] M. Sastry, A. Kumar, S. Datar, C. V. Dharmadhikari, K. N. Ganesh, Appl. Phys. Lett. 78 (2001) 2943.

[1-88] J. Y. Tseng, M. H. Lin, L. K. Chan, Colloids Surf. A 182 (2001) 239.

[1-89] M. T. Wang, L. D. Zhang, J. Mater. Res. 16 (2001) 765.

[1-90] T. Farhat, J. Schlenoff, Electrochem. Solid State Lett. 5 (2002) B13.

[1-91] H. Hattori, Adv. Mater. 13 (2001) 51.

[1-92] P. A. Ngankam. P. Lavalle, J. C. Voegel, L. Szyk, G. Decher, P. Schaaf, F. J. G. Cuisinier, J. Am. Chem. Soc. 122 (2000) 8998.

[1-93] L. Q. Zhang, A. K. Dutta, G. Jarero, P. Stroeve, Langmuir 16 (2000) 7095.

[1-94] M. Muller, T. Rieser, K. Lunkwitz, J. Meierhaack, Macromol. Rapid Commun. 20 (1999) 607.

[1-95] T. Rieser, K. Lunkwitz, S. Berwald, J. Meierhaack, M. Muller, F. Cassel, Z. Dioszeghy, F. Simon, ACS Symp. Ser. 744 (2000) 189.

[1-96] D. L. Elbert, C. B. Herbert, J. A. Hubbell, Langmuir 15 (1998) 5355.

[1-97] J. J. Hwang, K. Jaeger, J. Hancock, S. I. Stupp, J. Biomed. Mater. Res. 47 (1999) 504.

[1-98] F. Caruso, K. Niikura, D. N. Furlong, Y. Okahata, Langmuir 13 (1997) 3427.

[1-99] T. Chen, K. A. Friedman, I. Lei, A. Heller, Anal. Chem. 72 (2000) 3757.

[1-100] T. Hoshi, H. Saiki, S. Kuwazawa, Y. Kobayashi, J. Anzai, Anal. Sci. 16 (2000) 1009.

[1-101] S. H. Lee, J. Kumar, Langmuir 16 (2000) 10482.

[1-102] A. Narvaez, G. Suarez, I. C. Popescu, I. Katakis, E. Dominguez, Biosens. Bioelectron. 15 (2000) 43.

[1-103] H. C. Yoon, H. S. Kim, Anal. Chem. 72 (2000) 922.

[1-104] K. Sirkar, A. Revzin, M. V. Pishko, Anal. Chem. 72 (2000) 2930.

[1-105] J. H. Dai, A. W. Jensen, D. K. Mohanty, J. Erndt, Langmuir 17 (2001) 931.

[1-106] C. Pearson, J. Nagel, M. C. Petty, J. Phys. D, Appl. Phys. 34 (2001) 285.

[1-107] M. Onda, Y. Lvov, K. Ariga, T. Kunutake, Biotechnol. Bioeng. 51 (1996) 163.

[1-108] S. Mecking, R. Thomann, Adv. Mater. 12 (2000) 953.

[1-109] M. Ferreira, M. F. Rubner, B. R. Hsieh, Mater. Res. Soc. Symp. Proc 328 (1994) 119.

[1-110] H. Hong, D. Davidov, Y. Avny, H. Cahyet, E. Z. Faraggi, R. Neumann, Adv. Mater. 7 (1995) 846.

[1-111] J. Tian, C. C. Wu, M. E. Thompson, J. C. Sturm, R. A. Register, M. J. Marsella, T. M. Swager, Adv. Mater. 7 (1995) 395.

[1-112] Tian, C. C. Wu, M. E. Thompson, J. C. Sturm, R. A, Chem. Mater. 7 (1995) 2190.

[1-113] H. Hong, M. Tarabia, H. Chayet, S. Davidov, E. Z. Faraggi, Y. Avny, R. Neumann, S. Kirstein, J. Appl. Phys. 79 (1996) 3082.

[1-114] F. J. Arregui, Y. J. Liu, I. R. Matias, R. O. Claus, Sens. Actuators 59 (1999) 54.

[1-115] A. Wu, D. Yoo, J. K. Lee, M. F. Rubner, J. Am. Chem. Soc. 121 (1999) 4883.

[1-116] H. Mattoussi, M. F. Rubner, F. Zhou, J. Kumar, S. K. Tripathy, L. Y. Chiang, Appl. Phys. Lett. 77 (2000) 1540.

[1-117] T. Sonoda, T. Fujisawa, A. Fujii, K. Yoshino, Appl. Phys. Lett. 76 (2000) 3227.

[1-118] T. Piok, R. Schroeder, C. Brands, J. R. Heflin, G. Leising, W. Graupner, Synth. Met. 121 (2001) 1589.

[1-119] M. Eckle, G. Decher, Nanoletters, 1 (2001) 45.

[1-120] L. Krasemann, B. Tieke, Langmuir, 16 (2000) 287.

[1-121] J. J. Harris, M. L. Bruening, Langmuir, 16 (2000) 2006.

[1-122] J. Meierhaak, W. Lenk, D. Lehmann, K. Lunkwitz, J. Membr. Sci. 184 (2001) 233.

[1-123] B. Tieke, F. Vanackern, L. Krasemann, A. Toutianoush, Eur. Phys. J. E. 5 (2001) 29.

[1-124] T. R. Farhat, J. B. Schlenoff, Langmuir 17 (2001) 1184.

[1-125] S. Shiratori, T. Ito and T. Yamada, Colloid. Surf. A 198 (2002) 415.

[1-126] J. B. Schlenoff, S. T. Dubas, and T. Farhat, Langmuir 16 (2000) 9968.

[1-127] A. Izquierdo, S. Ono, J. C. Voegel, P. Schaaf, and G. Decher, Langmuir 21 (2005) 7558.

[1-128] K. Krogman, N. Zacharia, S. Schroeder, and P. Hammond, Langmuir 23 (2007) 3137.

[1-129] C. Lu, I. Dönch, M. Nolte, and A. Fery: Chem. Mater. 18 (2006) 6204.

[1-130] O. Félix, Z. Zheng, F. Cousin, and G. Decher, C. R. Chimie 12 (2009) 225.

[1-131] N. Laugel, J. Hemmerle, C. Porcel, J. C. Voegel, P. Schaaf, and V. Ball, Langmuir 23 (2007) 3706.

[1-132] S. S. Ono and G. Decher, Nano Lett. 6 (2006) 592.

[1-133] X. Zhao, C. Hinchliffe, C. Johnston, P. J. Dobson, S. Patrick, and P. S. Grant, Mater. Sci. and Eng. B 151 (2008) 140.

[1-134] C. H. Porcel, A. Izquierdo, V. Ball, G. Decher, J. C. Voegel, and P. Schaaf, Langmuir 21 (2005) 800.

[1-135] J. Cho, K. Char, J. D. Hong, and K. B. Lee, Adv. Mater. 13 (2001) 1076.

[1-136] C. Jiang, S. Markutsya, and V. V. Tsukruk, Adv. Mater. 16 (2004) 157.

[1-137] M. S. Johal, J. L. Casson, P. A. Chiarelli, D. G. Liu, J. A. Shaw, J. M. Robinson, and H. L. Wang, Langmuir 19 (2003) 8876.

[1-138] M. H. Merrill and C. T. Sun, Nanotechnology 20 (2009) 075606.

[1-139] C. Jiang, X. Wang, R. Gunawidjaja, Y. H. Lin, M. K. Gupta, D. L. Kaplan, R. R.

Naik, and V. V. Tsukruk, Adv. Funct. Mater. 17 (2007) 2229.

[1-140] B. S. Shim, P. Podsiadlo, D. G. Lilly, A. Agarwal, J. Lee, Z. Tang, S. Ho, P. Ingle, D. Psterson, W. Lu, and N. A. Kotov, Nano Lett. 7 (2007) 3266.

[1-141] コーティングのすべて」，加工技術研究会 編 (1999).

[1-142] 原崎勇次,「コーティング工学」，槙書店 (1978).

[1-143] 原崎勇次,「コーティング方式」，槙書店 (1979).

[1-144] R. Ota, S. Seki, M. Ogawa, T. Nishide, A. Shida, M. Ide and Y. Sawada, Thin Solid Films 411 (2002) 56.

[1-145] P. Chrysicopoulou, D. Davazoglou, Chr. Trapalis, and G. Kordas, Thin Solid Films 323 (1998) 188.

[1-146] K. Yonaiyama, H. Saito, M. Higuchi, T. Asaka, K. Katayama and Y. Azuma, J. Ceram. Soc. Jpn. 111 (2003) 413

[1-147] P. Stroeve, V. Vasquez, M. Coelho, J. Rabolt, Thin Solid Films 284 (1996) 708.

[1-148] V. Jain, H. Yochum, H. Wang, R. Montazami, M. A. V. Hurtado, A. Mendoza-Galvan, H. W. Gibson, J. R. Heflin, Macromolecular Chemistry and Physics 209(2) (2008) 150.

[1-149] V. Jain, R. Sahoo, J. R. Jinschek, R. Montazami, H. M. Yochum, F. L. Beyer, A. Kumar, J. R. Heflin, Chemical Communications 31 (2008) 3663.

[1-150] N. A. Kotov, I. Dekany, J. H. Fendler, The Journal of Physical Chemistry 99 (2002) 13065.

[1-151] N. Malikova, I. Pastoriza-Santos, M. Schierhorn, N. Kotov, L. Liz-Marzan, Langmuir 18 (2002) 3694.

[1-152] A. Mamedov, N. Kotov, Langmuir 16 (2000) 5530.

[1-153] J. Anzai, Y. Kobayashi, N. Nakamura, M. Nishimura, T. Hoshi, Langmuir 15 (1999) 221.

[1-154] R. Aroca, P. Goulet, D. Dos Santos, R. Alvarez-Puebla, O. Oliveira, Analytical chemistry(Washington, DC) 88 (2005) 378.

[1-155] F. Crespilho, F. Huguenin, V. Zucolotto, P. Olivi, F. Nart, O. Oliveira: Electrochemistry Communications 8 (2006) 348.

[1-156] S. Jaffar, K. Nam, A. Khademhosseini, J. Xing, R. Langer, A. Belcher: Nano Letters 4 (2004) 1421.

[1-157] C. Constantine, K. Gattas-Asfura, S. Mello, G. Crespo, V. Rastogi, T. Cheng, J. DeFrank, R. Leblanc, J. Phys. Chem. B 107 (2003) 13762.

[1-158] K. Sarathy, P. Thomas, G. Kulkarni, C. Rao: J. Phys. Chem. B 103 (1999) 399.

[1-159] J. Hong, K. Lowack, J. Schmidt, G. Decher: Progress in Colloid and Polymer Science 93 (1993) 98.

[1-160] T. Cassier, K. Lowack, G. Decher, Supramolecular Science 5 (1998) 309.

[1-161] J. Lang, M. Liu, J. Phys. Chem. B 103 (1999) 11393.

[1-162] L. Lu, S. Wang, X. Lin, Analytica Chimica Acta 519 (2004) 161.

[1-163] R. K. Iller, Journal of Colloid and Interface Science 21 (1966) 569.

[1-164] G. Decher, Macromol. Chem. Macromol. Symp 46 (1991) 231.

[1-165] G. Decher, M. Eckle, J. Schmitt, B. Struth, Current Opinion in Colloid & Interface Science 3 (1998) 32.

[1-166] G. Decher, Science 277 (1997) 1232.

[1-167] G Decher, J. D. Hong, J. Schmitt, Thin Solid Films 210 (1992) 831.

[1-168] W. B. Stockton, M. F. Rubner, Macromolecules 30 (1997) 2717.

[1-169] S. A. Sukhishvili, S. Granick, Journal of the American Chemical Society 122 (2000) 9550.

[1-170] J. L. Lutkenhaus, P. T. Hammond, Soft Matter 3 (2007) 804

[1-171] M. Rubner, Multilayer thin films: sequential assembly of nanocomposite materials 2003 133.

[1-172] S. Shiratori, M. Rubner, Macromolecules 33 (2000) 4213.

[1-173] Bungenberg, H. D. Jong, Colloid Science 2 (1949) 232.

[1-174] S. L. Clark, M. Montague, P. T. Hammond, Supramolecular Science 4 (1997) 141.

[1-175] S. Clark, M. Montague, P. T. Hammond, Polymeric Materials Science and Engineering 77 (1997) 620.

[1-176] Y. Lvov, G Decher, H. Moehwald, Langmuir 9 (1993) 481.

[1-177] A. Krozer, S. Nordin, B. Kasemo, Journal of Colloid and Interface Science 176 (1995) 479.

[1-178] A. Xie, S. Granick, Macromolecules 35 (2002) 1805.

[1-179] H. Van de Steeg, M. Cohen Stuart, A. De Keizer, B. Bijsterbosch, Lanmuir 8 (1992) 2538.

[1-180] B. C. Bonekamp, H. A. Vanderschee, J. Lyklema, Journal of Croatica Chemica Acta 56 (1983) 695.

[1-181] M. A. C. Stuart, H. Tamai, Langmuir 4 (1988) 1184.

[1-182] D. Yoo, S. Shiratori, M. Rubner, Macromolecules 31 (1998) 4309.

[1-183] S. S. Shiratori, M. F. Rubner, Macromolecules 33 (2000) 4213.

[1-184] S. Dubas, J. Schlenoff, Macromolecules 34 (2001) 3736.

[1-185] M. Bohmer, O. Evers, J. Scheutjens, Macromolecules 23 (1990) 2288.

[1-186] J. Blaakmeer, M. Bohmer, M. Stuart, G. Fleer, Macromolecules 23 (1990) 2301.

[1-187] M. Böhmer, Y. El Attar Sofi, A. Foissy, Journal of Colloid and Interface Science 164 (1994) 126.

[1-188] L. Dupont, A. Foissy: Colloids and Surfaces A, Physicochemical and Engineering Aspects 110 (1996) 235.

[1-189] S. S. Shiratori, M. F. Rubner, Macromolecules 33 (2000) 4213.

[1-190] J. Y. Choi and M. F. Rubner, Macromolecules 38 (2005) 116.

[1-191] T. D. Stephan, J. B. Schlenoff, Macromilecules, 34 (2001) 3736.

[1-192] G. Decher, J. Schmitt, Progr. Colloid Polym. Sci. 89 (1992) 160.

[1-193] J. B. Schlenoff, L. Hiep, L. Ming, J. Am. Chem. Soc. 120 (1998) 7626.

[1-194] T. R. Farhat, J. B. Schlenoff, Langmuir 17 (2001) 1184.

[1-195] O. J. Rojas, M. Ernstsson, R. D. Neuman, P. M. Claesson, Langmuir 18 (2002) 1640.

[1-196] D. K. Kim, S. W. Han, C. H. Kim, J. D. Hong, K. Kim, Thin Solid Films 350 (1999) 153.

[1-197] A. V. Dobrynin, A. Deshkovski, M. Rubinstein, Macromolecules, 34 (2001) 3421.

[1-198] R. A. McAloney, M. Sinyor, D. Vyaacheslav, M. C. Goh, Langmuir 17 (2001) 6655.

[1-199] J. D. Mendelsohn, C. J. Barrett, V. V. Chan, A. J. Pal, A. M. Mayes, M. F. Rubner, Langmuir 16 (2000) 5017.

[1-200] D.M. Dotzauer, J. Dai, L. Sun, M.L. Bruening, Nano Letters 6 (2006) 2268.

[1-201] M. Michel, Y. Arntz, G. Fleith, J. Toquant, Y. Haikel, J.C. Voegel, P. Schaaf, V. Ball, Langmuir 22 (2006) 2358.

[1-202] D.I. Gittins, F. Caruso, Advanced Materials 12 (2000) 1947.

[1-203] G. Schneider, G. Decher, Nano Letters 4 (2004) 1833.

[1-204] H. Shimomura, Z. Gemici, R. E. Cohen, and M. F. Rubner: Appl. Mater.

Interfaces 2 (2010) 813.

[1-205] S.F. Manaco, J. Opt. Soc. Am. 51 (1961) 280.

[1-206] H.A. Macleod, Thin-fllm Optical Filters, 2nd edition, McGraw-Hill, New york, 1989, p. 48.

[1-207] D. Chen Solar EnergyMaterials & Solar Cells 68 (2001) 313

CHAPTER 2

Investigation of TiO$_2$ thin film growth by layer-by-layer self assembly for application to optical devices

2. 1 Introduction

Over the past several decades, titanium oxide (TiO$_2$) has been widely used in various forms in various field applications. The TiO$_2$ thin film is a promising candidate for such varied applications owing to its high refractive index, high relative dielectric constant, remarkable solar energy conversion, and ability for photocatalysis [1-3]. Titanium(IV) bis(ammonium lactate) dihydroxide (TALH) is relatively stable at ambient temperature in neutral solutions [4-6], which makes it an ideal precursor for the fabrication of titania-based thin films from aqueous solutions [7-9].

There are many different techniques used for depositing TiO$_2$ films: sol-gel method [10], sputtering [11], chemical vapor deposition (CVD) [12], and other chemical deposition methods. In the sol-gel method, volatile solvents are used and film thickness control is difficult, because film quality is affected by humidity and temperature. Sputtering is carried out in vacuum. It entails high fabrication cost and requires expensive equipment. CVD requires vacuum equipment and high deposition energy. Other chemical depositions can be carried out at normal pressure; however, they use non- environmentally sound solutions such as TiF$_6$. All the methods discussed above have some environmental demerits in their fabrication processes.

On the other hand, layer-by-layer self-assembly (LBL-SA) is based on the alternate adsorption of oppositely charged materials in aqueous solutions via electrostatic

attraction [13, 14]. Thus, LBL-SA has many advantageous features as follows: process simplicity, water-based room-temperature deposition at normal pressures, lack of thickness limit, and no need for complex equipment [15-17]. In addition, the thickness of the film can be controlled up to nanoscale accuracy [18-20]. Although this method has many advantages, it requires a very long fabrication time. This presents unacceptable demerits if this technology is to be extended to industrial applications.

For the fabrication of practical devices using LBL-SA, a high-speed fabrication technique is highly required. In particular, for optical application, the uniformity of the film and the precise control of film thickness are essential.

The spray method is a very rapid technique for fabricating thin films. However, its uniformity on a wide area is not always sufficiently good for optical applications. Moreover, there are still numerous unknown factors affecting optical flatness and the force of adhesion to the substrate.

It is generally known that conditions of a solution (such as pH [21-25], concentration of solution, and salt content[26-28]) have strong effects on the amount of adsorption on thin films in LBL-SA. Therefore, the properties of thin films with polyelectrolyte and inorganic precursors are affected by a solution's conditions.

In this study, the effects of the pH and concentration of a solution, immersion time, number of rinsing times, and the addition of NaCl on the film thickness, morphology, surface roughness, and transmittance of fabricated thin films in order to increase film fabrication speed. In this chapter also present high-quality films with high-speed deposition that maintains the optical flatness of the TiO_2 thin film surface.

2. 2 Experimental Procedure

2.2.1 Materials

Poly(diallyl dimethyl ammonium chloride) (PDDA, 20 wt% in water) as a positively charged solution and titanium(IV) bis(ammonium lactate) dihydroxide (TALH, 50 wt%) as a negatively charged solution were obtained from Aldrich. Sodium silicate solution was obtained from Kanto Chemical. All materials were used without further purification. PDDA solution was used without pH adjustment. TALH solution was adjusted to pHs 2.5 to 6.3 by adding HCl. The concentrations of the PDDA solution prepared were from 10 to 100 mM, which were achieved by adding NaCl.

2.2.2 Preparation of thin films

The glass and silicon wafer substrates were ultrasonically agitated in KOH solution (1.0 wt%) mixed with ultrapure water and ethanol (2:3 in v/v) for 5 min and then rinsed with ultrapure water. By this treatment, negatively charged substrates were prepared.

The negatively charged substrates were immersed in cationic PDDA solution and then rinsed three times in pure water for 1 min each. The positively charged substrates produced by the deposition of PDDA were subsequently immersed in the negatively charged TALH solution and then the same rinsing procedure (three times for 1 min each) was carried out. This coating sequence was automatically repeated up to 10 bilayers without stopping using an automatic dipping machine. Hereafter, when we

deposit the material B over A, we describe the system as (A/B) and when we repeat this sequence 10 times, we describe it as $(A/B)_{10}$.

2.2.3 Characterization of thin films

Surface morphology was investigated by field-emission scanning electron microscopy (FE-SEM; Hitachi S-4700), and the root mean square (RMS) surface roughness of films was measured by atomic force microscopy (AFM; Digital Instrument Nanoscope IIIa) in the tapping mode. RMS roughness was calculated according to the following equation:

$$RMS = \sqrt{\frac{\sum(Z_i - Z_{ave})^2}{N}} \;;$$

(1)

where Z_i is the height on the Z-axis of the feature i, Z_{ave} is the average height of the entire image, and N is the number of points in an image.

The thickness of the prepared films was measured by ellipsometry (ULVAC ESM-1A) and a surface profile measurement system (Salon DEKTAK 3030). By profiling, the average value of five measurements was chosen to represent the thickness of the thin film. Surface profile measurement system data not shown here due to the film thickness is almost same, which is confirmed using ellipsomety and a surface profile measurement system. The transmittance and reflectance of the prepared thin films deposited on glass were measured using an ultraviolet-visible (UV-vis) spectrophotometer (Shimadzu UV mini-1240) and a reflectance meter (Olympus USPM-RM).

2. 3 Results and Discussion

The chemical structures of the starting materials are shown in Fig. 1. PDDA and TALH are positively and negatively charged in solution, respectively. The precipitation of TALH solution by the destabilization of the chelate proceeds when acid is added. At low pHs, the formation of intermediate complexes of titanium oxychloride is initiated. During the decomposition of optimized solutions of TALH, cationic complexes of titanium hydroxide [$Ti(OH)_4$] precursors change into TiO_2 precipitate phases. It is known that the amount of absorption is increased by the concentration of polyelectrolyte and the amount of salt added. The adsorption of polyelectrolyte onto an oppositely charged surface is an ion exchange phenomenon, where charged segments replace small salt ions to compensate for the surface charge.

The film fabrication conditions are shown in Table I, and the optical characteristics of the thin film are also shown in Fig. 2. As shown in the table and figure, the thickness of the (PDDA/TALH) thin film was increased from ca. 15 to ca. 42 nm (ca. 2.5-fold) by changing the pH of TALH solution from 6.3 to 2.5. Then, the thickness of the (PDDA/TALH) thin film was increased from ca. 15 to ca. 30 nm (ca. 2-fold) by increasing the concentration of PDDA from 10 to 100 mM. By adding NaCl (1.0 M) to PDDA solution, the thickness of the thin films was increased from 15 to ca. 25 nm (ca. 1.5-fold). Figure 2 represents the absorbance characteristics at 460 nm. Figures 3(a)-3(c) show that the absorbance increased with the increase in film thickness, which is caused by the deposition conditions mentioned above.

Figure 3 shows the FE-SEM images of the prepared thin film with the coating sequence of (PDDA/TALH)$_{10}$ as a function of the pH of TALH solution, the

54

concentration of PDDA solution, and the amount of NaCl added. As shown in this figure, clusters agglomerated and the average size of the clusters was affected by the pH of TALH solution, the concentration of PDDA solution, and the amount of NaCl added. TALH in aqueous solutions is hydrolyzed at low pHs to yield TiO_2 nanocrystals in pure anatase form. At low pHs, the destabilization of the chelate occurs by the protonation of lactate groups. It is possible to control the TiO_2 particle size of TALH solution by adjusting the pH of TALH solution. At lower pHs, the TiO_2 particles are larger. Therefore, the amount of absorption increases with decreasing pH of TALH solution [4]. Moreover, the amount of absorption increases with increasing concentration of PDDA solution because of the strong coulombic interactions at high concentrations. This is caused by the extrinsic charge compensation, that is, the increase in the number of loopy structures in the polyelectrolyte induced by the partial neutralization of positively charged PDDA. Therefore, the amount of absorption increases with increasing ionic strength up to a certain salt concentration.[26] The results showed that the thickness of the thin films was increased by approximately 2.5-, 2-, and 1.5-fold by changing the pH of TALH solution and the concentration of PDDA solution, and by adding NaCl to the solution, respectively.

Figures 4(a)-4(c) show the surface roughness of the (PDDA/TALH)$_{10}$ film measured by AFM as a function of the pH of TALH solution. The results of AFM are similar to the results of FE-SEM. The surface roughness of the (PDDA/TALH) thin films (a, b, and c) were ca. 1.5, 4.1, and 11.3 nm, respectively. These figures show that the surface roughness increased with the decrease in TALH solution pH. By comparing the previously mentioned Figs. 2(a) and 4(a)-4(c) we found that when film thickness was increased, surface roughness was also increased. This means that the error bars of the

film thickness shown in Fig. 2(a) correspond to the surface roughness shown in Figs. 4(a)-4(c). Next, by comparing Figs. 4(a) and 4(d), we found that film thickness and surface roughness increased with the increase in PDDA solution concentration. Finally, by comparing Figs. 4(a) and 4(e), it was shown that the surface roughness of the thin film was also increased by the NaCl addition to the PDDA solution. This was caused by the extrinsic charge compensation, that is, the increase in the number of loopy structures in the polyelectrolyte by the partial neutralization of positively charged PDDA. [26]

Table II shows the properties of the prepared thin film when we combine the best combination of all the factors that we obtained from the previous experiments: 100 mM PDDA with the addition of 0.5 M NaCl and pH 3.5 TALH solution. The thickness of the (PDDA/TALH) thin film was increased from ca. 15 to ca. 87 nm (ca. 6-fold) by changing the conditions of the solutions.

Figure 5 shows the FE-SEM and AFM images of the (PDDA/TALH)$_{10}$ thin film fabricated under the selected deposition conditions shown in Table II. As shown in these images, the surface roughness of the films was increased by the combination of the deposition conditions, and the size of the clusters was also increased. As shown in these figures, TiO$_2$ small crystals approximately 100 nm in diameter were observed on the surface, and surface roughness increased; however, the crystals had little effect on the optical characteristics of the films, as shown in Fig. 6. We consider that this point is very important for the fabrication of practical optical devices.

Figure 6(a) shows the transmittance and absorbance of the composed (PDDA/TALH)$_{10}$ thin film. It is found that absorbance from 400 to 800 nm had no effect on transmittance. We fabricated an AR thin film by depositing a low-refractive-index layer consisting of (PDDA/Na$_2$SiO$_3$)$_{40}$ and a high-refractive-index

56

layer composed of (PDDA/TALH)$_{10}$ by LBL-SA while controlling the thickness and roughness of the thin film. Figure 6(b) shows the reflectance and transmittance of the film. As shown in this figure, the highest transmittance in the visible range is 97% and the lowest reflectance of the film is 0.3%. Although the average surface roughness was slightly larger than 10 nm, the film could be applied in optical devices. From the industrialization point of view, a 6-fold increase in fabrication speed is very welcome. We consider that by suppressing surface roughness within approximately 10 nm, optical quality can be maintained even if deposition speed is markedly increased. We are now fabricating optical devices for practical applications.

2. 4 Conclusions

The thickness of the (PDDA/TALH) thin film was confirmed to increase by controlling the pH of TALH solution and the concentration of PDDA solution, and by adding NaCl.

Deposition conditions for satisfying the three parameters were chose: pH of TALH solution, concentration of PDDA solution, and amount of NaCl added. The thickness of the thin film increased approximately 6-fold from 15 to 87 nm using a combination of the deposition conditions. There are three reasons for the phenomenon: (1) hydrolysis of TALH solution induced by adjusting pH, (2) strong coulombic interactions at high concentrations of PDDA solution, and (3) electrostatic effect induced by the addition of NaCl. Therefore, the fabrication speed of thin film could be increased by controlling the deposition conditions. Moreover, deposition speed could be increased while maintaining optical quality (the highest transmittance in the visible range is 97% and the lowest

reflectance of the film is 0.3%) by suppressing the surface roughness within 10 nm. Although surface roughness increased to 10.7 nm, it was still sufficiently good for optical devices used in the visible range. The optimization of the fabrication conditions for thin films is very important for the production of optical devices such as antireflection and infrared reflective films using LBL-SA.

Table I. Properties of prepared (PDDA/TALH) thin film as function of deposition

conditions.

pH of (PDDA/ TALH)	Concentration of PDDA (mM)	Amount of NaCl added to PDDA (M)	Thickness (nm)	Surface roughness (nm)	Transmittance (400-800 nm) (%)
(5.5/6.3)	10	0	15	1.5	87-90
(5.5/5.5)	10	0	18	2.9	87-90
(5.5/4.5)	10	0	24	4.1	83-90
(5.5/3.5)	10	0	33	5.2	75-88
(5.5/2.5)	10	0	42	11.3	71-86
(5.5/6.3)	50	0	27	4.9	79-89
(5.5/6.3)	100	0	30	4.9	78-89
(5.5/6.3)	10	0.5	23	3.8	82-90
(5.5/6.3)	10	1.0	25	6.3	80-90

Table II. Properties of prepared (PDDA/TALH) thin film under combined condition.

pH of (PDDA/TALH)	Concentration of PDDA (mM)	Amount of NaCl added to PDDA (M)	Thickness (nm)	Surface roughness (nm)	Transmittance (400-800nm)
(5.5/6.3)	10	0	15	1.5	87-90
(5.5/3.5)	100	0.5	87	10.7	82-90
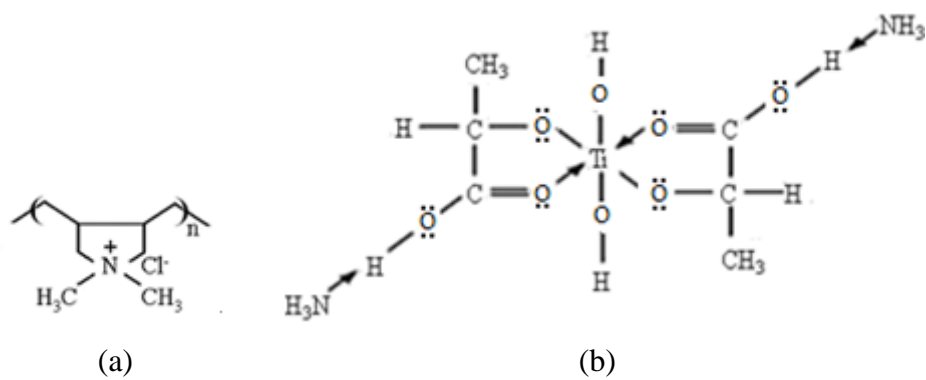
Fig. 1. Chemical structures of starting materials: (a) PDDA and (b) TALH.
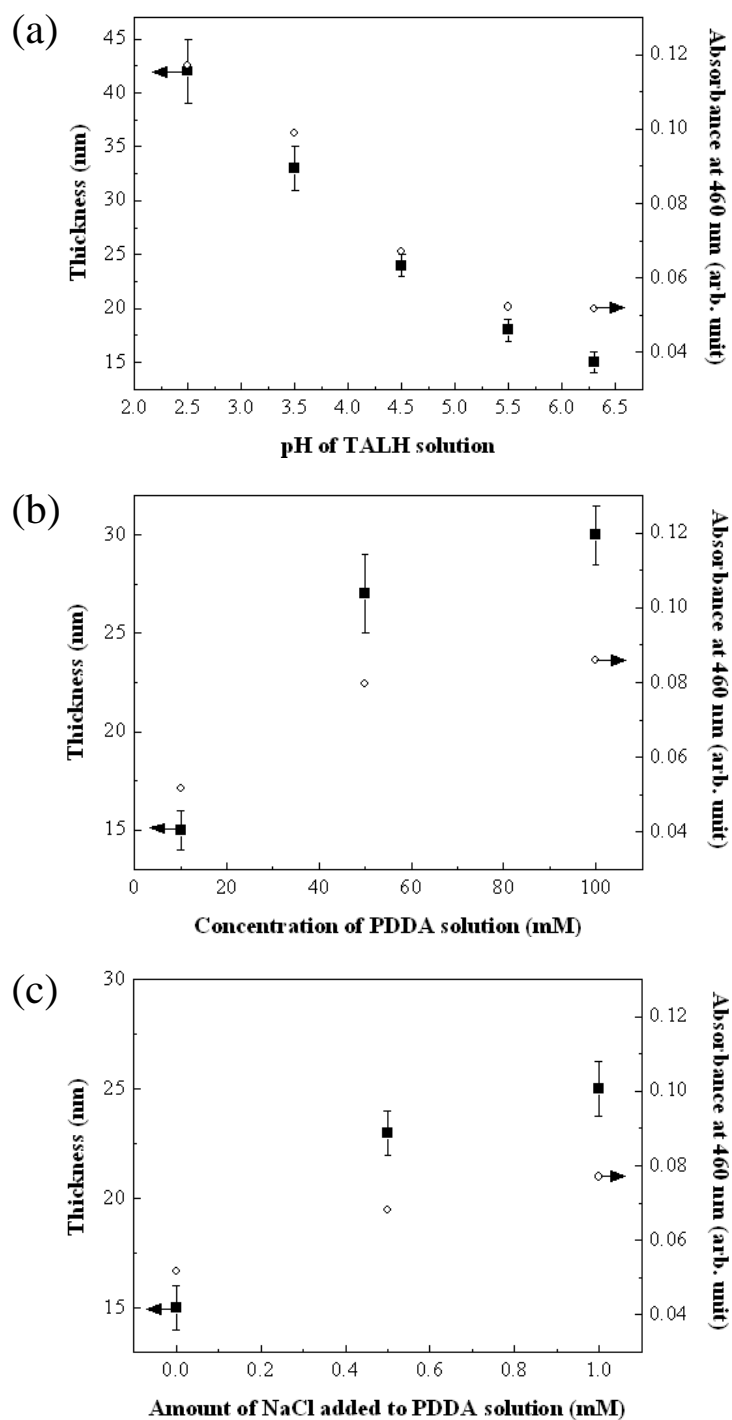
Fig. 2. Thickness and absorbance at 460 nm of (PDDA/TALH)$_{10}$ films as a function of (a) the pH of TALH solution, (b) the concentration of PDDA solution, and (c) the amount of NaCl added to PDDA solution.
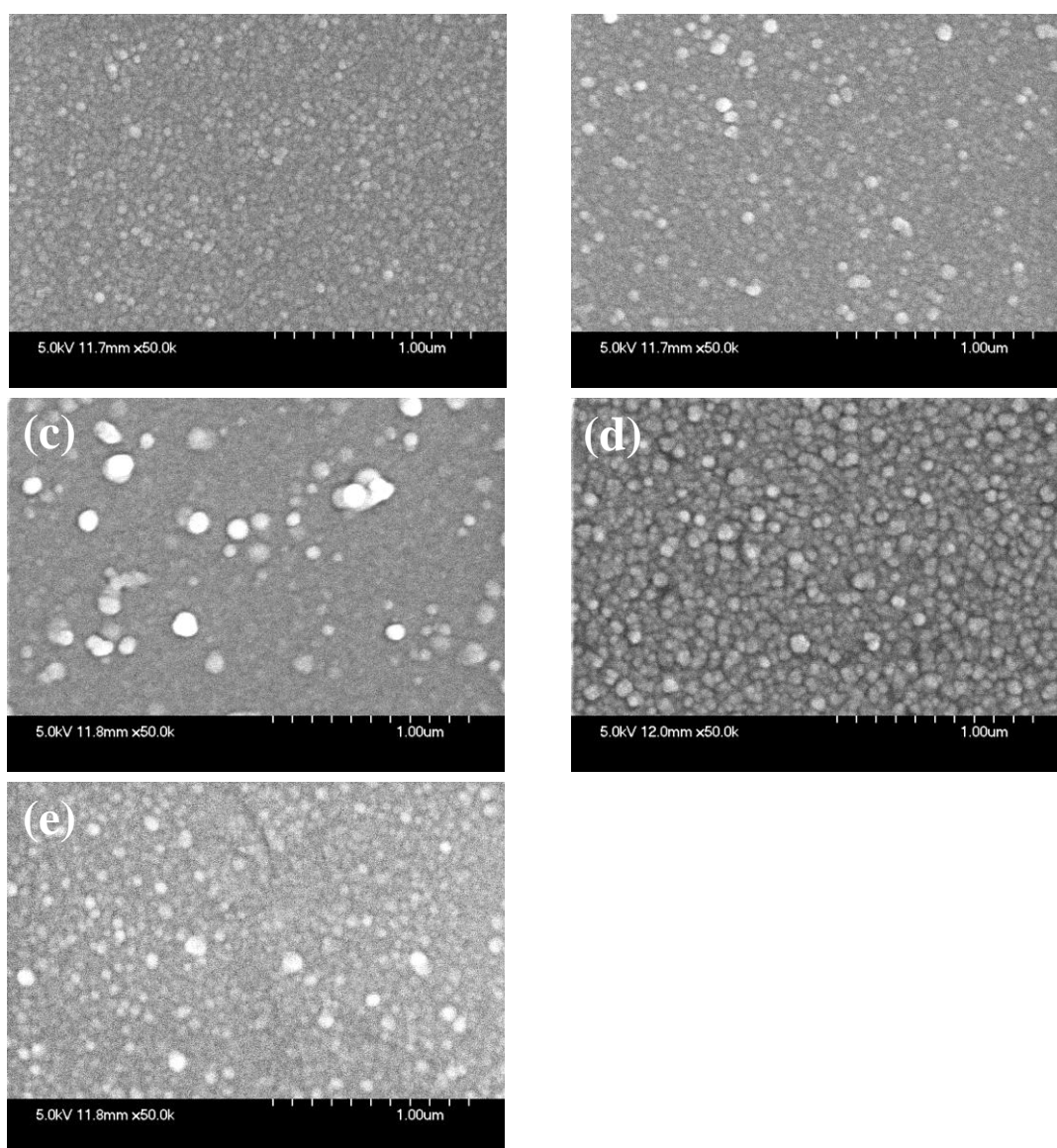
Fig. 3. FE-SEM images of (PDDA/TALH)$_{10}$ for comparing (1) (a), (b), and (c); (2) (a) and (d); and (3) (a) and (e). The fabrication conditions are as follows : (1) (a) pH 6.3 TALH solution, (b) pH 4.5 TALH solution, and (c) pH 2.5 TALH solution; the other conditions are the same. (2) (a) 10 mM PDDA solution and (d) 100 mM PDDA solution; the other conditions are the same. (3) (a) 0 mM NaCl added to PDDA. (e) 1.0 M NaCl added to PDDA; the other conditions are the same.
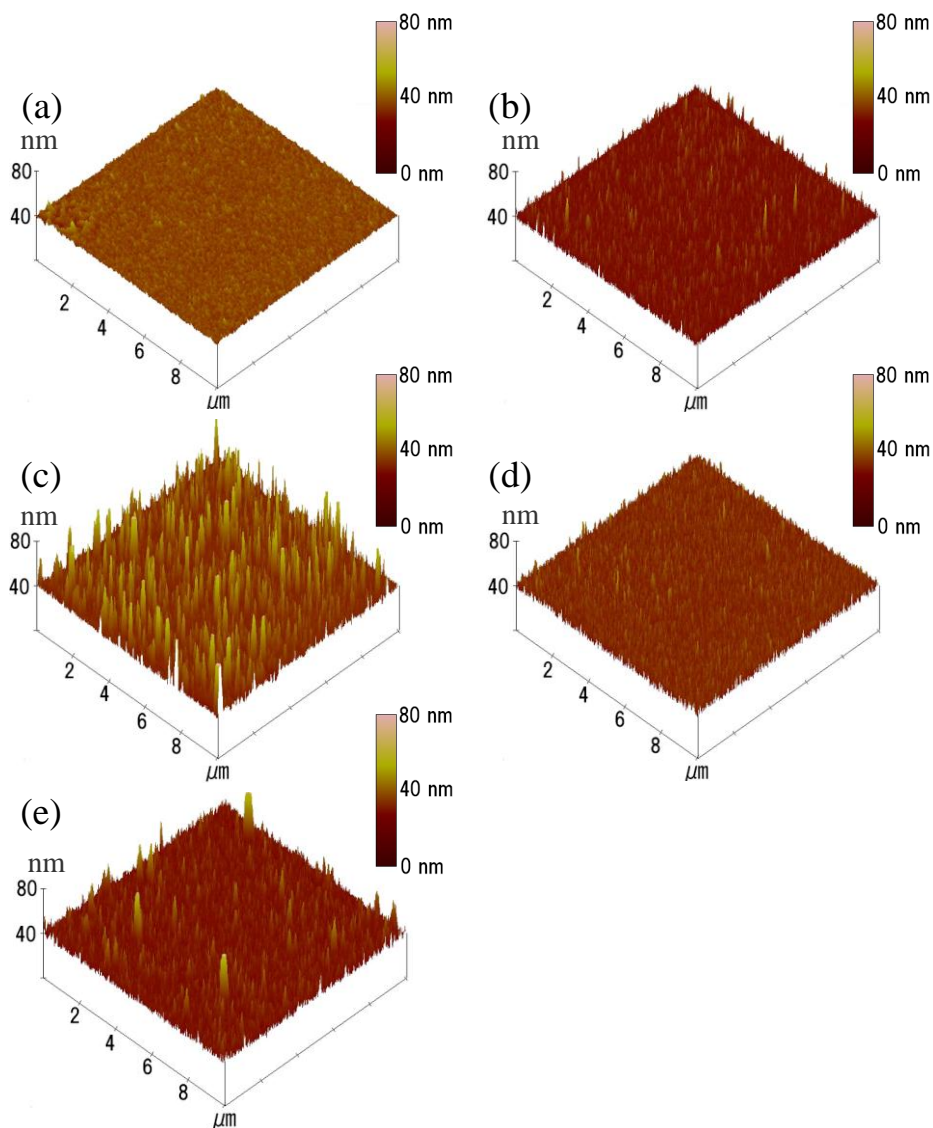
Fig. 4. (Color online) AFM images of (PDDA/TALH)$_{10}$ for comparing (1) (a), (b), and (c); (2) (a) and (d); and (3) (a) and (e). The fabrication conditions are as follows: (1) (a) pH 6.3 TALH solution, (b) pH 4.5 TALH solution, and (c) pH 2.5 TALH solution; the other conditions are the same. (2) (a) 10 mM PDDA solution, and (d) 100 mM PDDA solution; the other conditions are the same. (3) (a) 0 mM NaCl added to PDDA. (e) 1.0 M NaCl added to PDDA; the other conditions are the same.

(a)

5.0kV 11.4mm ×50.0k   1.00um

(b)
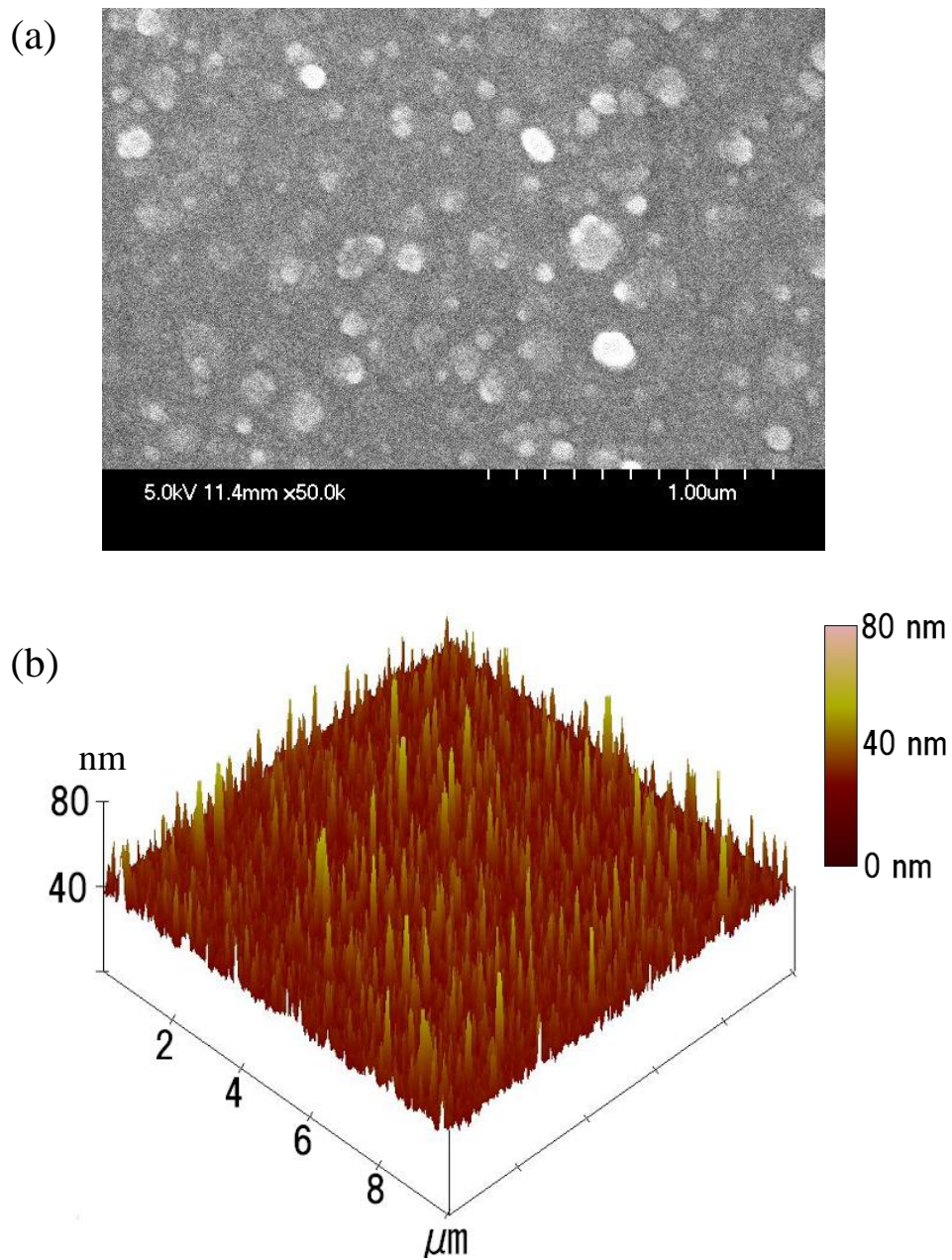
Fig. 5. (Color online) (a) FE-SEM and (b) AFM images of $(PDDA/TALH)_{10}$ with the addition of 0.5 M NaCl to 100 mM PDDA solution and the pH of TALH solution being 3.5.
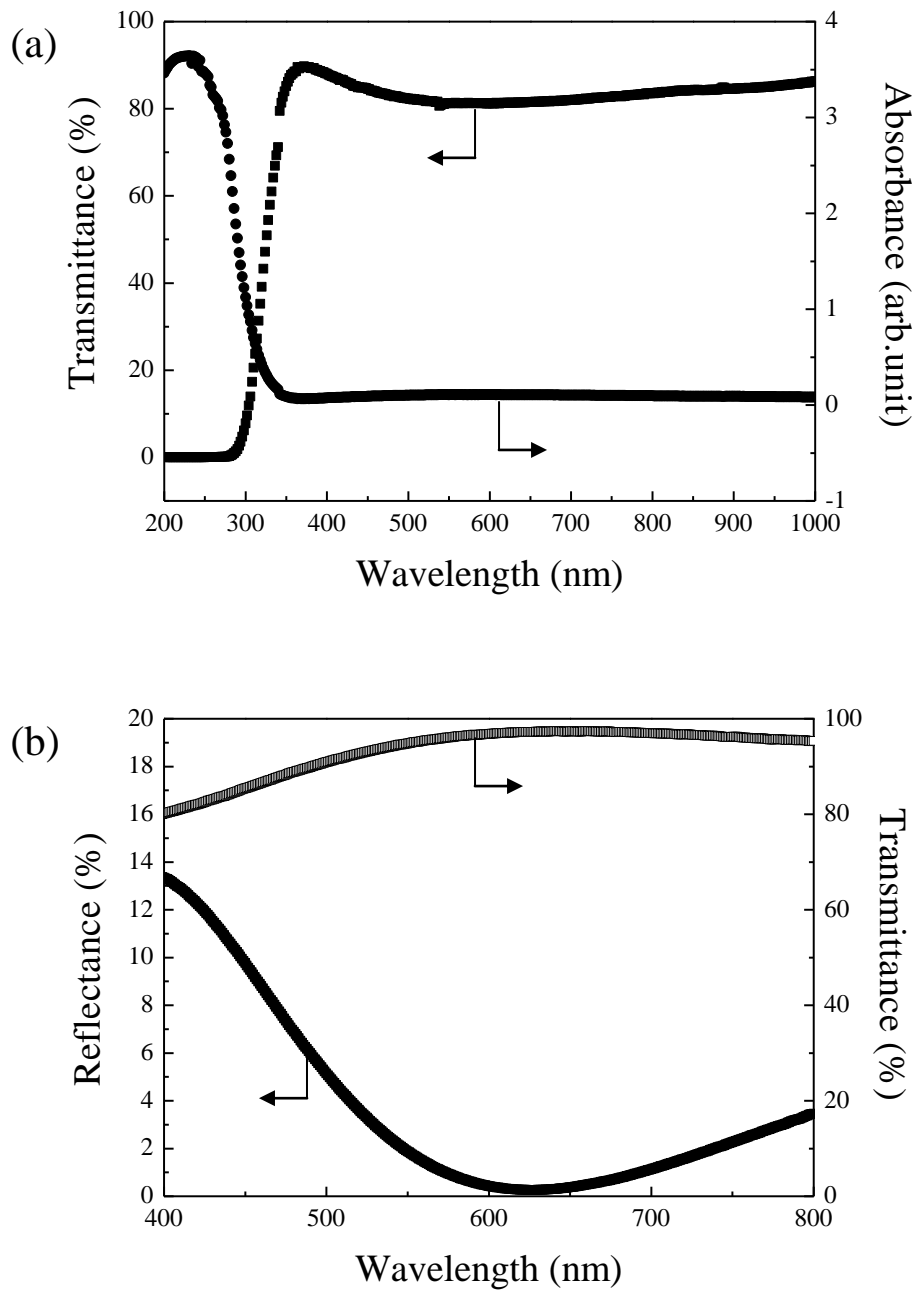
Fig. 6. (a) Transmittance and absorbance of $(PDDA/TALH)_{10}$ thin film and (b) transmittance and reflectance of fabricated $(PDDA/TALH)_{10}$-$(PDDA/Na_2SiO_3)_{40}$ thin film.

References

[2-1] E. T. Fitzgibbons, K. J. Sladek, and W. H. Hartwig: J. Electrochem. Soc. 119 (1972) 735.

[2-2] K. Rajeshwar: Chem. Ind. 17 (1996) 454.

[2-3] A. Sclafani, M. N. Mozzanega, and P. Pichat: J. Photochem. Photobiol A. 59 (1991) 181.

[2-4] S. Baskaran, L. Song, J. Liu, Y. L. Chen, and G. L. Graff: J. Am. Ceram. Soc. 81 (1998) 401.

[2-5] A. Hanprasopwattana, T. Rieker, A. G. Sault, and A. K. Datye: Catal. Lett. 45 (1997) 165.

[2-6] H. Mockel, M. Giersig, and F. Willig: J. Mater. Chem. 9 (1999) 3051.

[2-7] K. S. Mayya, D. I. Gittins, and F. Caruso: Chem. Mater. 13 (2001) 3833.

[2-8] X. Y. Shi, T. Cassagneau, and F. Caruso: Langmuir 18 (2002) 904.

[2-9] F. Caruso, X. Y. Shi, R. A. Caruso, and A. Susha: Adv. Mater. 13 (2001) 740.

[2-10] P. Chrysicopoulou, D. Davazoglou, Chr. Trapalis, and G. Kordas: Thin Solid Films 323 (1998) 188.

[2-11] M. Takeuchi, T. Itoh, and H. Nagasaka: Thin Solid Films 51 (1978) 83.

[2-12] K. S. Yeung and Y. W. Lam: Thin Solid Films 109 (1983) 169.

[2-13] Y. Lvov, K. Ariga, M. Onda, I. Ichinose, and T. Kunitake: Langmuir 13 (1997) 6195.

[2-14] B. G. De. Geest, N. N. Sanders, G. B. Sukhorukov, J. Demeestera, and S. C. De. Smedt: Chem. Soc. Rev. 36 (2007) 636.

[2-15] G. Decher, J. D. Hong, and J. Schmitt: Thin Solid Films 210-211 (1992) 831.

[2-16] G. Decher: Science 277 (1997) 1232.

[2-17] Y. Wang, A. S. Angelatos, and F. Caruso: Chem. Mater. 20 (2008) 848.

[2-18] S. Shiratori, T. Ito, and T. Yamada: Colloids Surf. A 198 (2002) 415.

[2-19] K. Ariga, J. P. Hill, M. V. Lee, A. Vinu, R. Charvet, and S. Acharya: Sci. Technol. Adv. Mater. 9 (2008) 014109.

[2-20] K. Ariga, J. P. Hill, and Q. Ji: Phys. Chem. Chem. Phys. 9 (2007) 2319.

[2-21] J. H. Kim, S. Fujita, and S. Shiratori: Thin Solid Films 499 (2006) 83.

[2-22] B. S. Kim, H. Gao, A. A. Argun, K. Matyjaszewski, and P. T. Hammond: Macromolecules 42 (2009) 368.

[2-23] S. S. Shiratori and M. F. Rubner: Macromolecules 33 (2000) 4213.

[2-24] J. Cho and F. Caruso: Macromolecules 36 (2003) 2845.

[2-25] J. L. Lutkenhaus, K. McEnnis, and P. T. Hammond: Macromolecules 41 (2008) 6047.

[2-26] J. B. Schlenoff and S. T. Dubas: Macromolecules 34 (2001) 592.

[2-27] S. T. Dubas and J. B. Schlenoff: Macromolecules 32 (1999) 8153.

[2-28] O. Mermut and C. J. Barrett: J. Phys. Chem. B 107 (2003) 2525.

CHAPTER 3

Spray Layer-by-Layer Method

Several LBL modifications have been proposed recently, including spray-LBL [1-10]. Compared with dipping self-assembly coating, spraying self-assembly coatings has the advantages that the desired thin film with large surface area can be fabricated in short time and with small volume of solution. These thin films deposited by spraying coatings may be expected for the many device applications such as external coatings to protect corrosion, large area membrane, and biomaterial coatings with the fine design and controlling of the structure of multilayers thin film.

Schlenoff introduced a new preparation method "spraying" respectively in 2000 [1]. This method can accelerate the adsorption time polymers adsorption time from 25 to 150 times depending on the chemical nature of the compounds and the experimental parameters. In fact, spraying is much more that a technology used for dispersing liquids in air or to point objects. One can consider spraying as a very powerful method to bring a surface into contact with a liquid producing a very homogeneous liquid film at the interface. It is thus extremely well suited for LBL-assembly, especially for the homogeneous wetting of large or uneven surface.

In the spraying process, substrate is vertically set up and liquid is horizontally sprayed onto the substrate. Once liquid reaches substrate surface, drainage caused by gravity will ensure the liquid coverage on the surface (Fig. 1, step1). Because of the vertically installed substrate and the gravity-induced drainage, weakly adsorbed polymer chains are difficult to attach the surface. Nevertheless, a rinse step is necessary

to remove weakly adsorbed polyelectrolyte on the surface. Rinse solution is sprayed onto the substrate and an additional waiting time is necessary for the drainage of rinse solution (Fig. 1, step2). After the rinse step, oppositely charged polymer solution can be sprayed again onto the surface (Fig. 1, step3), followed by another rinse step (Fig. 1, step4).

3. 1. Comparison of preparation methods: dipping, spraying and spin coating

Dipping, spraying and spin coating are the three major preparation methods used in LBL assembly. Since the use of spin coating is limited in both substrate size and planarity, dipping and spraying are two most frequently used preparation methods. Similar to the LB adsorption, dipping is the first preparation method used in polyelectrolyte multilayer construction. The substrate is brought into contact with polyelectrolyte solutions. After a certain adsorption time, polymer chains will diffuse from bulk solution to the surface and get adsorbed. The necessary adsorption time for a single layer pair varies from 20 to 60 min in different systems.

Multilayers thin films by LBL self-assembly dipping, spraying or spin coating methods have been fabricated and compared the properties of films obtained by different deposition method. Hong [10, 11], Wang [12, 13], and Char [14] demonstrated the deposition phenomenon of polyelectrolytes or nanoparticles by spin coating. The thickness growth of multilayers thin films deposited by spin coating is larger than that of thin films assembled by dipping coating in the adsorption of oppositely charged polyelectrolytes as shown in Fig. 2 [11]. However, when the multilayers thin films are assembled with polyelectrolytes and oppositely charged nanoparticles, the thickness

growth of thin film obtained by spin coating is smaller than that of thin film deposited by dipping coating as shown in Fig. 3 [14] because the thin film deposited by spin coating has a layered structure of nanoparticles by centrifugal force. On the other hand, the thin films deposited by dipping coating are assembled without layered structure [14].

Schlenoff [1] and Porcel [2] introduced the alternative or continuous and simultaneous spraying deposition of polyelectrolytes. Fig. 4 shows the comparison of thickness growth of multilayers thin film deposited by spray or dipping coating [1]. The thickness increasing of PDDA/PSS multilayers thin film deposited by alternative spraying coating for 10 s is a little larger than that of thin film by dipping coating as the number of layers is increased and these films prepared by two method shows the exponential thickness growth. On the other hand, the PGA/PAH thin films deposited by continuous and simultaneous spray coating show the linear thickness growth according to spray time as shown in Fig. 5 [2]. When the PGA/PAH thin films are assembled by the dipping coating, this film shows the exponential thickness growth [15].

Compared with dipping self-assembly coating, spraying and spin self-assembly coatings have the advantages that the desired thin film with large surface area can be fabricated in short time and with small volume of solution.

Finally, these thin films deposited by spin and spraying coatings may be expected for the many device applications such as external coatings to protect corrosion, large area membrane, and biomaterial coatings with the fine design and controlling of the structure of multilayers thin film.

3. 2 Principle of spray-LBL method

Some controllable and uncontrollable parameters in spray-LbL method can also explain this phenomenon. Examples of controllable parameters include spray distance, spray volume, concentrations of polyelectrolyte while droplet size, droplet speed and speed distribution during spraying process, concentrations of polyelectrolyte in droplets are examples of parameters that are not easy to control.

3. 2. 1 Fluids

In this chapter we learn about the behavior of fluids. We will see how Archimedes' principle can be used to determine which materials will float in a given fluid. Bernouilli's equation, which relates the pressure to the flow speed in a fluid, will also be presented. As we will see, Archimedes' principle and Bernouilli's equation are responsible for many important and common phenomena. [16-18]

(1) States of Matter

There are essentially three states of ordinary matter: solid liquid and gas. Solid objects are characterized by their rigidity and incompressibility. That is, they cannot easily be deformed into different shapes without breaking. (Rubber is a somewhat special solid: it can be deformed, but as soon as the applied force is removed, it returns to its original state.) Incompressibility means that it is very difficult to change a solid's

density, which is defined as

$$D = M / V \quad (Density = mass\ per\ unit\ volume) \quad (1)$$

Liquids on the other hand have no shape of their own. They take on the shape of whatever container they happen to be in. However, liquids, like solids, are difficult to compress. Finally, gases have not a definite shape and density. They tend to fill whatever container they occupy, as long as the container is sealed. Otherwise the gases leak out and spread out as far as they can. All types of matter are made of molecules. The difference between solids, liquids and gases has to do with how tightly the molecules are held together by electromagnetic forces. In solids, the molecules are very tightly bound into rigid structures, whereas in liquids the binding forces are looser, allowing the molecules to slide over each other (flow). Gas molecules on the other hand have virtually no binding forces between them, so that they tend to get as far away from each other as their container allows.

A fluid is defined to be any matter which can flow without significant external forces being applied.

This definition can apply to either liquids or gases, but in this Chapter we will for simplicity assume that the fluids are essentially incompressible. Although this strictly speaking restricts us to liquids, most of our considerations will also apply, at least approximately, to gases under certain conditions. Thus, for example, we will be

applying to apply our results to the air in our atmosphere.

(2) Fluid flow and the continuity equation

Fluids, by definition can flow, but are essentially incompressible. This provides some very useful information about how fluids behave when they flow through a pipe, or a hose. Consider a hose whose diameter decreases along its length, as shown in the Figure below. The continuity equation is a direct consequence of the rather trivial fact that what goes into the hose must come out. The volume of water flowing through the hose per unit time (i.e. the flow rate at the left must be equal to the flow rate at the right or in fact anywhere along the hose. Moreover, the flow rate and point in the hose is equal to the area of the hose at that point times the speed with which the fluid is moving:

Q (Flow rate) =A (area) × v (velocity)   (2)

You can easily verify that $A \times v$ has units m^3/t which is correct for volume per unit time (Fig 6). These considerations lead us directly to the continuity equation, which states that

A (Area) × v (velocity) = C (constant)   (3)

Everywhere along the hose. This has the important consequence that as the area of the hose decreases, the velocity of the fluid must increase, in order to keep the flow rate constant. Anyone who has pinched one end of a garden hose has experienced this effect:

74

the smaller you pinch the end of the hose, the faster the water comes out.

An important property of fluids is pressure. Suppose we imagine surrounding a given volume of fluid (liquid or gas) by a container. The atoms and molecules of the fluid will bounce off the walls of the container, thereby changing their velocity. This change of velocity, by Newton's 2nd law, comes from a force, which is the action of the wall on the molecule. By Newton's 3rd law the molecule exerts an equal and opposite force on the wall. The pressure of the fluid is defined as the average force of the molecules on the wall per unit area:

P (Pressure) = Fa / A (average force / area) (4)

Given a large volume of fluid, you can image putting a wall anywhere within the fluid, so that pressure is not something that is just defined at the boundaries (i.e. by the container), but is in fact defined, and can be felt or measured throughout the fluid. This is why the pressure increases as one goes down in the ocean - as one descends, there is more and more fluid above, which exerts a larger and larger force on a given area. Similarly, the pressure in the atmosphere is quite literally due to the weight of the air over our heads pressing down on us. As one goes up in altitude, there is less air above and the air pressure decreases. The forces due to air pressure are very large near sea level: 100,000 N per square meter of force pressing against us. The reason we don't implode is that the pressure of fluids inside our body (blood in veins, air in lungs etc) is equal to the pressure from the atmosphere outside, and there is no net force inward. However, slight pressure changes can have devastating effects. This is why diving too deep underwater can be dangerous. The extra pressure due to the weight of the water

75

over your head causes huge forces which can literally crush you. This also explains why deep sea divers must have air under high pressure in their tanks. This way the air that they take into their lungs is approximately at the same pressure as the water pushing inward on their lungs, which would otherwise collapse.

(3) Bernoulli's Principle [16-18]

This is an important principle involving the movement of a fluid through a pressure difference. Suppose a fluid is moving in a horizontal direction and encounters a pressure difference. This pressure difference will result in a net force, which by Newton's 2nd law will cause an acceleration of the fluid. The fundamental relation,

Work done = change in kinetic energy

in this situation can be written as

$$\Delta P \text{ (change in pressure)} \times A \text{ (area)} \times D \text{ (distance)} = \Delta K \text{ (change in kinetic energy)} \qquad (6)$$

which furthermore can be expressed as

$$\Delta P \text{ (change in pressure)} + \Delta(K/V) \text{ change in (kinetic energy / volume)} = 0 \qquad (7)$$

In other words,

P (Pressure) + (K / V) (kinetic energy / volume) = C (constant) (8)

which is known as Bernoulli's principle. This is very similar to the statement we encountered before for a freely falling object, where the gravitational potential energy plus the kinetic energy was constant.

Bernoulli's principle thus says that a rise (fall) in pressure in a flowing fluid must always be accompanied by a decrease (increase) in the speed, and conversely, if an increase (decrease) in, the speed of the fluid results in a decrease (increase) in the pressure. This is at the heart of a number of everyday phenomena. As a very trivial example, Bernouilli's principle is responsible for the fact that a shower curtain gets "sucked inwards" when the water is first turned on. What happens is that the increased water/air velocity inside the curtain (relative to the still air on the other side) causes a pressure drop. The pressure difference between the outside and inside causes a net force on the shower curtain which sucks it inward. A more useful example is provided by the functioning of a perfume bottle: squeezing the bulb over the fluid creates a low pressure area due to the higher speed of the air, which subsequently draws the fluid up. This is illustrated in the following Fig. 7.

Bernouilli's principle also tells us why windows tend to explode, rather than implode in hurricanes: the very high speed of the air just outside the window causes the pressure just outside to be much less than the pressure inside, where the air is still. The difference in force pushes the windows outward, and hence explodes. If you know that a hurricane is coming it is therefore better to open as many windows as possible, to equalize the pressure inside and out.

Another example of Bernoulli's principle at work is in the lift of aircraft wings and

the motion of "curve ball" in baseball. In both cases the design is such as to create a speed differential of the flowing air past the object on the top and the bottom - for aircraft wings this comes from the movement of the flaps, and for the baseball it is the presence of ridges. Such a speed differential leads to a pressure difference between the top and bottom of the object, resulting in a net force being exerted, either upwards or downwards.

Applying the Bernoulli equation between the shown (Fig. 8) stations (A) and (B) along the center:

$$P_1 + Pgz_1 + P\frac{V_1^2}{2} = P_2 + Pgz_2 + P\frac{V_2^2}{2} \tag{9}$$

Assuming that the venturi meter is horizontal ($z_1 = z_2$), and that the flow is uniform at both stations (thus: $V_1 = Q/A_1$ and $V_2 = Q/A_2$), the above equation becomes:

$$P_1 + P\frac{(Q/A_1)^2}{2} = P_2 + P\frac{(Q/A_2)^2}{2} \tag{10}$$

Solving the above equation with respect to Q:

$$Q = \sqrt{\frac{2\Delta P}{P(A_1^2 - A_2^2)}} A_1 A_2 = \frac{A_2}{\sqrt{1 - (A_2/A_1)^2}} \sqrt{2\Delta P/P} \tag{11}$$

The above equation relates the flow rate Q to the pressure $\Delta P = P_1 - P_2$ differential. This pressure differential can be measured (as in the case of the Pitot tube we described in class) through pressure taps (holes) on the walls of the venturi meter, at stations (A) and (B) that are connected with the sides of a U-manometer. A modified formula for Q is given which also includes the effects of viscous forces (which are completely ignored

when applying the Bernoulli equation). The venturi meter is covered in more detail in advanced Fluid Mechanics courses.

3. 3 Optimization of the spray-LBL method for thin film deposition

In spraying, we are simply taking potential energy, supplied by a pump, and converting it to kinetic energy, as provided by the spray. Impact in this sense is the force and force distribution evidenced on a target surface due to the expenditure of kinetic energy. Because the impingement of individual water droplets on a surface is generally considered to be inelastic, the total impact from a spray can be estimated with reasonable accuracy from a simple reaction force equation:

$$Ft = \rho \times Q \times v \qquad\qquad (9)$$

where Ft is the total force, ρ is the fluid density, Q is the total volume flux, and v is the exit velocity of the spray from the nozzle.

Although this formula is only technically correct when applied immediately outside the nozzle, there is a large body of empirical data showing that it applies at a target surface as well. Application of the formula usually involves the incorporation of a bulk efficiency factor that accounts for spray variables such as target distance, energy losses internal to the nozzle, drop size, spray angle, and spray type.

The situation may be further complicated by spray rebound, which increases the impulse and resulting impact force. Consider for example a spray impacting on a solid surface (Fig. 9).

In case A, the spray hits the target surface and deflects horizontally. A real situation could be any combination of these situations. Cases A would be the type of behavior expected when spraying at lower relative pressures onto smooth surfaces. Cases B represent higher pressures, rougher surfaces, and closer target distances. In case A, the impact force is the same as the reaction force formula predicts. Total impact would be same as case A multiplied by the cosine of incident angle relative to "vertical". In case B, the total impact will be larger than the reaction force calculated from the equation. This is because impact results from a change in vector momentum. Since the liquid rebounds toward the nozzle, it imparts additional momentum to the target. If spray droplets collided in a perfect elastic manner with the target, the resulting impact could be as much as double that calculated from the simplified reaction force equation.

The observable trend of decreasing film thickness with increasing spray distance is a combination of the two effects of spray distance, the amount of droplets that impact the surface and the force of impact. At close distances, more droplets impact the film surface at one time, as well as impacting with more force, reducing the diffusion distance. The combination of more droplets and shorter diffusion distances results in thicker films than films made at greater distances.

3. 3. 1 Characteristics of spray parameters

Each of the operational parameters of the spray-LBL system were adjusted individually and systematically to determine the best parameters to control and adjust the film thickness and roughness. These parameters are polyelectrolyte concentration, polyelectrolyte spray time, the distance between the spray nozzles and the substrate, the

air pressure and number of bilayers etc.

(1) Polyelectrolyte concentration

As the polyelectrolyte concentration increases, the overall film thickness also increases.

Increasing the polyelectrolyte concentration, increase the number of polyelectrolyte molecules in each sprayed droplet. Having more polyelectrolyte molecules in each droplet require less time for a specific number of polyelectrolyte chains to adsorb to the surface once the droplets impact the surface and spread into a liquid film on the surface. Increasing concentration is thus lead to more polyelectrolyte molecules available for adsorption to the film during the short droplet contact time.

Films are deposited using electrostatic interactions between the substrate and the two oppositely charged polyelectrolyte. As a charged surface is exposed to the oppositely charged polyelectrolyte solution the polymer chains adsorb to the surface building a layer. After enough of the polyelectrolyte chains have adsorbed, the surface experiences a charge reversal. If the surface is exposed to enough polyelectrolyte, the charge reversal is strong enough to prevent other liked charged polyelectrolyte from adsorbing to the surface. This is the point of polyelectrolyte saturation on the film surface layer. This indicated that spray-LBL technique is also an electrostatic controlled adsorption process. And adjusting the concentration of the polyelectrolyte solutions used in the spray-LBL technique is an effective way to change the thickness of the films produced.

(2) Polyelectrolyte spray time

Another significant parameter to control film thickness is the spraying time or contact time between the polyelectrolyte and the film surface. Like concentration, the contact time parameter is also found in traditional LBL deposition in the form of dipping time. Increasing the contact time should have a similar effect to that of concentration. Increasing the contact time, increase the amount of polyelectrolyte available for adsorption to the surface. Increasing the contact time allows more time for the diffusion process through the liquid coating resulting from the droplets impacting the surface. If the exposure time is equal to or greater than the diffusion time of the polyelectrolyte in this liquid surface coating, then the polyelectrolyte chains are able to diffuse to and adsorb to the surface. Instead of increasing the amount of polyelectrolyte in the droplets, as was done in the concentration study, the exposure of the polyelectrolyte solution was increased, thus increasing the number of chains that diffuse to the surface. Polyelectrolyte spray time affects the film roughness in a similar manner as it affects film thickness.

(3) Spraying distance

As the distance from the nozzle increases, the diameter of the spray cone expands. If the substrate is too close to the nozzles, the cone was not large enough to cover the entire surface. However, if the substrate is too far away from the nozzles then the cone was much larger than the substrate surface and most of the droplets will not impact the surface. As distance increases the number of droplets impacting the surface decreases,

and thus the number of polyelectrolyte chains available near the surface decreases. This effect can be viewed similarly to decreasing the concentration of polyelectrolyte in each droplet

Another affect of increasing the spraying distance is a decrease in droplet velocity, as seen in Table 1. By increasing the spray distance the droplets must travel further through the ambient environment, increasing the decelerating effects of air resistance, gravity, and droplet collisions.

The observable trend of decreasing film thickness with increasing spray distance is a combination of the two effects of spray distance, the amount of droplets that impact the surface and the force of impact. At close distances, more droplets impact the film surface at one time, as well as impacting with more force, reducing the diffusion distance. The combination of more droplets and shorter diffusion distances results in thicker films than films made at greater distances.

(4) Pressure

The effect of droplet velocity on film thickness was previously discussed in the spraying distance investigation. To summarize, increasing the droplet impact velocity will cause the droplet to deform at impact and reduce the diffusion length for the polyelectrolyte chains inside. This was result in more polyelectrolyte chains reaching the surface during the set contact time, and thus a thicker film. While the impact velocity of the droplets is always be less than the nozzle exit velocity, due to air resistance, gravity and droplet collisions.

Increasing the air pressure increase the droplet impact velocity resulting in a shorter

diffusion length for the polyelectrolyte chains in the droplets and a thicker, but rougher film. Both film thickness and roughness have a direct relationship with air pressure; increasing the air pressure increases both the film thickness and film roughness.

(5) Number of bilayers

The number of bilayers has a very logical affect on the film thickness; increasing the number of bilayers increases the film thickness. Typically, LBL film thickness grows linearly with the number of bilayers, except in cases where polyelectrolyte interdiffusion results in an exponential growth regime. [18] The effect of increasing the number of bilayers is that the film thickness and roughness increase.
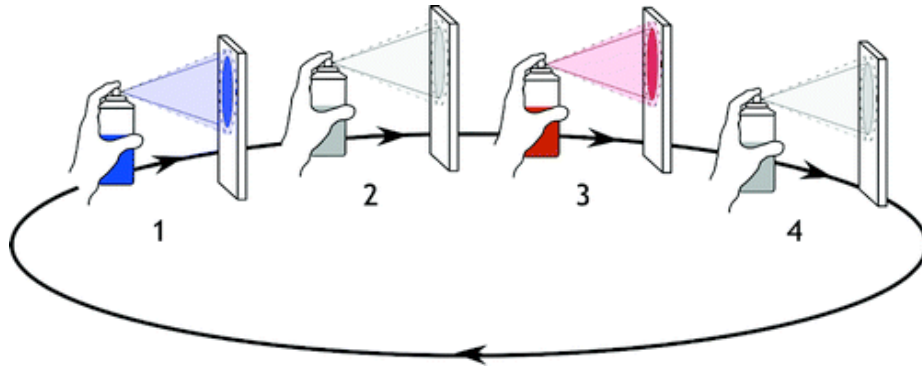
Fig. 1. Simplified spray process. Figures are adapted from [1]
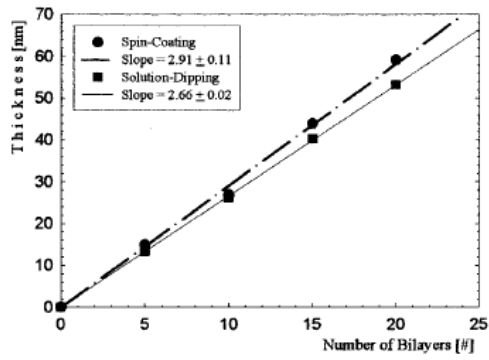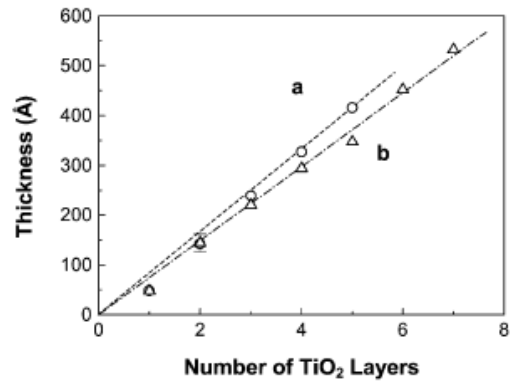
(a)   **(b)**

Fig. 2. Thickness difference of thin film deposited by spin or dipping coating: (a) thin film consisted of polyelectrolytes and (b) thin film consisted of polyelectrolyte and nanoparticles. Figures are adapted from [11] and [14].
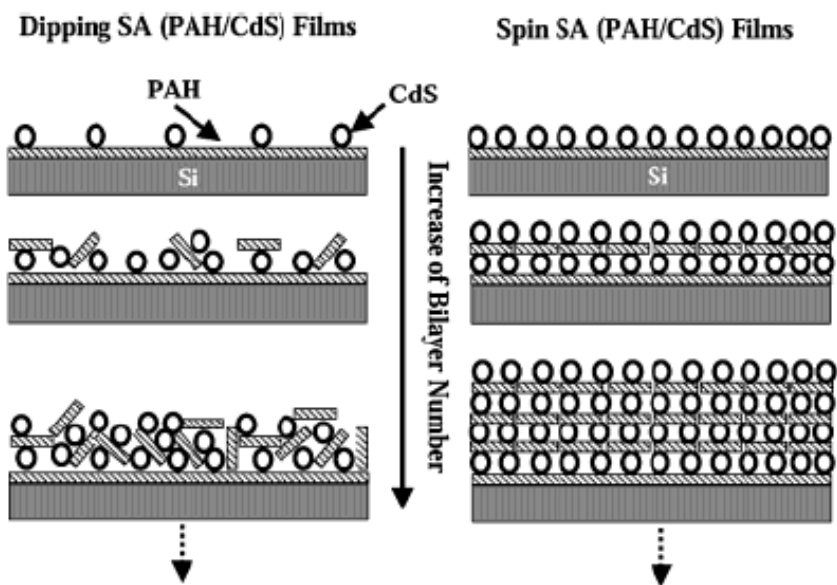
Fig. 3. Schematic diagram of the internal structure of films consisted of PAH and CdS by spin or dipping coating. Figure is adapted from [10].
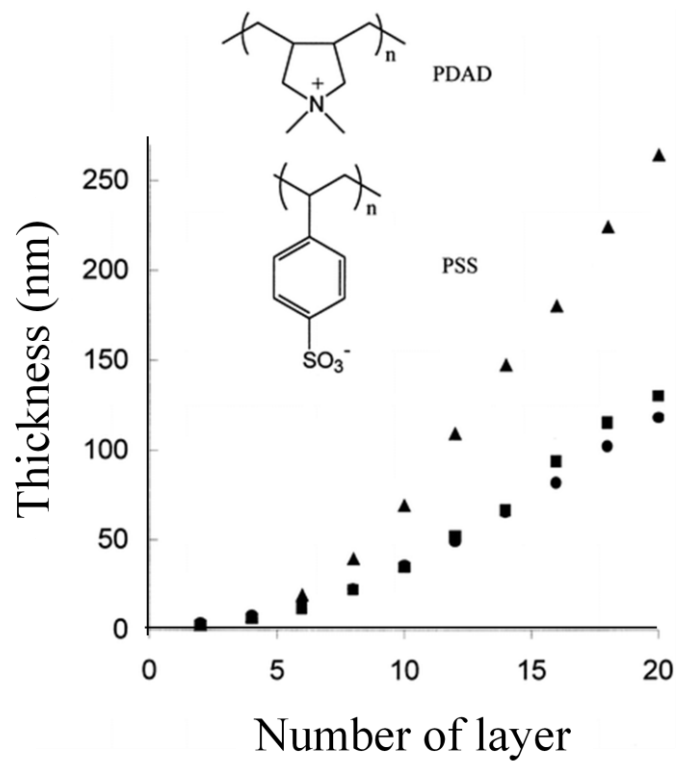
Fig. 4. Thickness of a polyelectrolyte layer as a function of number of layers deposited for sprayed and dip-coated silicon wafers. For both methods, the contact time of the solution with the substrate was approximately 10 s for each layer: circles, dip-coated; squares, sprayed. Figure is adapted from [1].
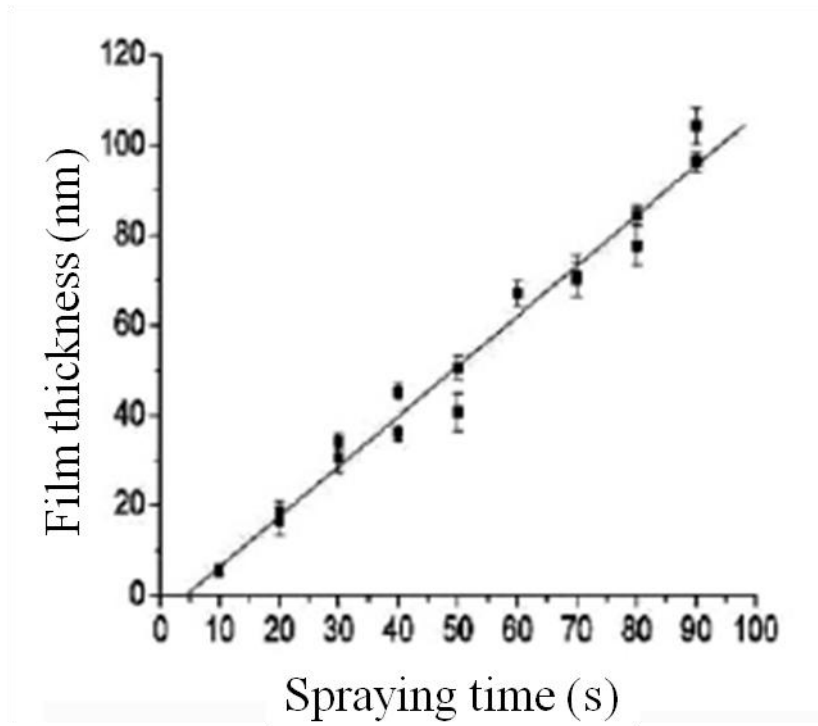
Fig. 5. Thickness of PEI-PGA/PAH film buildup versus spraying time. Figure is adapted from [2].
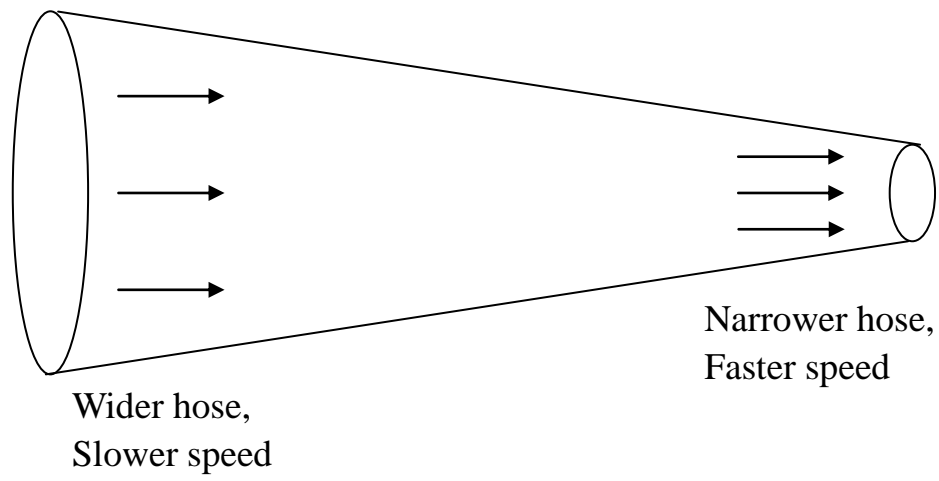
Fig. 6. Fluid flow in a hose of variable size. [16]
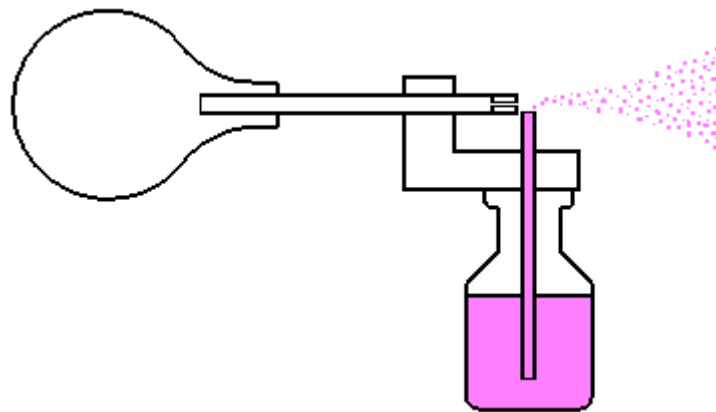
Fig. 7. Scheme of action of spray atomizer. The air jet which comes out of the
horizontal cane causes a depression on the vertical cane which draws liquid from the
small bottle and disperses it in tiny drops. [16]
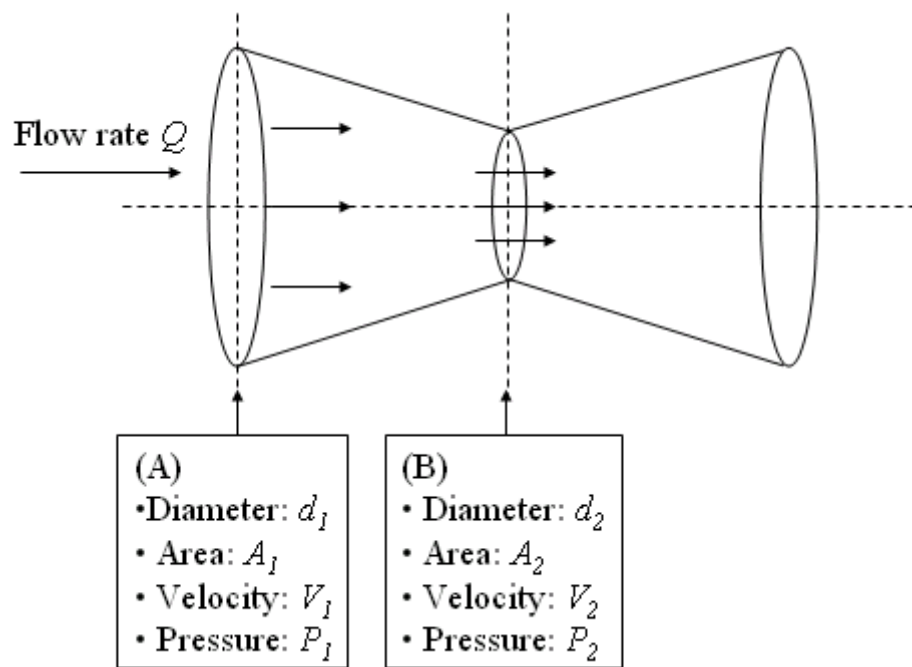
Fig. 8. One-dimensional duct showing control volume. [16]

Table I. Impact velocity of the PAA solution droplets at the adjusted spraying distances.
[18]

Spraying Distance (in)	Impact Velocity (m/s)
5.0	6.8
6.0	6.2
6.5	5.7
7.0	5.5
7.5	5.2
8.5	5.0
9.0	4.7
10.0	4.0
11.0	3.2
12.0	2.3
13.0	1.4
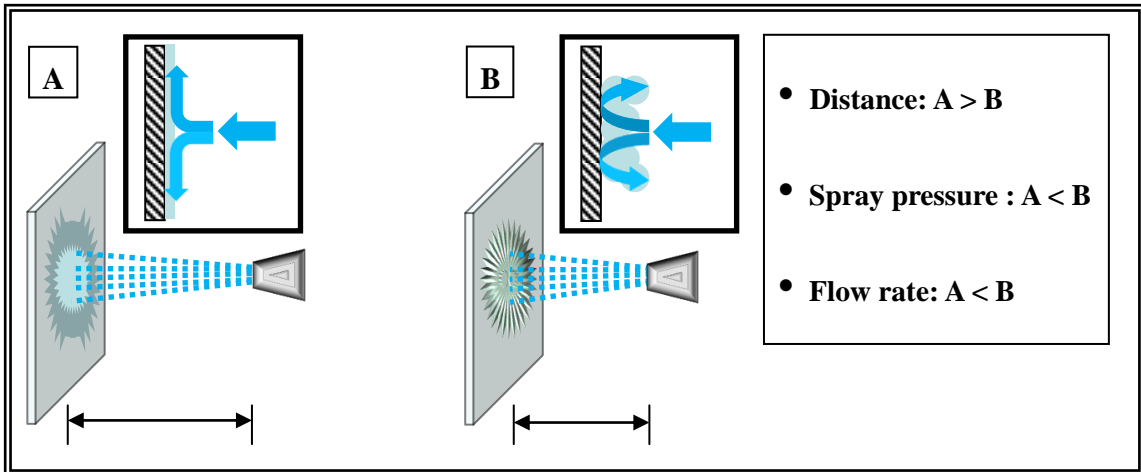
Fig. 9. Shape of spray impacting on a solid surface.

References

[3-1] J. B. Schlenoff, S. T. Dubas, and T. Farhat, Langmuir 16 (2000) 9968.

[3-2] C. H. Porcel, A. Izquierdo, V. Ball, G. Decher, J. C. Voegel, and P. Schaaf, Langmuir 21 (2005) 800.

[3-3] A. Izquierdo, S. Ono, J. C. Voegel, P. Schaaf, and G. Decher, Langmuir 21 (2005) 7558.

[3-4] C. Lu, I. Dönch, M. Nolte, and A. Fery: Chem. Mater. 18 (2006) 6204.

[3-5] O. Félix, Z. Zheng, F. Cousin, and G. Decher, C. R. Chimie 12 (2009) 225.

[3-6] N. Laugel, J. Hemmerle, C. Porcel, J. C. Voegel, P. Schaaf, and V. Ball, Langmuir 23 (2007) 3706.

[3-7] S. S. Ono and G. Decher, Nano Lett. 6 (2006) 592.

[3-8] X. Zhao, C. Hinchliffe, C. Johnston, P. J. Dobson, S. Patrick, and P. S. Grant, Mater. Sci. and Eng. B 151 (2008) 140.

[3-9] K. Krogman, N. Zacharia, S. Schroeder, and P. Hammond, Langmuir 23 (2007) 3137.

[3-10] J. H. Cho, K. H. Char, J. D. Hong, K. B. Lee, Adv. Mater. 13 (2001) 1076.

[3-11] S. S. Lee, J. D. Hong, C. H. Kim, K. Kim, J. P. Koo, K. B. Lee, Macromolecules, 34 (2001) 5358.

[3-12] P. A. Chiarelli, M. S. Johal, J. L. Casson, J. B. Roberts, J. M. Robinson, H. L. Wang, Adv. Mater. 13 (2001) 1167.

[3-13] P. A. Chiarelli, M. S. Johal, D. J. Holmes, J. L. Casson, J. M. Robinson, H. L. Wang, Langmuir 18 (2002) 168.

[3-14] B. H. Sohn, T. H. Kim, K. H. Char, Langmuir 18 (2002) 7770.

[3-15] F. Boulmedais, V. Ball, P. Schwinte, B. Frisch, P. Schaaf, J. C. Voegel, Langmuir 19 (2003) 440.

[3-16] D. F. Young, B.R. Munson, T. H. Okiishi, Fundamentals of Fluid Mechanics(6th)

[3-17] N. Eastlake, N. Charles, The Physics Teacher 40 (2002) 166.

[3-18] C. Porcel, P. Lavalle, G. Decher, B. Senger, J. C. Voegel, P. Schaaf. Langmuir 24(4) (2007) 1898

CHAPTER 4

Nanoscale Texture Control of Polyelectrolyte Multilayer Using Spray Layer-by-Layer Method

4. 1. Introduction

The fabrication of polyelectrolyte multilayer thin films [1-3] has received much attention recently owing to their various applications such as sensors, [4] electronic devices, [5] drug delivery carriers, [6, 7] micropatterning, [8] membranes, [9-14] microcontainers for molecules encapsulation, [15] and particle surface modification. [16-23] There are many different techniques used for depositing thin films: sol-gel method, [24] sputtering, [25] chemical vapor deposition (CVD), [26] and other chemical deposition methods. In the sol-gel method, volatile solvents have to be used and film thickness control is difficult, because film quality is affected by humidity and temperature. Sputtering is carried out in vacuum. It entails high fabrication cost and requires expensive equipment. CVD also requires vacuum equipment and high deposition energy. Chemical deposition can be carried out at normal pressure; however, it requires non-environmentally friendly solutions such as TiF_6. All the methods discussed above have some environmental demerits in their fabrication processes.

The layer-by-layer (LBL) technique for the fabrication of a multilayer thin film was introduced at the beginning of 1991 by Decher and Hong. [27] It is based on the alternate adsorption of oppositely charged materials in aqueous solutions via electrostatic attraction. It has many advantages such as a simple process, water-based

room-temperature deposition at normal pressure, no limit of thickness, and no need for complicated equipment. In addition, the thickness of the thin films can be controlled with nanoscale accuracy. Although this method has many advantages, it requires long fabrication time. Because the process is driven in part by diffusion, LBL cycles usually take several minutes to complete. This is an unacceptable demerit if this technology is to be applied in industrial fields.

Several LBL modifications have been proposed recently, including spray LBL, [28–36] spin-assisted LBL, [37–41] or dewetting LBL (d-LBL). [42] These new methods have primarily focused on decreasing the cycle time required by LBL, and have achieved reductions from cycle times of about 20 min to 60–80 s. They succeeded in shorening deposition time at least one order of magnitude down to 6 s for polymer/polymer films. [29] They have also provided some abilities to build LBL films on unique substrates, such as fiber substrates [30] or the control of the in-plane nanostructure of nanoparticles or polymers. [42]

In 2000, Schlenoff et al. reported the fabrication of a poly(diallyl dimethyl ammonium)/poly(styrene sulfonate) (PDDA/PSS) multilayer film by spraying the respective solutions on the substrate. [28] Izquierdo et al. studied the fabrication of multilayer films by dipping versus spraying. [29] Krogman et al. described a fully automated system capable of depositing thin polymer films using atomized mists of solutions containing species of complementary functionality. [30] They found that such films had a composition and thickness similar to those of multilayer films constructed by the conventional deposition method in solution. In addition, the spraying method is convenient, fast, and more generally applicable to the coating of large surfaces. However, they did not monitor the nanoscale control of the structures formed by the

spray-LBL method. Shiratori and Rubner reported that dramatic changes in the thickness of a sequentially adsorbed polyelectrolyte layer can be realized by making very small changes in solution pH. [1] Mendelsohn et al. also reported the texture structure formation by the dip LBL method in 2003. [43] High degrees of opposite ion pairing of train conformations occur, consequently leading to the formation of thin layers that are molecularly smooth. However, for a weak polyelectrolyte adsorbed at pH values at which the charge density of one molecule is low, the electrostatic forces are reduced; therefore, opposite ions cannot pair up as readily. Therefore, nonfully charged molecules are deposited with a high number of loops and tails, forming thicker, so called loopy, and rougher layers. When poly(allylamine hydrochloride) (PAH) and poly(acrylic acid) (PAA) are deposited at pHs 7.5 and 3.5, respectively (7.5/3.5), the PAA chains adsorb at a low pH with a low degree of ionization onto fully charged chains of PAH. This produces a loopy conformational arrangement. [44] In this case, a highly organized texture structure was formed on the film surface. By changing the surface texture structure, Mendelsohn et al. [43] and Choi and Rubner [44] reported a rational design of cytophillic and cytophobic polyelectrolyte multilayer thin films. They also suggest the possibility of fabricating cell-adhesive and cell-resistant thin films.

Recently, we have also found that texture structures were the formed for the (9.5/5.0) PAH/PAA film. It is found that this (9.5/5.0) film is thicker than the (7.5/3.5) film. There is a possibility to form nanoscale texture structures very rapidly. If these structures can be formed by the spray-LBL method, it should be much faster. If nanoscale texture structures are formed by the spray-LBL method, the possibility for biological applications of this method will increase.

Thus far, there is no report on the formation of nanoscale texture structures using the

spray-LBL method. In this study, the first fabrication process for nanoscale texture structure formation using the spray-LBL method was reported. The influences of the concentration of spraying solution, quantity of spray, and flow rate on the surface morphology of fabricated thin films were studied. In addition, the important factors for the control of the surface morphology of polyelectrolyte multilayer thin films prepared by the spray-LBL method were demonstrated. Differences in nanoscale texture structure formation between the conventional LBL method and the spray-LBL method are also discussed.

4. 2. Experimental Procedure

4.2.1 Materials

PAH (M_W = 70,000) as a positively charged solution PAA (M_W = 90,000) as a negatively charged solution were obtained from Aldrich and Polysciences, respetively. All the materials were used without any further purification. PAH solution and PAA solution were adjusted to pHs 9.5 and 5.0 with NaOH, respectively. The concentration of PAH and PAA solutions was 10 mM.

4.2.2 Preparation of thin films

A thin film was also deposited on the silver electrode of a quartz crystal microbalance (QCM; AT-cut, 10 MHz) to measure the amounts of PAH and PAA adsorbed. Glass and QCM substrates were ultrasonically agitated in KOH solution (1.0 wt%), mixed with

ultrapure water and ethanol (2:3 in volume ratio) for 5 min, and then rinsed with ultrapure water. By this treatment, negatively charged substrates were prepared.

The spray-LBL process is shown in Fig. 1. PAH solution was sprayed onto the negatively charged substrate. Then, it was rinsed for 20 s with pure water. Positively charged substrates prepared by the spraying of PAH solution were subsequently sprayed with negatively charged PAA solution and then the same rinsing steps were carried out. This cycle was repeated until five bilayers were formed.

4.2.3 Characterization of thin films

The QCM device was used to determine the deposited mass after each adsorption step. The resonance frequency of the QCM electrodes was 10 MHz. The piezoelectric quartz crystal changes its fundamental oscillation frequency f^2 as mass is deposited onto or depleted from the surface. According to the Sauerbrey equation, the resonant frequency shift, Δf, of a QCM is proportional to the mass change Δm:

$$\Delta f = -\frac{f^2}{N\rho A}\Delta m \quad \cdot \tag{1}$$

Thin films were built up on glass slide substrates. Thin films on glass slides were scratched with a razor blade to form lines. By profiling, the average value of three measurements was chosen to represent the thickness of a thin film. Film thickness was investigated by a surface profile measurement system (Salon DEKTAK 3030). Surface morphology was investigated by field-emission scanning electron microscopy (FE-SEM; Hitachi S-4700), and the root mean square (RMS) surface roughness of films was measured by atomic force microscopy (AFM; Digital Instrument Nanoscope IIIa) in the tapping mode.

4. 3. Results and Discussion

Figure 2 shows a brief schematic illustration of train conformation and loop-rich conformation (PAH/PAA) films. When PAH and PAA are deposited at pHs 9.5 and 5.0, respectively, both the partially ionized PAA and PAH molecules are adsorbed in loop-rich conformations, forming thick layers with a high degree of internal charge pairing. In this case, highly organized texture structures were formed on the film surface, as depicted in Fig. 2(b). This loop-rich conformation texture structure film has a large surface area compared with the train conformation film [Fig. 2(a)]. The advantages of these loopy structures are that (1) they have a high deposition speed, (2) they can obtain a large thickness, (3) they have a large rough surface area and (4) they can be applied in air cleaning filters or sensor devices.

4. 3.1 Structural changes of (PAH/PAA)$_5$ films prepared by the dip-LBL method

The (PAH/PAA)$_5$ thin films prepared by the LBL method were fabricated in order to compare them with thin films prepared by the spray-LBL. Figure 3 shows an AFM image of a (PAH/PAA)$_5$ thin film prepared by the conventional dip LBL method. The substrate was first immersed in PAH solution (10 mM, pH 9.5) and rinsed with pure water. The substrate was then transferred to PAA solution (10 mM, pH 5.0) and rinsed with pure water. The surface roughnesses of the prepared (PAH/PAA)$_5$ thin films (a, b, c, and d) were ca. 2.0, 2.6, 3.6, and 3.8 nm, respectively. By comparing Figs. 3(a)-3(d), it was found that for (a) there is no texture structure, whereas for (b) - (d) we can find a

102

clear texture structure. The time of dipping in PAH and PAA is from 1 to 15 min. As a result, when the using the dip LBL method, more than 3 min of dipping was necessary for fabricating the texture structure. The texture structure was not formed on the surface in the case of less than 3 min dipping [Fig. 3(a)]. Even if the dipping time was increased to 15 min, there was almost no change in the surface structure [Figs. 3(b)-3(d)]. This means that there was a limit for the surface structural change even if dipping time was increased. We consider that this is because the adsorption of PAH and PAA saturates within a period of time.

4. 3. 2 Influence of spray solution concentration

Next, the effect of the concentration of spray solution was studied. $(PAH/PAA)_5$ films were prepared by spraying PAH and PAA at 3 ml each. Surface observations by FE-SEM are shown in Fig. 4. As shown in Fig. 4, texture structures were formed when using the spray solution of more than 10 mM. Using the solution of 1 and 5 mM, islandlike structures were formed [Figs. 4(a) and 4(b)]. On the other hand, the width and height of texture structures were increased by increasing the concentration of the spray solution from 10 to 20 mM. By comparing Figs. 4(c) and 4(d), it was demonstrated that the width and height of the texture structures increased because the contrast of the top of the mountainlike structures shown in Fig. 4(d) was higher than that shown in Fig. 4(c). Moreover, the speed of fabricating (PAH/PAA) thin films could be increased by spray-LBL under 10 mM solution condition. As shown in Figs. 3(d) and 4(c), although one-deposition time decreased from 15 to 1 min, the texture structure size is maintained at ca. 110 nm.

Figure 5 shows film thickness as a function of the concentration of spray solution. Thickness was measured using a surface profile measurement system. As a result, the thickness of the (PAH/PAA)$_5$ thin film was increased from ca. 21 to ca. 57 nm (ca. two fold) by increasing the concentration of spray solution from 1 to 20 mM, because the amount of PAH and PAA adsorbed increased with the concentration of spray solution. The adsorption of PAH and PAA was monitored by QCM measurement. The QCM was sprayed with PAH and PAA solutions and dried by air blowing; then resonance frequency was measured. The frequency shift was measured using QCM according to the bilayer number of (PAH/PAA). As shown in Fig. 6, frequency shift gradually increased with the bilayer number of (PAH/PAA). Frequency shift also increased with the concentration of spray solution.

Frequency shift measured using QCM was increased from 1898 to 3118 Hz by changing the concentration of spray solution from 1 to 20 mM. By comparing Figs. 5 and 6, it is clearly demonstrated that the amount of PAH and PAA adsorbed for one layer increased with polymer concentration. We can notice that LBL film thickness can be controlled either by changing the concentration of spray solution or the number of bilayers. Considering film deposition speed, a relatively higher concentration has the advantage; however, it is preferable to change the number of bilayers for precise thickness control.

4. 3. 3 Structural change of (PAH/PAA)$_5$ films prepared by spray-LBL method

We prepared (PAH/PAA) films with changing spray quantity and flow rate. FE-SEM (Fig. 7) and AFM (Fig. 8) images show that the film surfaces had fine porous structures,

which have cluster sizes ranging from 100 to 200 nm. The quantities (1 − 4 ml) of PAH and PAA sprayed on each layer were controlled by keeping the flow rate at the same value (0.05 − 0.1 ml/s). It was found that a peculiar texture structure of (PAH/PAA)$_5$ films was formed, as shown in Figs. 7 and 8, under a variety of spraying conditions. Cluster size was increased by increasing spray quantity and by decreasing flow rate. The texture structure was not formed on the surface when the flow rate was 0.1 ml/s, because the agglomeration time of PAH and PAA decreases with increasing flow rate. Moreover, the amounts of PAH and PAA adsorbed increased with spray solution quantity. Figure 7(a) shows an image of a film fabricated at a small spray quantity and a low flow rate. Although the amount adsorbed was small, since the agglomeration time was long, texture structures were successfully formed. In Fig. 7(i), the flow rate was two times larger than that in Fig. 7(a), and texture structures did not form because the agglomerate time was short. If we compare Figs. 7(a) and 7(d), the spraying quantity was larger for the latter. We found that the cluster size of texture structures increased with the amount of PAH and PAA adsorbed. Cluster size, as shown in Figs. 7(a) to 7(d) increased from ca. 130 to ca. 180 nm.

The effects of spray quantity and flow rate on surface morphology are more clearly seen by AFM than by FE-SEM. Figure 8 shows AFM images of the (PAH/PAA)$_5$ film as a function of flow rate and spray quantity. The results of AFM were very similar to the results of FE-SEM. In these figures of AFM, the changes in the width and height of the texture structure are much clearly demonstrated.

Figure 9 shows the surface RMS roughness and film thickness of the (PAH/PAA)$_5$ film prepared   as a function of flow rate and spray quantity. RMS roughness was calculated according to the following equation:

$$RMS = \sqrt{\frac{\sum(Z_i - Z_{ave})^2}{N}} \ ;$$

(2)

where Z_i is the height on the Z-axis of the feature i, Z_{ave} is the average height of the entire image, and N is the number of points in an image. The RMS roughness of the prepared (PAH/PAA)$_5$ film were from 2 to 24.1 nm and the thickness were from 27 to 138 nm. As flow rate decreased and/or spray quantity increased, the surface roughness of the prepared thin films became large. Film thickness also increased with increasing surface roughness. It was clearly demonstrated that we can control the nanoscale structures and thickness of (PAH/PAA) thin films by the spray-LBL method. For engineering applications of the spray-LBL method, especially for the application of ultrathin films in optical devices, a small surface roughness is required. We can prepare thin films at a high flow rate by the spray-LBL method. Therefore, these films can be applied in optical devices. In contrast, when the flow rate was low, the surface became porous. Therefore, this method at a low flow rate can be applied to fabricating high-surface-area thin films such as air cleaning filters or sensor devices.

We confirmed that the structure and thickness of thin films can be controlled by controlling the concentration of spray solution, spray quantity, and flow rate in the spray-LBL method. A scheme of (PAH/PAA) film growth by the spray-LBL method is shown in Fig. 10.

In an early step, the film was deposited partially appearing like islands structures on the substrate surface [Fig. 10(a)]. Islandlike structures appeared in the film with a thickness of about 30 nm or less. Clusters formed when other clusters aggregated. Then, the film surface became flat with the increase in deposition quantity. The entire substrate surface was covered by the film [Fig. 10(b)]. As film thickness increased, the

(PAH/PAA) film formed texture structures [Fig. 10(c)]. The texture structures were enlarged [Fig. 10(d)] by changing the spray conditions such as concentration, quantity, or flow rate.

4. 4. Conclusions

Nanoscale texture structures of weak polyelectrolyte (PAH/PAA) multilayer films were successfully fabricated by the spray-LBL method. The surface morphology of (PAH/PAA) films was affected by spray solution concentration, spray quantity, and flow rate was determined. By controlling the conditions, it was demonstrated that the nanoscale texture structures can be successfully fabricated by the spray-LBL method. This method can control film thickness and the surface morphology with nm accuracy. Moreover, the speed of fabricating thin films by the spray-LBL method was markedly increased compared with that by the dip-LBL method. By changing spray quantity, flow rate, and concentration in the spray-LBL method, the phase transition for surface structure was discovered for the first time. It is expect that the spray-LBL method will be very useful for the fabrication of functional thin films for optical devices, filters, and sensors, or various surface coatings.
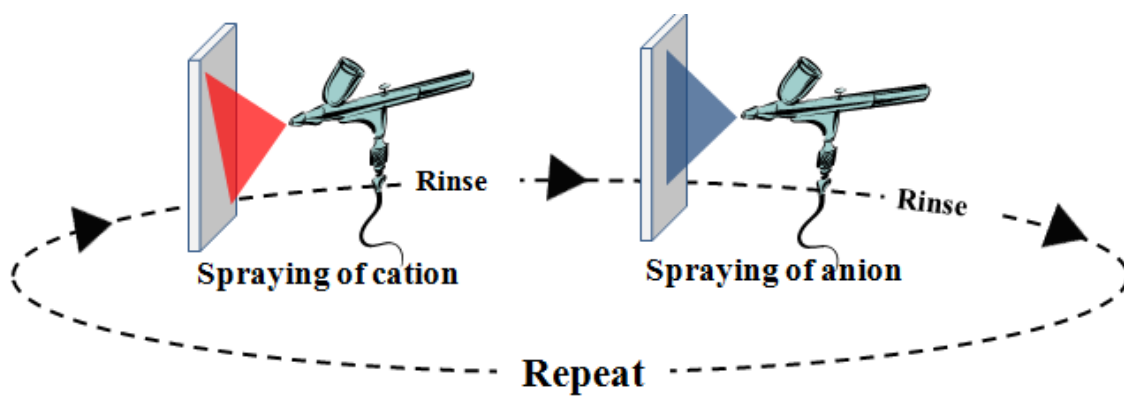
Fig. 1. Schematic illustration of spray layer-by-layer (spray-LBL) method.
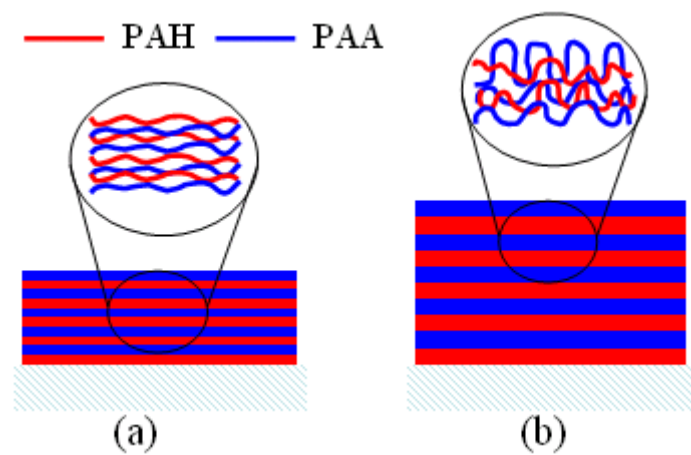
Fig. 2. Schematic illustration of (a) train conformation (PAH/PAA) films and (b) loop-rich conformation (PAH/PAA) films.
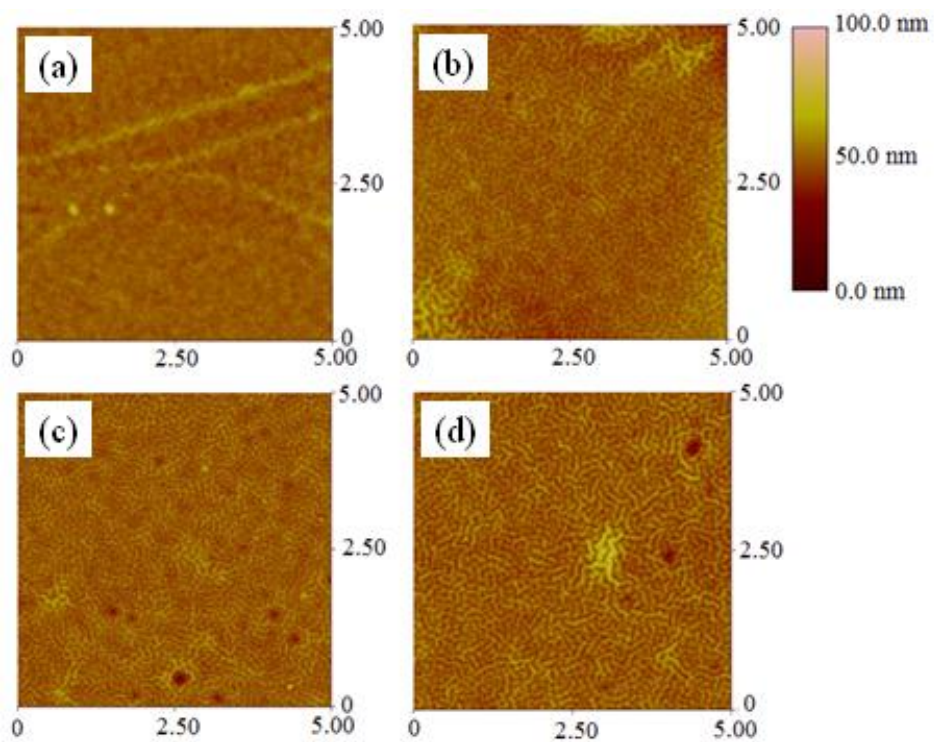
Fig. 3. AFM (top view; 5×5 µm^2) images of (PAH$_{9.5}$/PAA$_{5.0}$)$_5$ film prepared by LBL method as a function of dipping time: (a) 1, (b) 3, (c) 7, and (d) 15 min.
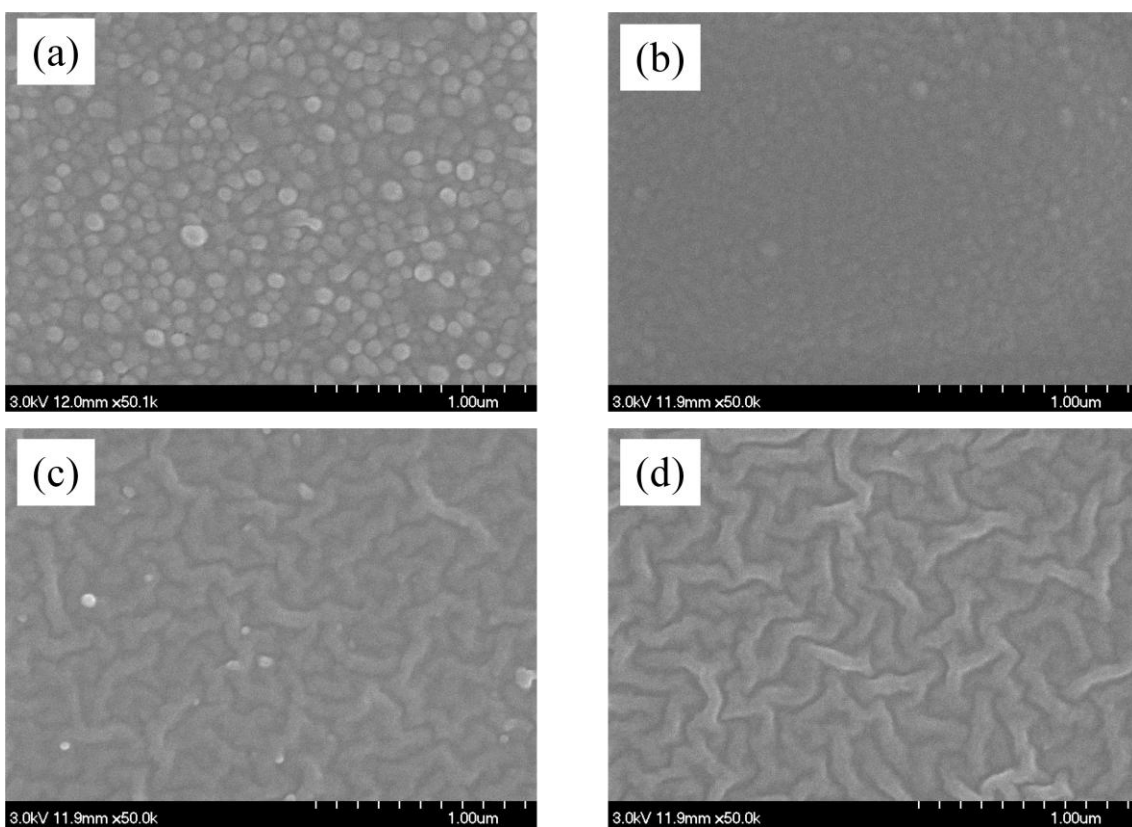
Fig. 4. FE-SEM images of $(PAH_{9.5}/PAA_{5.0})_5$ film as a function of concentration of spray solution: (a) 1, (b) 5, (c) 10, and (d) 20 mM.
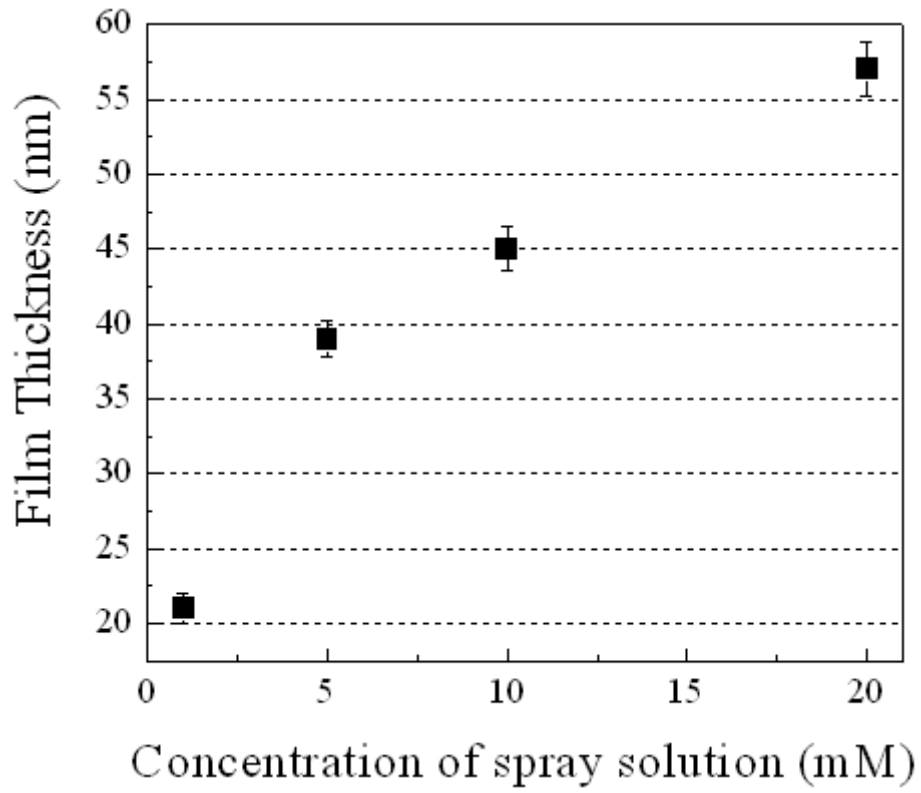
Fig. 5. Thickness of $(PAH_{9.5}/PAA_{5.0})_5$ film as a function of concentration of spray solution.
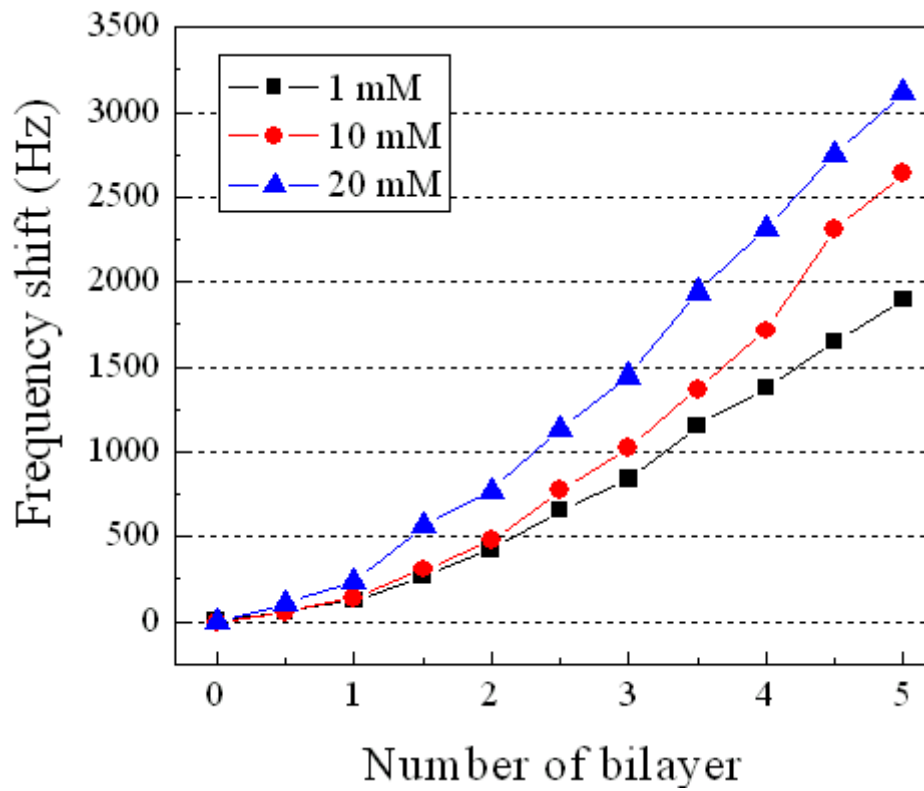
Fig. 6. QCM frequency shift of $(PAH_{9.5}/PAA_{5.0})_5$ film as a function of concentration of spray solution.
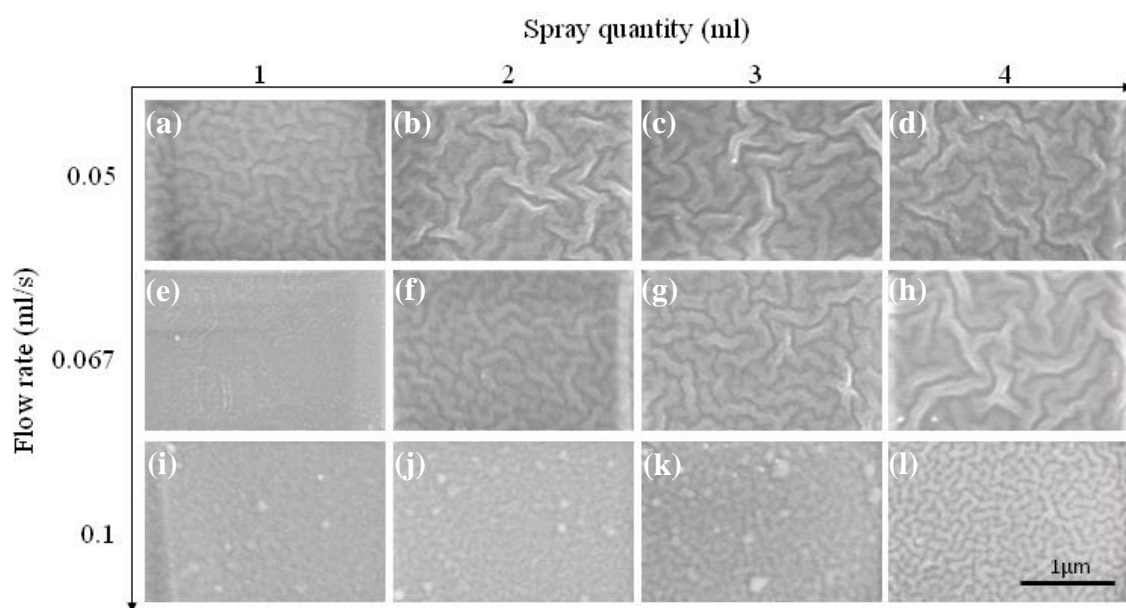
Fig. 7. FE-SEM images of $(PAH_{9.5}/PAA_{5.0})_5$ film as a function of flow rate and spray quantity.
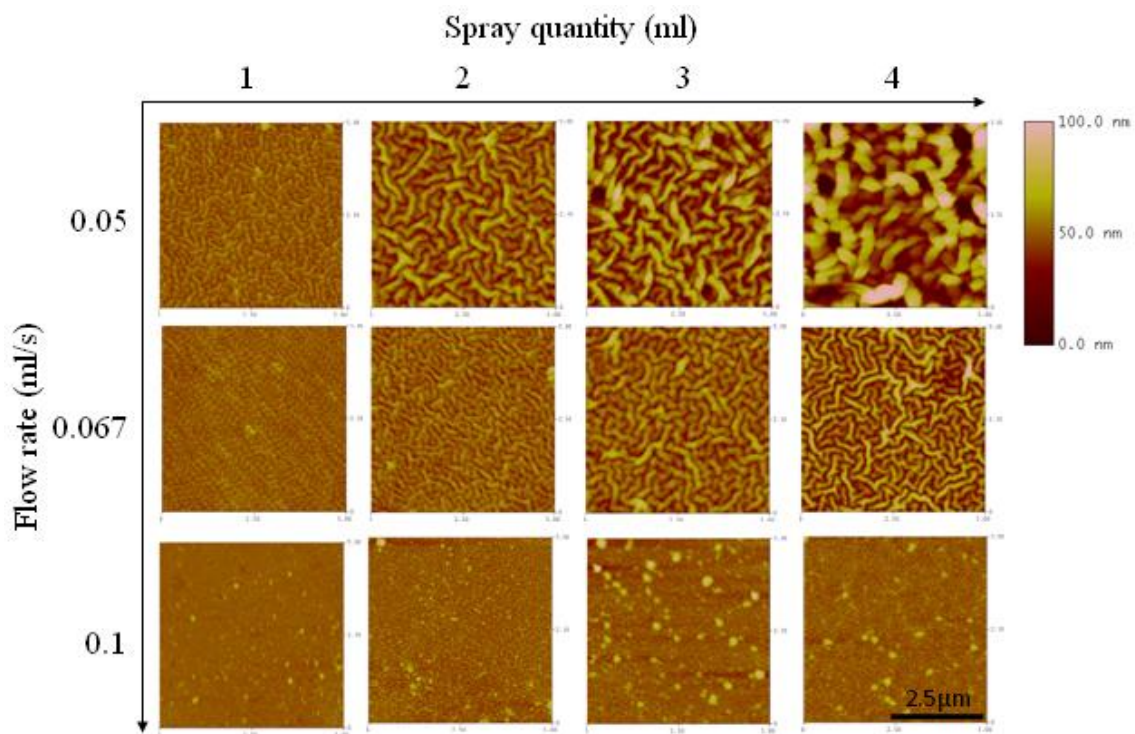
Fig. 8. AFM (top view; $5 \times 5 \ \mu m^2$) images of (PAH$_{9.5}$/PAA$_{5.0}$)$_5$ film as a function of flow rate and spray quantity.
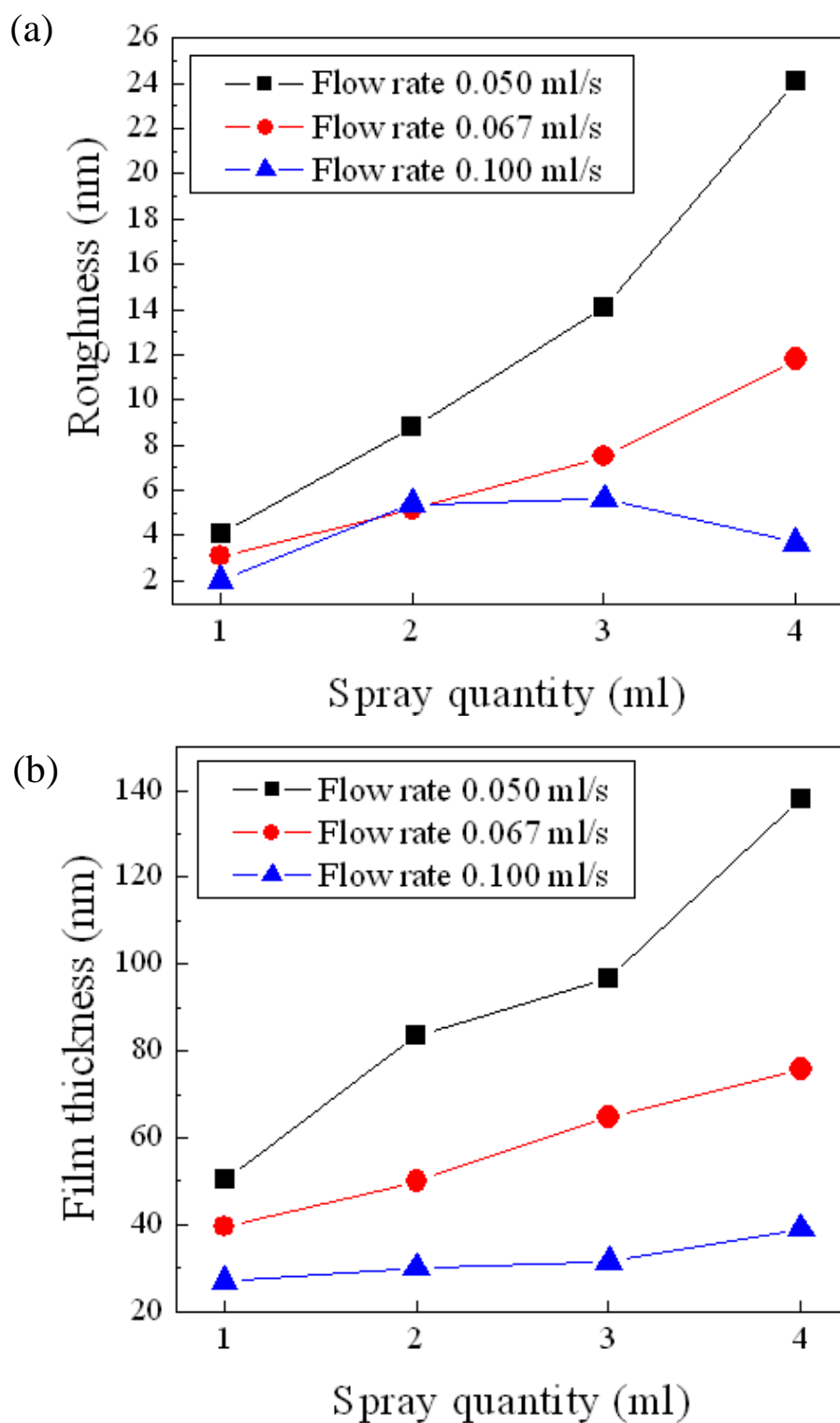
Fig. 9. Surface roughness (a) and thickness (b) of $(PAH_{9.5}/PAA_{5.0})_5$ film as a function of flow rate and spray quantity.
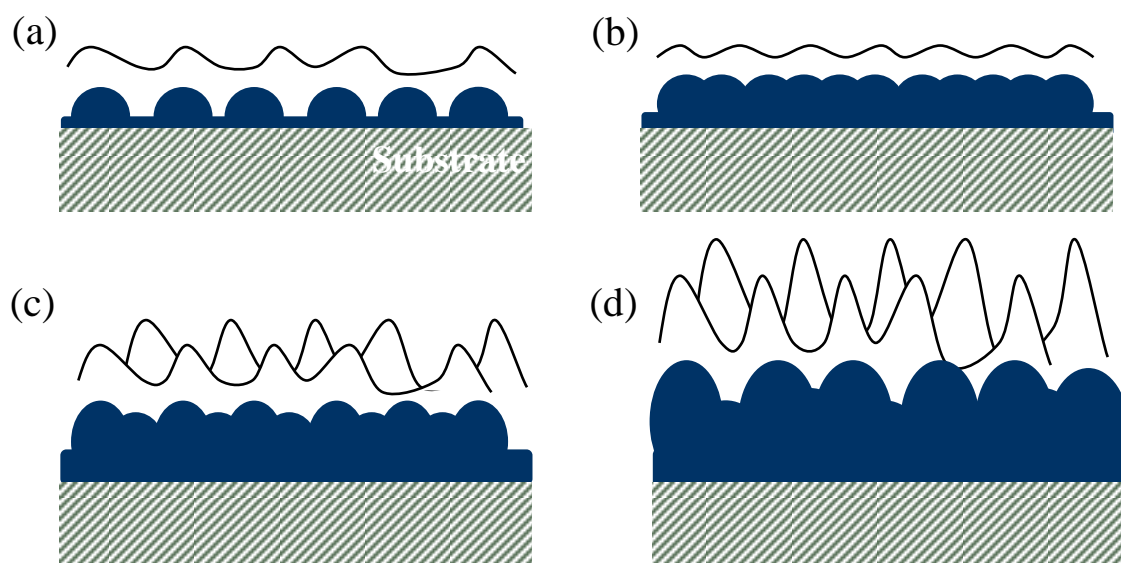
Fig. 10. Schematic illustrations of film growth by spray layer-by-layer (spray-LBL) method: (a) islandlike adsorption, (b) surface coverage, (c) formed texture structure, and (d) growth of mountainlike texture structure.

Reference

[4-1] S. Shiratori and M. F. Rubner: Macromolecules 33 (2000) 4213.

[4-2] J. D. Mendelsohn, C. J. Barrett, V. V. Chan, A. J. Pal, A. M. Mayes, and M. F. Rubner: Langmuir 16 (2000) 5017.

[4-3] S. Fujita S. Shiratori: Nanotechnology 16 (2005) 1821.

[4-4] W. Zhao, J. J. Xu, and H. Y. Chen: Electroanal. 18 (2006) 1737.

[4-5] K. H. H. Peter, J. S. Kim, J. H. Burroughes, H. Becker, F. Y. L. Sam, T. M. Brown, F. Cacialli, and R. H. Friend: Nature (London) 404 (2000) 481.

[4-6] K. Ariga, J. P. Hill, and Q. Ji: Phys. Chem. Chem. Phys. 9 (2007) 2319.

[4-7] F. Caruso, R. A. Caruso, and H. Moehwald:. Science 282 (1998) 1111.

[4-8] S. C. Olugebefola, W. A. Kuhlman, M. F. Rubner, and A. M. Mayes: Langmuir 24 (2008) 5172.

[4-9] M. Nolte and A. Fery: Nanobiotechnol 153 (2006) 112.

[4-10] F. Caruso and C. Schüler: Langmuir 15 (2000) 9595.

[4-11] S. T. Dubas, T. R. Farhat, and J. B. J. Schlenoff: Am. Chem. Soc. 123 (2001) 5368.

[4-12] A. M. Balachandra, J. Dai, and M. L. Bruening: Macromolecules 35 (2002) 3171.

[4-13] J. Dai, A. M. Balachandra, J. I. Lee, and M. L. Bruening: Macromolecules 35 (2002) 3164.

[4-14] D. M. Sullivan and M. L. J. Bruening: Am. Chem. Soc. 123 (2001) 11805.

[4-15] C. S. Peyratout and L. Daehne: Angew. Chem. Int. Ed. 43 (2004) 3762.

[4-16] F. Caruso, R. A. Caruso, and H. Möhwald: Science 282 (1998) 1111.

[4-17] F. Caruso, H. Lichtenfeld, H. Möhwald, and M. J. Giersig: Am. Chem. Soc. 120 (1998) 8523.

[4-18] F. Caruso and H. Möhwald: Am. Chem. Soc. 121 (1999) 6039.

[4-19] F. Caruso, H. Lichtenfeld, E. Donath, and H. Möhwald: Macromolecules 32 (1999) 2317.

[4-20] F. Caruso, X. Shi, R. A. Caruso, and A. Susha: Adv. Mater. 13 (2001) 740.

[4-21] F. Caruso, M. Spasova, V. Salgueiriño-Maceira, and L. M. Liz-Marzán: Adv. Mater. 13 (2001) 1090.

[4-22] D. I. Gittins, A. S. Susha, B. Schoeler, and F. Caruso: Adv. Mater. 14 (2002) 508.

[4-23] Y. Lvov, K. Ariga, M. Onda, I. Chinose, and T. Kunitake: Langmuir 13 (1997) 6195.

[4-24] P. Chrysicopoulou, D. Davazoglou, C. Trapalis, and G. Kordas: Thin Solid Films 323 (1998) 188.

[4-25] M. Takeuchi, T. Itoh, and H. Nagasaka: Thin Solid Films 51 (1978) 83.

[4-26] K. S. Yeung and Y. W. Lam: Thin Solid Films 109 (1983) 169.

[4-27] G. Decher and J. D. Hong: Macromol. Chem. Macro. Symp. 46 (1991) 321.

[4-28] J. B. Schlenoff, S. T. Dubas, and T. Farhat: Langmuir 16 (2000) 9968.

[4-29] A. Izquierdo, S. Ono, J. C. Voegel, P. Schaaf, and G. Decher: Langmuir 21 (2005) 7558.

[4-30] K. Krogman, N. Zacharia, S. Schroeder, and P. Hammond: Langmuir 23 (2007) 3137.

[4-31] C. Lu, I. Dönch, M. Nolte, and A. Fery: Chem. Mater. 18 (2006) 6204.

[4-32] O. Félix, Z. Zheng, F. Cousin, and G. Decher: C. R. Chimie 12 (2009) 225.

[4-33] N. Laugel, J. Hemmerle, C. Porcel, J. C. Voegel, P. Schaaf, and V. Ball:

Langmuir 23 (2007) 3706.

[4-34] S. S. Ono and G. Decher: Nano Lett. 6 (2006) 592.

[4-35] X. Zhao, C. Hinchliffe, C. Johnston, P. J. Dobson, S. Patrick, and P. S. Grant: Mater. Sci. and Eng. B 151 (2008) 140.

[4-36] C. H. Porcel, A. Izquierdo, V. Ball, G. Decher, J. C. Voegel, and P. Schaaf: Langmuir 21 (2005) 800.

[4-37] J. Cho, K. Char, J. D. Hong, and K. B. Lee: Adv. Mater. 13 (2001) 1076.

[4-38] C. Jiang, S. Markutsya, and V. V. Tsukruk: Adv. Mater. 16 (2004) 157.

[4-39] M. S. Johal, J. L. Casson, P. A. Chiarelli, D. G. Liu, J. A. Shaw, J. M. Robinson, and H. L. Wang: Langmuir 19 (2003) 8876.

[4-40] M. H. Merrill and C. T. Sun: Nanotechnology 20 (2009) 075606.

[4-41] C. Jiang, X. Wang, R. Gunawidjaja, Y. H. Lin, M. K. Gupta, D. L. Kaplan, R. R. Naik, and V. V. Tsukruk: Adv. Funct. Mater. 17 (2007) 2229.

[4-42] B. S. Shim, P. Podsiadlo, D. G. Lilly, A. Agarwal, J. Lee, Z. Tang, S. Ho, P. Ingle, D. Psterson, W. Lu, and N. A. Kotov: Nano Lett. 7 (2007) 3266.

[4-43] J. D. Mendelsohn, S. Y. Yang, J. Hiller, A. I. Hochbaum, and M. F. Ruber: Biomacromolecules 4 (2003) 96.

[4-44] J. Y. Choi, and M. F. Rubner: J. Macromol. Sci.-Pure Appl. Chem. A 38 (2001) 1191.

CHAPTER 5

Control of structure and film thickness using spray layer-by-layer method for application to double-layer anti-reflection film

5. 1 Introduction

Anti-reflection (AR) films have numerous applications in optical and display devices [1] such as cathode ray tubes (CRTs), plasma display panels (PDPs), and liquid crystal displays (LCDs). For example, Rubner and coworkers introduced an AR thin film consisting of polyelectrolytes by controlling the porosity and thickness of a multilayer thin film using the LBL self-assembly method. [2] Shimomura et al. reported the fabrication of uniform, conformal multistack nanoparticle thin films for optical applications with precise thickness control over each stack using the electrostatic layer-by-layer assembly method. [3] In particular, for AR films, the uniformity of the film and the precise control of film thickness and refractive index are essential. The advantage of double-layer anti-reflectance films is that they have higher transmittance and lower reflectance than single-layer anti-reflectance films. Double-layer AR coatings [3-6] consisting of low- and high-refractive-index layers on a substrate have been researched to increase the efficiency of the AR range. The best AR efficiency is determined by the index obtained from the following equations: [7-8]

$$n_1^3 = n_0^2 n_s \text{ and } n_2^3 = n_0 n_s^2, \tag{1}$$

where n_0 and n_s are the refractive indices of air and the substrate, respectively, and n_1 and n_2 are the refractive indices of the first layer with a low refractive index and

the second layer with a high refractive index, respectively. Therefore, n_2 is equal to n_1^2.

In addition, the thickness of each layer is determined by the following equation:

$$d = \frac{1}{n} \times \frac{\lambda}{4} \; .$$
(2)

The high- and low-refractive-index layers of a multilayer optical film depend on the elemental properties of the materials. Therefore, the film thickness was adjusted to $\lambda/4n$ by repeating the deposition process.

Multilayer films fabricated by the LBL method were built up to nanoscale order film thickness and morphology on a three-dimensional substrate. The LBL method is based on the alternate adsorption of oppositely charged materials in aqueous solutions via electrostatic attraction. [9-11] The LBL method has lots of advantages such as a simple process, water based room-temperature deposition at normal pressure, no limit of thickness, and no need for complicated equipment. [12-13] In addition, the thickness of the thin film can be controlled with nanoscale accuracy. [14-16] Although this method has many advantages, it requires long fabrication time. Furthermore, this technique is also wasteful, limiting its practicality in manufacturing. Because the process is driven in part by diffusion, LBL cycles usually take on the order of several minutes to complete. This presents unacceptable demerits if this technology is to evolve into industrial applications. Several LBL modifications have been proposed recently, including spray-LBL, [17-25] spin-assisted LBL, [26-30] or dewetting-LBL (d-LBL). [31] The recently developed practice of spraying solutions onto a substrate to fabricate thin films via the LBL method has been further investigated and extended.

Recently, we have reported that texture-type nanostructure was successfully fabricated by the spray-LBL method. [32] By controlling the conditions such as spray solution concentration, spray quantity, and flow rate, it was demonstrated that the

nanoscale texture structures can be successfully fabricated by the spray-LBL method. This method can control film thickness and the surface morphology with nm accuracy.

In this study, the fabrication of a double-layer AR film with controlled film thickness and structure by the spray-LBL method was studied. An AR film by depositing a low-refractive-index layer consisting of (PAH/PAA)$_7$ and a high-refractive-index layer composed of (PDDA/TALH)$_{10}$ by spray-LBL while controlling the thickness and roughness of the thin film was fabricate.

5. 2. Experimental Procedure

5.2.1 Materials

Poly(diallyldimethylammonium chloride) (PDDA; M_W = 200,000 – 300,000, 20 wt% in water) and poly(allylamine hydrochloride) (PAH; M_W = 70,000) were obtained from Aldrich as positively charged solutions. Titanium(IV) bis(ammonium lactato) dihydroxide (TALH; 50 wt%) with double negative charges and poly(acrylic acid) (PAA; M_W = 100,000, 25% aqueous solution) were obtained from Aldrich as negatively charged solutions. All materials were used without any further purification. The concentration of PDDA was adjusted to 25 mM, those of PAH and PAA were adjusted to 10 mM and that of TALH was adjusted to 1.0 wt% with ultrapure water (>18 MΩcm). TALH, PAH, and PAA solutions were adjusted to pH 3.5, 9.5, and 5.0 with HCl or NaOH. PDDA solution was used without pH adjustment.

5.2.2 Preparation of thin films

The high-refractive-index layer was fabricated using the PDDA and TALH solutions. PAH and PAA solutions were used for the low-refractive-index layer. Figure 1(a) shows the chemical structures of PDDA, TALH, PAH, and PAA.

The glass and Ag quartz crystal microbalance (QCM) substrates were ultrasonically agitated in KOH solution (1.0 wt%) mixed with ultrapure water and ethanol (2:3 in volume ratio) for 5 min and then rinsed with ultrapure water. By this treatment, negatively charged substrates were prepared.

Double-layer anti-reflection (AR) films with high- and low-reflective-index layers were successfully fabricated by the spray-LBL method. Figure 1(b) shows a schematic diagram of the prepared AR film. For the high-refractive-index layer, PDDA solution was sprayed onto the negatively charged substrate. Then, it was rinsed for 20 s with pure water. Positively charged substrates formed by the spraying of PDDA solution were subsequently sprayed with a negatively charged solution of TALH and then the same rinsing procedures were carried out. This cycle was repeated. The low-refractive-index layer was formed by the same procedures as for the high-refractive-index layer.

5.2.3 Characterization of thin films

A QCM device was used to determine the deposited mass after each adsorption step. The resonance frequency of the QCM electrodes was 10 MHz. The piezoelectric quartz crystal changes its fundamental oscillation frequency as mass is deposited onto or

depleted from the surface. Thin films were built up on glass slide substrates. Thin films on glass slides were scratched with a razor blade to form lines. By profiling, the average value of three measurements was chosen to represent the thickness of the thin film. Film thickness was investigated using a surface profile measurement system (Salon DEKTAK 3030). Surface morphology was investigated by field emission scanning electron microscopy (FE-SEM; Hitachi S-4700). The transmittance and reflectance of the prepared thin films deposited on glass were measured using an ultraviolet-visible (UV-vis) spectrophotometer (Shimadzu UV mini-1240) and a reflectance meter (Olympus USPM-RM)m respectively.

5. 3. Results and Discussion

The adsorptions of (PDDA/TALH) and (PAH/PAA) were monitored by QCM measurement. The QCM was sprayed with cation (PDDA and PAH) and anion (TALH and PAA) solutions, dried by air blowing, and then the resonance frequency was measured. The frequency shift of the QCM was measured according to the number of bilayers of (PDDA/TALH) and (PAH/PAA).

Figure 2 shows the frequency shift as a function of the number of layers of (PDDA/TALH) and (PAH/PAA). As shown in Fig. 2, the frequency shift was regularly increased according to the bilayer number of (PDDA/TALH) and (PAH/PAA). The frequency shifts for the deposition of one layer of (PDDA/TALH) and (PAH/PAA) were about 630 and 410 Hz, respectively. As a result, we confirmed the successful deposition of (PDDA/TALH) and (PAH/PAA) by the spray-LBL method. Since the density of TALH is higher than that of polymers such as PDDA, PAH, PAA, the frequency change

of TALH adsorption has a steeper pitch than those of the three polymers. This high mass adsorption of the material including Ti leads to the formation of the high-refractive-index layer during the spray-LBL deposition.

The (PDDA/TALH) film growth was followed by UV-vis measurement. Figure 3 shows the absorbance of the composed (PDDA/TALH) film as a function of the number of bilayers and represents the absorbance characteristics at 460 nm. The absorbance linearly increased with the increase in the number of bilayers. As shown in the figure, the absorbance of UV-vis data is in good accordance with the frequency shift of QCM data. The gradual formation of the high-refractive-index layer successfully proceeded with the increase in the number of layers formed by the spray-LBL.

Figure 4 shows the transmittance and thickness of the prepared high-refractive-index layer (PDDA/TALH) film and low-refractive-index layer (PAH/PAA) film deposited on one side of a slide glass. The thicknesses of the (PDDA/TALH) and (PAH/PAA) films were regularly increased by increasing the number of bilayers. The average thicknesses of (PDDA/TALH) and (PAH/PAA) films were determined to be ca. 7 and ca. 14 nm, respectively. This means that the thickness of the films was well controlled by the spray-LBL method. Although the thickness of the film is increased, the transmittance was almost the same. The experimental results show that for the high-refractive-index layer, the control of the surface roughness was successfully achieved and indicate that the formation of aggregated particles during the film deposition was prevented. On the other hand, for the low-refractive-index layer, the experimental results indicate that the formation of the texture did not have an effect on the transparency of the film.

A double-layer AR film was fabricated on one side of a slide glass by the spray-LBL method. The AR film was composed of a double layer of a high-refractive-index layer

and a low-refractive-index layer. The AR film was formed by depositing a low-refractive-index layer consisting of (PAH/PAA)$_7$ and a high-refractive-index layer composed of (PDDA/TALH)$_{10}$ by the spray-LBL method while controlling the thickness and roughness of the thin film.

Table I shows the film thickness and refractive index of the prepared high- and low-refractive-index layers deposited on the glass ($n = 1.53$). From these results, the film thickness and refractive index of the high-refractive-index layer (PDDA/TALH)$_{10}$ film are 75.3 ± 4 nm and 1.75 at 550 nm, respectively, and those of the low-refractive-index layer (PAH/PAA)$_7$ are 90 ± 3 nm and 1.48 at 550 nm.

The optical properties of the prepared AR film were determined by the results of measurement of the transmittance and reflectance. Figure 5 shows the reflectance and transmittance of the prepared AR films and the glass substrate. As shown in this figure, the highest transmittance in the visible range is 94.5% and the lowest reflectance of the film is 0.5%. This film has AR properties because the transmittance of the prepared (PDDA/TALH)$_{10}$/(PAH/PAA)$_7$ film was increased approximately 3.1% at 550 nm and the reflectance was decreased approximately 3.3% at 550 nm compared with the glass substrates. During the transmittance increase and reflectance decrease, there is a 0.22% difference in the transmittance and reflectance. This 0.22% is the loss due to light scattering and absorption by the change of surface structure. These results of transmittance and reflectance are not good enough yet, as the results are based on the one side coating on the glass substrate. It is expect them to be better when both sides are coated.

Figure 6 shows FE-SEM images of the prepared AR film. Figure 6(a) shows an FE-SEM image of the high-refractive-index layer (PDDA/TALH)$_{10}$ film. As shown in

127

the figure, TiO$_2$ small crystals approximately 40 – 100 nm in diameter were observed on the surface. As depicted in Fig. 6(b), FE-SEM characterization reveals that the low-refractive-index layer (PAH/PAA)$_7$ film exhibits a porous texture structure. The FE-SEM image of the cross-sectional view of the prepared double-layer AR film with the coating sequence of (PDDA/TALH)$_{10}$/(PAH/PAA)$_7$ is shown in Fig. 6(c). As shown in the figure, it is clear that the prepared film consisted of a double layer. The film thicknesses of the high- and low-refractive-index layer layers were 70 – 80 and 90 – 100 nm, respectively. This result is the same as the film thickness shown in Fig. 4.

5. 4. Conclusions

Double-layer AR films by depositing a high-refractive-index layer composed of (PDDA/TALH)$_{10}$ and a low-refractive-index layer consisting of (PAH/PAA)$_7$ by the spray-LBL method while controlling the thickness and roughness of the thin film was successfully fabricated. This AR thin film showed the maximum transmittance (94.5%) and the minimum reflection (0.5%) at approximately 550 nm in wavelength. Moreover, the deposition speed was increased by more than 10 times compared with the conventional LBL method, while keeping the optical characteristics of the films. It is expect that this will be very useful for fabrication of the functional thin films by the spray-LBL method for various surface coatings etc.
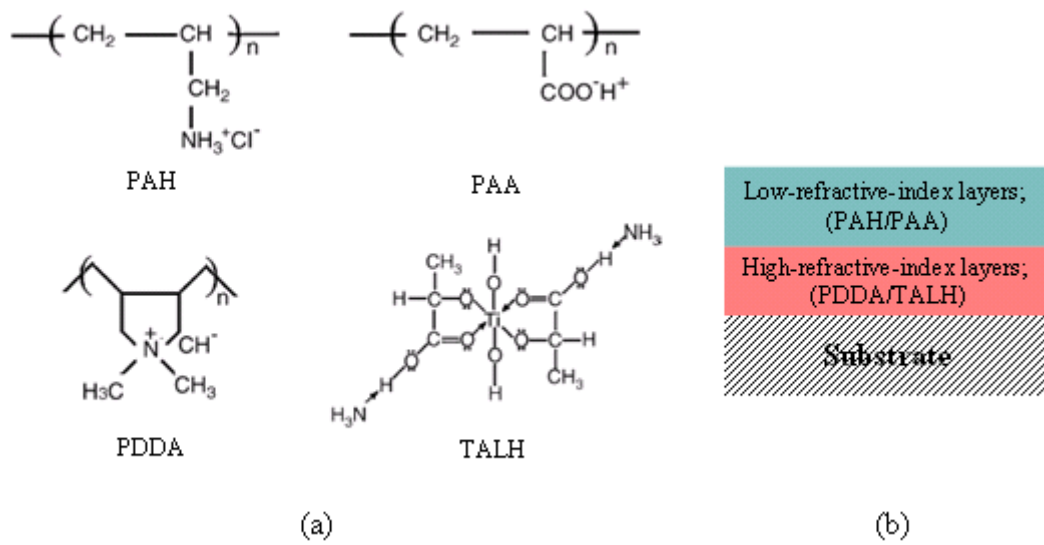
Fig. 1. (Color online) (a) Chemical structures of PDDA, TALH, PAH, and PAA. (b) Schematic diagram of prepared AR film.
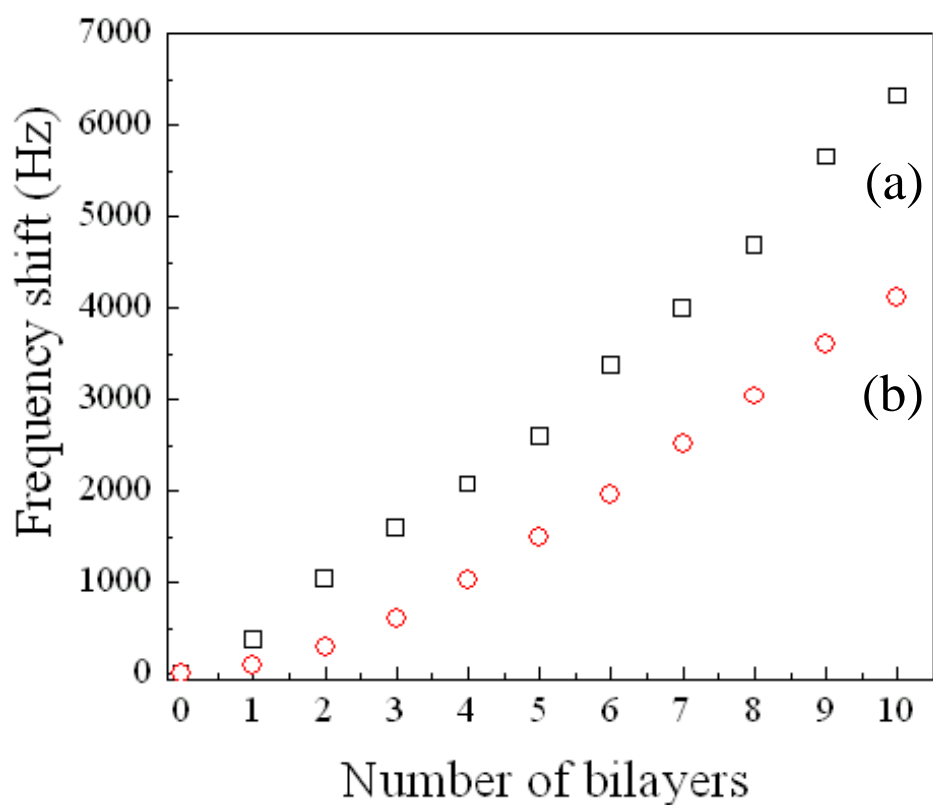
Fig.2. QCM frequency shift of (a) (PDDA/TALH) and (b) (PAH/PAA) films as a function of the number of bilayers.
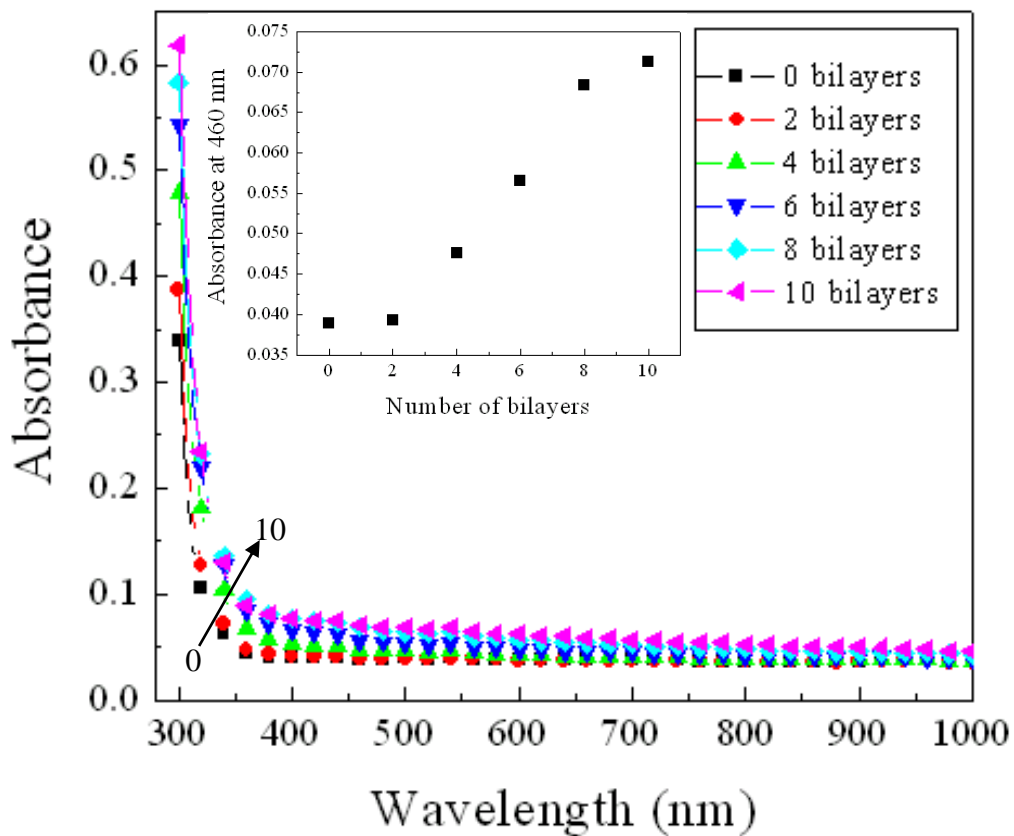
Fig. 3. (Color online) Absorbance of (PDDA/TALH) film and the absorbance characteristics at 460 nm as a function of the number of bilayers.
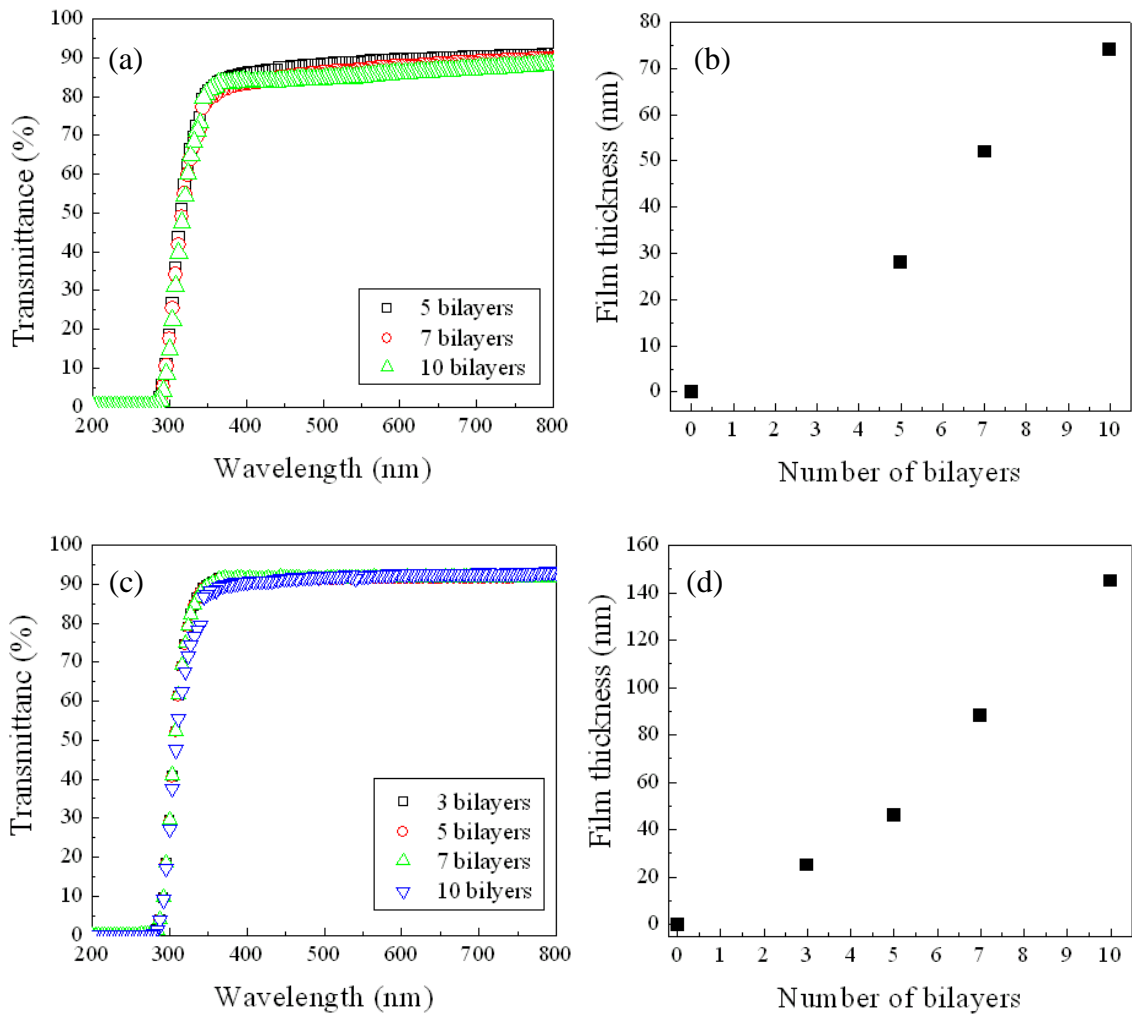
Fig. 4. (Color online) (a) Transmittance and (b) film thickness of prepared high-refractive-index layer (PDDA/TALH) film and (c) transmittance and (d) film thickness of prepared low-refractive-index layer (PAH/PAA) film deposited on a slide glass.

Table I. Film thickness and refractive index of high-refractive-index layer and low-refractive-index layer deposited on a glass substrate ($n = 1.53$).

(PDDA/TALH)$_{10}$ High-n layer		(PAH/PAA)$_7$ Low-n layer	
d (nm)	n	d (nm)	n
75.3 ± 4	1.75	90 ± 3	1.48

The refractive index and film thickness were estimated coated on a slide glass at $\lambda = 550$ nm using a reflectance meter (USPM-RU Olympus).
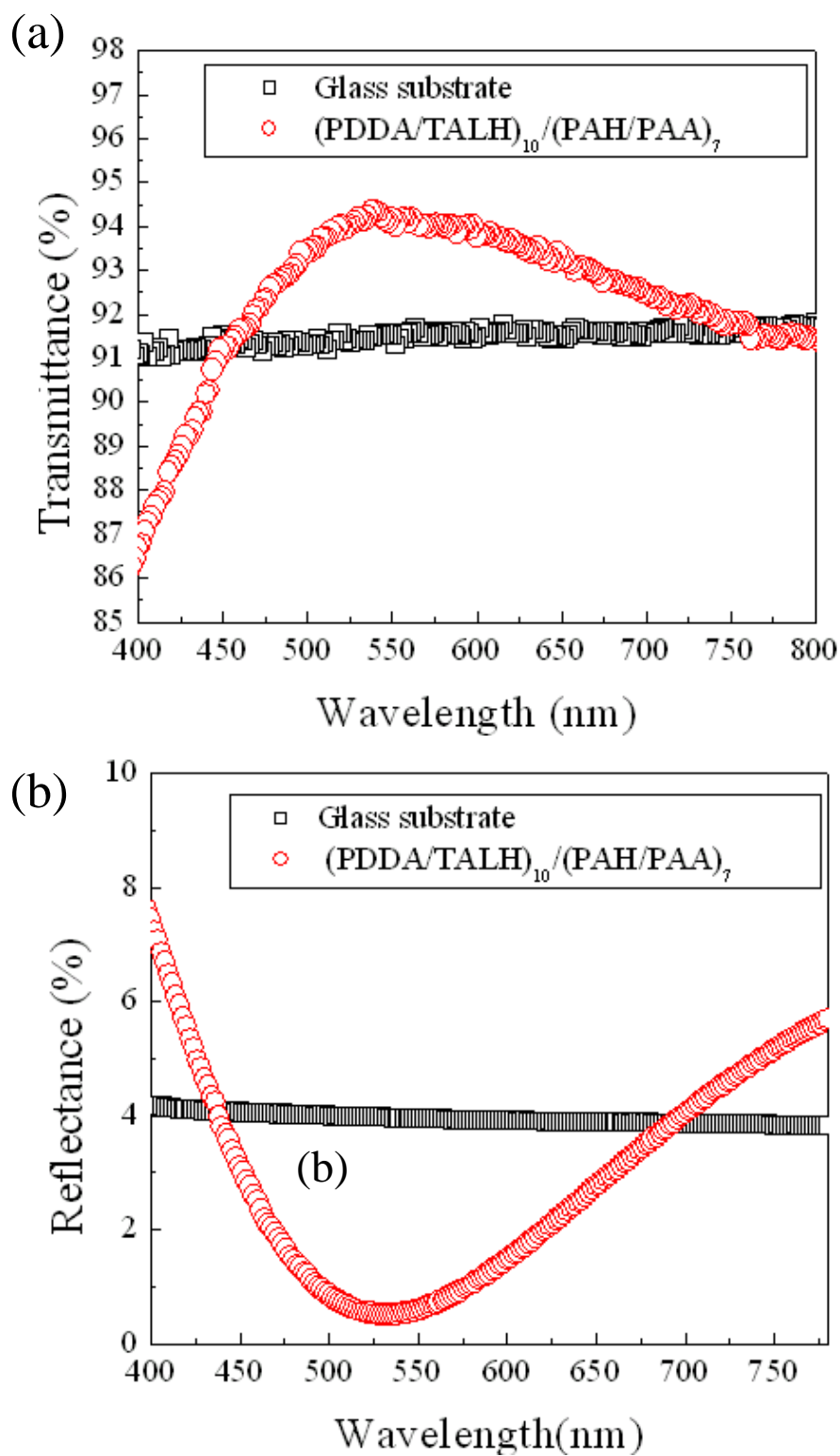
Fig. 5. (Color online) (a) Transmittance and (b) reflectance of the prepared film deposited on slide glass.

134
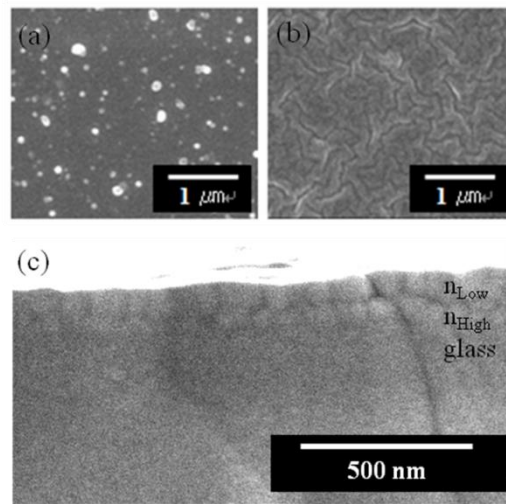
Fig. 6. FE-SEM image of prepared film: (a) high-refractive-index layer (PDDA/TALH)$_{10}$, (b) low-refractive-index layer (PAH/PAA)$_7$, and (c) the cross-sectional image of the interface between the high-refractive-index layer and the low-refractive-index layer : (PDDA/TALH)$_{10}$/(PAH/PAA)$_7$.

References

[5-1] J. Sczybowski, G. Bräuer, G. Teschner, and A. Zmelty: Surf. Coat. Technol. 98 (1998) 1460.

[5-2] J. Hiller, J. D. Mendelsohn, and M. F. Rubner: Nat. Mater. 1 (2002) 59.

[5-3] H. Shimomura, Z. Gemici, R. E. Cohen, and M. F. Rubner: Appl. Mater. Interfaces 2 (2010) 813.

[5-4] B. A. Moys: Thin Solid Films 21 (1974) 145.

[5-5] J. H. Kim, S. Fujita, and S. Shiratori: Colloids Surf. A 284-285 (2006) 290.

[5-6] C. Martinet, V. Paillard, A. Gagnaire, and J. Joseph: J. Non-Cryst. Solids 216 (1997) 77.

[5-7] H. A. Macleod: Thin-Film Optical Filters (Elsevier, New York, 1969).

[5-8] F. Abeles: Ann. Phys. 5 (1950) 706.

[5-9] G. Decher and J. Schmitt: Prog. Colloid Polym. Sci. 89 (1992) 160.

[5-10] Y. Lvov, K. Ariga, M. Onda, I. Ichinose, and T. Kunitake: Langmuir 13 (1997) 6195.

[5-11] B. G. De. Geest, N. N. Sanders, G. B. Sukhorukov, J. Demeestera, and S. C. De Smedt: Chem. Soc. Rev. 36 (2007) 636.

[5-12] G. Decher: Science 277 (1997) 1232.

[5-13] Y. Wang, A. S. Angelatos, and F. Caruso: Chem. Mater. 20 (2008) 848.

[5-14] S. Shiratori, T. Ito, and T. Yamada: Colloids Surf. A 198 (2002) 415.

[5-15] K. Ariga, J. P. Hill, M. V. Lee, A. Vinu, R. Charvet, and S. Acharya: Sci. Technol. Adv. Mater. 9 (2008) 014109.

[5-16] K. Ariga, J. P. Hill, and Q. Ji: Phys. Chem. Chem. Phys. 9 (2007) 2319.

[5-17] J. B. Schlenoff, S. T. Dubas, and T. Farhat: Langmuir 16 (2000) 9968.

[5-18] A. Izquierdo, S. Ono, J. C. Voegel, P. Schaaf, and G.. Decher: Langmuir 21 (2005) 7558.

[5-19] K. Krogman, N. Zacharia, S. Schroeder, and P. Hammond: Langmuir 23 (2007) 3137.

[5-20] C. Lu, I. Dönch, M. Nolte, and A. Fery: Chem. Mater. 18 (2006) 6204.

[5-21] O. Félix, Z. Zheng, F. Cousin, and G. Decher: C. R. Chimie 12 (2009) 225.

[5-22] N. Laugel, J. Hemmerle, C. Porcel, J. C. Voegel, P. Schaaf, and V. Ball: Langmuir 23 (2007) 3706.

[5-23] S. S. Ono and G. Decher: Nano Lett. 6 (2006) 592.

[5-24] X. Zhao, C. Hinchliffe, C. Johnston, P. J. Dobson, S. Patrick, and P. S. Grant: Mater. Sci. Eng. B 151 (2008) 140.

[5-25] C. H. Porcel, A. Izquierdo, V. Ball, G. Decher, J. C. Voegel, and P. Schaaf: Langmuir 21 (2005) 800.

[5-26] J. Cho, K. Char, J. D. Hong, and K. B. Lee: Adv. Mater. 13 (2001) 10766.

[5-27] C. Jiang, S. Markutsya, and V. V. Tsukruk: Adv. Mater. 16 (2004) 157.

[5-28] M. S. Johal, J. L. Casson, P. A. Chiarelli, D. G. Liu, J. A. Shaw, J. M. Robinson, and H. L. Wang: Langmuir 19 (2003) 8876.

[5-29] M. H. Merrill and C. T. Sun: Nanotechnology 20 (2009) 7.

[5-30] C. Jiang, X. Wang, R. Gunawidjaja, Y. H. Lin, M. K. Gupta, D. L. Kaplan, R. R. Naik, and V. V. Tsukruk: Adv. Funct. Mater. 17 (2007) 2229.

[5-31] B. S. Shim, P. Podsiadlo, D. G. Lilly, A. Agarwal, J. Lee, Z. Tang, S. Ho, P. Ingle, D. Psterson, W. Lu, and N. A. Kotov: Nano Lett. 7 (2007) 3266.

[5-32] K. H. Kyung and S. Shiratori: to be published in Jpn. J. Appl. Phys.

CHAPTER 6

Summary

I. Establishment of experimental condition for fabrication of TiO$_2$ thin film and application to anti-reflective by layer-by-layer method
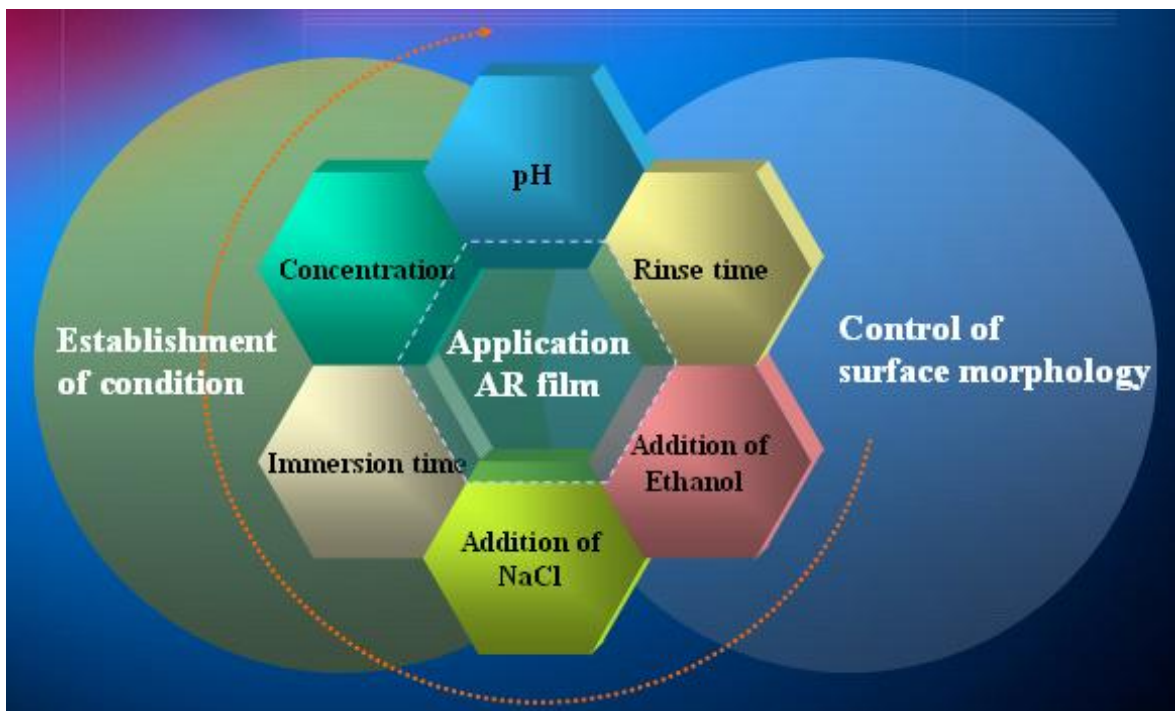
There are many different techniques used for depositing thin films: sol-gel method, sputtering, chemical vapor deposition (CVD), and other chemical deposition methods. Various techniques for fabrication of thin film are presented in Chapter 1. The Layer-by-layer (LBL) method in techniques for the thin film is based on the alternate adsorption of oppositely charged materials in aqueous solutions via electrostatic attraction. The LBL method has been paid much attention to the manufacture of multilayers thin films because the LBL method is very simple, environmentally friendly, and low-cost technique and does not need a vacuum system as well as other complete

apparatus. Though this method has many advantages, it requires long fabrication time. Because the process is driven in part by diffusion, LBL cycles usually take on the order of several minutes to complete. This presents unacceptable demerits if this technology is to evolve into industrial applications.

Over the past several decades, titanium oxide (TiO_2) has been widely used in various forms in various field applications. The TiO_2 thin film is a promising candidate for such varied applications owing to its high refractive index, high relative dielectric constant, remarkable solar energy conversion, and ability for photocatalysis. Titanium(IV) bis(ammonium lactate) dihydroxide (TALH) is relatively stable at ambient temperature in neutral solutions, which makes it an ideal precursor for the fabrication of titania-based thin films from aqueous solutions. Recently, optical thin films fabricated using a water-based process have been strongly demanded. We fabricated TiO_2 thin films consisting of poly(diallyl dimethyl ammonium chloride) (PDDA) and titanium(IV) bis(ammonium lactate) dihydroxide (TALH) for optical devices fabricated using layer-by-layer self-assembly.

The thickness of the (PDDA/TALH) thin film was confirmed to increase by controlling the pH of TALH solution and the concentration of PDDA solution, and by adding NaCl.

Deposition conditions for satisfying the three parameters were chose: pH of TALH solution, concentration of PDDA solution, and amount of NaCl added. The thickness of the thin film increased approximately 6-fold from 15 to 87 nm using a combination of the deposition conditions. There are three reasons for the phenomenon: (1) hydrolysis of TALH solution induced by adjusting pH, (2) strong coulombic interactions at high concentrations of PDDA solution, and (3) electrostatic effect induced by the addition of

NaCl. Therefore, the fabrication speed of thin film could be increased by controlling the deposition conditions. Moreover, deposition speed could be increased while maintaining optical quality (the highest transmittance in the visible range is 97% and the lowest reflectance of the film is 0.3%) by suppressing the surface roughness within 10 nm. Although surface roughness increased to 10.7 nm, it was still sufficiently good for optical devices used in the visible range. The optimization of the fabrication conditions for thin films is very important for the production of optical devices such as antireflection and infrared reflective films using LBL-SA.

II. Control of nano structure of polyelectrolyte (PAH/PAA) films by spray layer-by-layer method

The fabrication of polyelectrolyte multilayer thin films has received much attention recently. Polyelectrolyte multilayer thin films have strongly been paid attention to the various applications such as sensors, electronic devices, drug delivery carriers, micropatterning, membranes, microcontainers for molecules encapsulation, and particle surface modification.

Several LBL modifications have been proposed recently, including spray-LBL. Compared with dipping self-assembly coating, spraying self-assembly coatings has the advantages that the desired thin film with large surface area can be fabricated in short time and with small volume of solution. These thin films deposited by spraying coatings may be expected for the many device applications such as external coatings to protect corrosion, large area membrane, and biomaterial coatings with the fine design and controlling of the structure of multilayers thin film. These new methods have primarily

focused on decreasing the cycle time required by LBL. However, they did not monitor the nanoscale control of the structures formed by the spray-LBL method.

Weak polyelectrolyte multilayer thin films deposited by sequential spraying of poly(allylamine hydrochloride) (PAH) and poly(acrylic acid) (PAA) solutions are described. We have found that texture structures were the formed for the (9.5/5.0) PAH/PAA film. We found that this (9.5/5.0) film is thicker than the (7.5/3.5) film. There is a possibility to form nanoscale texture structures very rapidly. If these structures can be formed by the spray-LBL method, it should be much faster. If nanoscale texture structures are formed by the spray-LBL method, the possibility for biological applications of this method will increase. Thus far, there is no report on the formation of nanoscale texture structures using the spray-LBL method.

Therefore, nanoscale texture structures were fabricated considering several factors such as the concentration of spray solution, spray quantity, and the flow rate of spray solution using the spray layer-by-layer (spray-LBL) method.

Fabricated thin film by spray-LBL method is rapid and leads to high quality films. And nanoscale texture structures of weak polyelectrolyte (PAH/PAA) multilayer films were successfully fabricated by the spray-LBL method. We determined that the surface morphology of (PAH/PAA) films was affected by the spray solution concentration, quantity, and flow rate. By controlling the conditions, it was demonstrated that the nanoscale texture structures can be successfully fabricated by the spray-LBL method. This method can control film thickness and the surface morphology with nm accuracy. Moreover, the fabrication speed of thin films prepared by the spray-LBL method was markedly increased compared with that by the dip-LBL method. By changing spray quantity, flow rate, and concentration in the spray-LBL method, the phase transition for

surface structure was discovered for the first time. It is expect that the spray-LBL method will be very useful for the fabrication of functional thin films for optical devices, filters, and sensors, or various surface coatings.
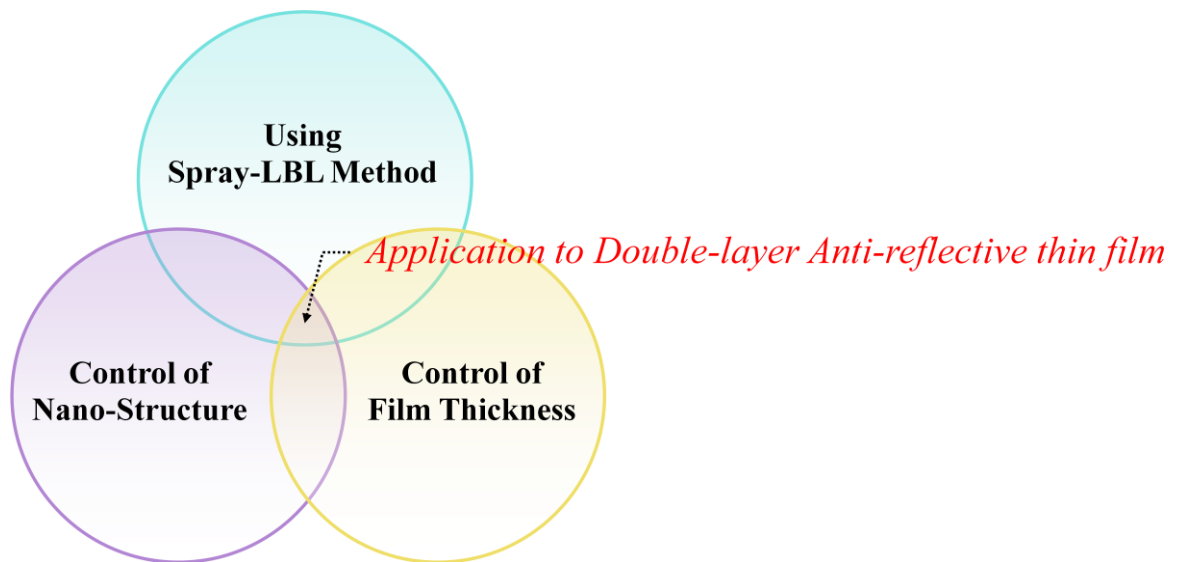
III. Application of double layer anti-reflective film

The recently developed practice of spraying solutions onto a substrate in order to fabricate thin film via LBL method has been further investigated and extended. Anti-reflection (AR) films have numerous applications in optical and display devices such as cathode ray tubes (CRTs), plasma display panels (PDPs), and liquid crystal displays (LCDs). We successfully fabricated double-layer anti-reflection (AR) thin film with high and low reflective index layers by spray-layer-by-layer (spray-LBL) method. For the deposition of high refractive index layer, poly(diallyldimethylammonium chloride) (PDDA) and titanium(IV) bis (ammoniumlactato) dihydroxide (TALH) were alternatively assembled. The average thickness of (PDDA/TALH) was determined to be

7 nm and the refractive index was n = 1.76 at 550 nm. Poly(allylamine hydrochloride) (PAH) and poly(acrylic acid) (PAA) were assembled on high refractive index layer for the deposition of low refractive index layer. The average thickness of (PAH/PAA) was determined to be 14 nm and the refractive index was n = 1.48 at 550 nm. This AR thin film showed the maximum transmittance (94.5 %) and the minimum reflection (0.5 %) around 550 nm in wavelength. Moreover, deposition speed was able to be increase more than 10 times compare with conventional LBL method, with keeping the optical characteristics of the films. It is expect that it will the very useful for the fabrication of the functional thin films by spray-LBL method for various surface coating etc.

Chapter 7

Future perspectives regarding the present research

LBL self-assembly technique has been promising method to the manufacture of multilayers thin films because the LBL deposition have a lot of merits such as very simple, environmentally friendly, and low-cost technique and needless of a vacuum system as well as other complete apparatus. The control of film thickness, surface properties, film morphology, degree of interpenetration, and transport properties can be readily carried out at low temperature and in simple process. In addition, many kinds of materials such as small organic molecules or inorganic compounds, macromolecules, biomacromolecules, and metallic or oxidic colloids can be employed for starting materials. Therefore the thin films fabricated by this technique are expected for various applications such as gradient thin films, organic/inorganic particle composite systems, molecularly ordered thin films, selective deposition/patterning, colloidal templates, membrane films, biomaterial coating, and nanocapsules.

Especially, the TiO_2 thin films are used for many optical, chemical, and electrical applications. Because TiO_2 has unique properties such as a very high refractive index as well as dielectric constant, and remarkable photocatalystic behavior. Therefore, the advance (TiO_2/polyelectrolyte) thin films fabricated by LBL self-assemble method are expected to be promising coating films for optical filter, air filter, AR thin film, and self-cleaning coating etc. For example, the AR coating film applications will be possible by using TiO_2 and polyelectrolytes thin films because the (TiO_2/PVS) thin films assembled at low temperature show a high density of anatase deposition, high refractive

index and transmittance. Hence, we can remarkably decrease the process expense to coat the AR thin film on display devices or solar cells compared with that of conventional methods. In addition, the AR coating film can be assembled on the flexible and low thermal resistance substrates by this method.

Recently, the polyelectrolytes thin films have been fabricated by continuous and simultaneous spraying. By using this method, we can expect lots of advantages such as the saving of deposition time, the decrease of solution loss, the possibility of very large surface coating, and the possibility of coating inside of tubes or microfluidic cells. The hydrophilic or hydrophobic thin films can be readily fabricated on many kinds of substrates such as glass, paper, cloth, metal, plastic materials by this ways.

The spray-LBL method is a very effective technique for depositing thin, multilayered films onto substrates with a surface charge. This technique provides more parameters for adjusting the deposition process and thus more control in fine-tuning the deposited thin films. By analyzing the effects on film thickness and roughness of each of the operational parameters of the system, it was determined that polyelectrolyte concentration, polyelectrolyte spraying time, spray distance, and polyelectrolyte charge density are the optimal parameters for adjusting the film thickness. If evident, trends were presented for each of the system parameters and their effect on film thickness. The parameter values that produced the smoothest films were also identified. These results allow for prediction and adjustment of the film properties based on the system parameter settings, prior to spraying any solutions. This can potentially eliminate the trial and error adjustment process that is currently conducted when film thickness and/or roughness must be modified.

Finally we can conclude that there is fortune possibility for the nano-scale control of

the film to create numerous functional products that are friendly and convenient to our

living.

Published papers and presentation lists regarding the present thesis

Papers

1. <u>Kyu-Hong Kyung</u> Kouji Fujimoto, Seimei Shiratori, Jin-Ho Kim, and Sae-Hoon Kim, Investigation of TiO_2 Thin Film Growth by Layer-by-Layer Self-Assembly for Application to Optical Devices, Jpn. J. Appl. Phys. 49 (2010) 045001

2. <u>Kyu-Hong Kyung</u> and Seimei Shiratori, Nanoscale Texture Control of Polyelectrolyte Multilayer using Spray Layer-by-Layer Method, Accepted to Jpn. J. Appl. Phys.

3. <u>Kyu-Hong Kyung</u>, Kouji Fujimoto, and Seimei Shiratori, "Control of Structure and Film Thickness using Spray-Layer-by-Layer Method: Application to Double-Layer Anti-Reflection Film, Accepted to Jpn. J. Appl. Phys.

4. Kouji. Fujimoto, <u>Kyu-Hong Kyung</u>, and Seimei Shiratori, Self-Assembled Hetero Structural Thin Film for Optical Lens, Submitted to Jpn. J. Appl. Phys.

International Conference

1. <u>Kyu-Hong Kyung</u> and Seimei Shiratori, Increase of the Fabrication Speed of Thin Film by Layer-by-Layer Self-Assembly Method, The IUMRS international Conference in Asia (2008).

2. <u>Kyu-Hong Kyung</u> and Seimei Shiratori, Control of Nano Structure and Film Thickness using Spray Layer- by-layer Method: Application to Double-layer

Anti-reflection Film, 13th International conference on Organic molecular films (2010).

3. Kyu-Hong Kyung and Seimei Shiratori, Nano-scale and film thickness control of texture structure of thin film using spray-layer- by-layer method, International Chemical Congress of Pacific Basin Societies (2010).

4. Kouji Fujimoto, Kyu-Hong Kyung, and Seimei Shiratori, Self assemble titania multilayer films from water base titanium complexes, 13th International conference on Organic molecular films (2010).

5. Nanae Fukao, Jyunichiro Abe, Kouji Fujimoto, Kyu-Hong Kyung, and Seimei Shiratori, Fabrication of Automatic Spray-LBL Machine with in-situ Monitoring Using QCM, 13th International conference on Organic molecular films (2010).

6. Kouji Fujimoto, Kyu-Hong Kyung, and Seimei Shiratori, Self assembly nano structural titania multilayer film from water base titanium complexes, Asian Nanotechnology on Nano science & Nanotechnology (2010).

Domestic Conference

1. Kyu-Hong Kyung, Seimei Shiratori, 交互積層法による超薄膜の成膜速度向上, 2008年秋季 第69回応用物理学会学術講演会

2. Kyu-Hong Kyung, Seimei Shiratori, 交互積層法における薄膜製作時 電圧印加の影響, 2009年春季第56回応用物理学関係連合講演

3. Kyu-Hong Kyung, Seimei Shiratori, Spray-LBL法による薄膜の構造制御と表面の濡れ性制御, 2009年秋季 第70回応用物理学会学術講演会

4. Kyu-Hong Kyung, Seimei Shiratori, Spray-LBL法による膜厚の制御と二層型反

射防止膜への応用, 2010年春季第57回応用物理学関係連合講演会

5. Kouji Fujimoto, <u>Kyu-Hong Kyung</u>, and Seimei Shiratori, Fabrication of optical multilayer thin films coated on lens using LBL process, 2010年春季第57回応用物理学関係連合講演会

6. Nanae Fukao, Jyunichiro Abe, Kouji Fujimoto, <u>Kyu-Hong Kyung</u>, and Seimei Shiratori, Fabrication and characterization of ultra thin film by automatic spray-LBL method, 2010年春季第57回応用物理学関係連合講演会

Acknowledgements

Kyu-Hong Kyung